Palacký University
Olomouc

Palacky University Olomouc

Faculty of Science

Department of Geology

Study programme: Geological Sciences (1201V022)

Field of study: Hydrogeology and Hydrogeochemistry

Integration of Hydrogeology and Geochemistry for Sustainable Groundwater Assessment, Modeling and Management in the Zagros Basin, the Kurdistan Region of Iraq

Doctoral Dissertation

Rebar Mahmmud M.Sc.

Supervisor: Professor Ing. Ondřej Šráček, Ph.D., M.Sc.

Co-Supervisor: Assistant Professor Dr Omed Mustafa

Olomouc 2023

Declaration

I hereby declare that this PhD dissertation of Geological Sciences study program, entitled (Integration of Hydrogeology and Geochemistry for Sustainable Groundwater Assessment, Modeling and Management in the Zagros Basin, the Kurdistan Region of Iraq) is entirely my own work and all the materials and resources are cited with regard to scientific ethics, copyrights and laws protecting knowledgeable property.

In Olomouc, Czech Republic, August 21, 2023

Rebar Mahmmud

Acknowledgements

I stand at the conclusion of this enriching journey of doctoral study, profoundly aware that I have not arrived here alone. My journey was made possible through the help, guidance, and support of many individuals, and it is my greatest pleasure to express my heartfelt gratitude to them.

First and foremost, I want to thank my supervisor, Professor Dr Ondra Sracek, who has been a beacon of knowledge, patience, and inspiration. His intellectual way, dedication, and unwavering faith in my capabilities have been invaluable to my academic growth. You challenged me to reach beyond my own expectations and for this, I am eternally grateful.

I would like to express my appreciation to my Co-Supervisor, Assistant Professor Dr Omed Mustafa, for his continuous support and advice throughout my PhD study journey.

Special thanks go to Professor Dr Howri Mansurbeg for his advice and support during my study. His advice and encouragement have always been such a great lesson for me during the long journey.

Thanks to the Head of the Geology Department at Palacky University Olomouc, Professor Dr Ondrej Babek and Dr Pavel Spirov for their continuous support during my study.

Thanks to my colleagues and friends at the Geology Department, Faculty of Science, Palacky University Olomouc.

My deep appreciation goes to Palacky University Olomouc for funding my PhD study and giving me Fischer Scholarship. The financial support and faith in my research contributed significantly to completing this journey.

Thanks to the Czech Geological Survey and Charles University in Prague for water sampling analysis, University of Tours in France for financial contribution of tritium analysis, University of Avignon for tritium analysis. In addition, thanks go to the Laboratories of Technische Universität Bergakademie Freiberg, Germany and Sulaimani Environmental Protection Office, Kurdistan Region, for the water analyses.

Thanks to the Directorate of Groundwater of Sulaimani for providing some hydrogeological data and my colleagues who are working there for continuous support. Thanks to the Ministry of Agriculture and Water Resources, Kurdistan Regional Government for giving support and financial contribution during my PhD journey.

On a personal message, I am profoundly indebted to my family. To my parents, thank you for instilling in me the values of hard work, perseverance, and curiosity. Your unconditional love

and support have been my rock. In addition, special thanks to my uncle Dr Amanj Ali for his continuous and financial support.

Finally, my heartfelt thanks go to my wife, Narmin and my daughter Nela; their unwavering support, patience, and sacrifices during this long journey have not gone unnoticed. They stood by me during the highs and lows of this challenging journey, and for that, you have my enduring love and gratitude.

This journey has taught me that knowledge is a collective endeavour and I am fortunate to have such a supportive community to contribute to this pursuit. If this dissertation is a mountain, it was built from pebbles of wisdom, assistance, encouragement, and love from each one of you.

Abstract

The Sulaimani-Warmawa Sub-basin is in the Kurdistan Region of Iraq, which is part of the Zagros Basin and has been comprehensively studied. A combination of hydrogeology and geochemistry has been utilised for sustainable groundwater assessment, a better understanding of this vital water resource and the establishment of a scientific and standard plan for better management and protection against contamination. The region is semiarid with seasonal rainfall in winter and dry and warm summer. The field parameters such as pH, electrical conductivity and temperature were measured in water wells located in the study area. In total, twenty-six water samples, including two from rain and one from the Tanjero River, have been collected for cation, anion, trace element, stable isotope (^{2}H, ^{18}O and ^{13}C), $^{87}Sr/^{86}Sr$ and radioactive isotope (^{3}H) analysis.

In general, the water chemistry changes from Ca-HCO_3 groundwater type at the basin boundaries to Ca-Mg-HCO_3 groundwater type towards the Tanjero River along the axis of the basin. Concentrations of Na, Cl, and SO_4 increase in some samples due to halite and gypsum dissolution embedded in carbonates. Redox parameters indicate a moderately reducing environment; the pH values are neutral or alkaline.

Barium (Ba) is the principal geogenic contaminant with concentrations up to 0.383 mg/l. The other geogenic contaminants such as As, F, Mn and Cr have low or below the detection limit concentrations as predicted based on their low carbonate rock contents. Inverse geochemical modeling on selected profiles calibrated using ^{13}C values provided mass transfer coefficients for possible geochemical reactions.

The result of isotopes ^{2}H and ^{18}O indicate groundwater recharge from winter precipitation with no evaporation. Values of dissolved inorganic carbon ^{13}C(DIC) correspond to equilibrium with carbonates and C4 plants as the source of CO_2. Groundwater $^{87}Sr/^{86}Sr$ values are consistent with carbonate dissolution as the primary process.

The tritium values of the rain sample were 7.3 TU and 4.4 TU for the Tanjero River inside Sulaimani City, respectively. The tritium values for groundwater samples were from less than 0.8 to 4.9 TU. Most groundwater samples do not seem to contain pre-bomb tritium, and the groundwater seems to be relatively young.

The most serious threat to groundwater quality are interactions of the studied aquifers with the heavily contaminated Tanjero River. Water treatment in the river is crucial and a water treatment plant should be built in Sulaimani. In addition, the determination of the depth and boundary of each aquifer, comprehensive hydrogeochemical and isotope study, water well monitoring system plan, and monitoring of geogenic contaminants of Ba, F and As are recommended for future research subjects.

Abstrakt

Hydrogeologický systém Sulaimani-Warmawa se nachází v irácké oblasti Kurdistán, která je součástí povodí Zagros, byl komplexně studován. Kombinace hydrogeologických a geochemických metod byla použita pro hodnocení využitelných podzemních vod, lepší pochopení tohoto životně důležitého zdroje a vytvoření plánu pro lepší management a ochranu před kontaminací. Oblast je semiaridní se sezónními srážkami v zimě a suchým a teplým létem. Terénní parametry jako pH, elektrická vodivost a teplota byly měřeny v ve studních ve studované oblasti. Celkem bylo odebráno dvacet šest vzorků vody, včetně dvou vzorků deště a jednoho vzorku z řeky Tanjero, pro analýzu kationtů, aniontů, stopových prvků, stabilních izotopů (^{2}H, ^{18}O, ^{13}C), $^{87}Sr/^{86}Sr$ a radioaktivních izotopů (^{3}H).

Obecně se chemismus vody mění z typu podzemní vody Ca-HCO_3 na hranicích povodí na typ podzemní vody Ca-Mg-HCO_3 ve směru proudění směrem k řece Tanjero podél osy povodí. Koncentrace Na, Cl a SO_4 jsou v některých vzorcích zvýšeny v důsledku rozpouštění halitu a sádrovce obsažených v karbonátech. Redoxní parametry indikují mírně redukční prostředí; hodnoty pH jsou neutrální nebo alkalické.

Baryum (Ba) je hlavní geogenní kontaminant s koncentracemi do 0,383 mg/l. Ostatní geogenní kontaminanty jako As, F, Mn a Cr mají nízké koncentrace nebo koncentrace pod detekčním limitem, jak bylo předpovězeno na základě jejich nízkého obsahu karbonátech. Inverzní geochemické modelování na vybraných profilech kalibrované pomocí hodnot δ^{13} poskytlo koeficienty přenosu hmoty pro možné geochemické reakce.

Hodnoty izotopů $\delta^{2}H$ a $\delta^{18}O$ indikují doplňování podzemní vody ze zimních srážek bez výparu. Hodnoty rozpuštěného anorganického uhlíku ^{13}C(DIC) odpovídají rovnováze s karbonáty a C4 rostlinám jako zdroji CO_2. Hodnoty $^{87}Sr/^{86}Sr$ v podzemní vodě jsou v souladu s rozpouštěním karbonátů jako primárním procesem.

Hodnoty tritia ve vzorku deště byly 7,3 TU a 4,4 TU v řece Tanjero ve městě Sulaimani. Hodnoty tritia pro vzorky podzemní vody byly od méně než 0,8 do 4,9 TU. Zdá se, že většina vzorků podzemní vody neobsahuje tritium z doby před nukleárními testy a podzemní voda se zdá být relativně mladá.

Nejzávažnější hrozbou pro kvalitu podzemních vod jsou interakce studovaných zvodní s silně kontaminovanou řekou Tanjero. Úprava vody v řece je zásadní a v Sulaimani by měla být vybudována úpravna vody. Kromě toho se pro budoucí výzkumné subjekty doporučuje stanovení hloubek a hranic zvodnělých vrstev, komplexní hydrogeochemická a izotopová studie, plán systému monitorování vodních vrtů a monitorování geogenních kontaminantů Ba, F a As.

Table Of Contents

List of Figures

LIST OF TABLES

1. Introduction

Groundwater is one of the vital resources in the world, especially in arid and semi-arid regions, and is used for drinking, domestic, agriculture, industrial, and other purposes. The effective management of groundwater resources in arid and semi-arid regions through different hydrogeological and hydrogeochemical tools is crucial for protecting them from the viewpoint of both quantity and quality. Several groundwater studies have been conducted in such areas; for instance, in the Kalahari Desert located in Namibia (Uugulu & Wanke, 2020), Botswana (Stadler et al., 2010), also in the northeastern region of Brazil (Halm et al., 2002), and central Australia (Harrington et al., 2002). The study conducted by Scanlon et al. (2006) revealed that groundwater quality in these regions is predominantly affected by intense evaporation and by the nature of recharge (diffuse vs. focused), in addition to the land use and land cover. Mountain front recharge is a commonly observed phenomenon in which the primary recharge zones of aquifers are located in mountainous regions with higher precipitation levels. As a result, groundwater flows from these mountain areas towards lower-lying regions, where the primary extraction of groundwater occurs (Markovich et al., 2019).

The United Nations Sustainable Development Goal (SDG6) emphasises that "2 billion people are living with the risk of reduced access to freshwater resources, and by 2050, at least one in four people is likely to live in a country affected by chronic or recurring shortages of fresh water" (UNDP, 2017). Therefore, more than 2 million people die annually from waterborne infections; in addition, 4.3 and 6.4 per cent of Sub-Sahara African and Indian GDP is negatively affected by poor sanitation. Iraq and the Kurdistan region are ranked 105/166 and the SDG index score was 64.8. It means that most of the local population uses at least basic drinking water services. However, it ranks poorly in the effort to achieve Sustainable Development Goal 6 (SDG6), a challenge which involves a proper understanding of relationships between land use, sea level rise, climate change, and groundwater quality.

The study area, Sulaimani-Warmawa Sub-basin (SWSB), is a hydrological Sub-basin which is a part of the Sulaimani-Sharazoor Basin. The SWSB is located southeast of the Kurdistan Region, northwest of the Zagros basin. It is mainly in Sulaimani Governorate and Sulaimani City is a part of the study area. It is a semi-arid region with a Mediterranean-type climate and precipitation occurs primarily in winter months. Groundwater is a crucial water resource because local streams are generally perennial and dry out during late summer. The region is economically significant because of its huge oil reserves and several towns are booming due to

the oil industry. Sulaimani is the principal city in the study area with about 800,000 inhabitants, primarily dependent on groundwater for water supply.

There is a lack of groundwater management in the Kurdistan Region of Iraq, especially in the SWSB. In addition, there is no clear management strategic plan from Kurdistan Regional Government and relevant authorities to preserve this vital water resource and protect them against contamination. Moreover, the unavailability of data and the limitation of scientific study in the area of interest is another challenge in the Kurdistan Region of Iraq for establishing the scientific standard to preserve groundwater.

Monitoring of groundwater is crucial to identify contamination early enough to prevent resource damage, as cleanup is costly and almost impossible after water quality declines. This task requires adequate knowledge and information on groundwater chemistry to develop a novel approach to achieve an inclusive and efficient integrated water resources framework that will accelerate SDG6 in the Kurdistan Region, Iraq, the Zagros basin and the Middle East.

This dissertation deals with the identification of processes responsible for the formation of groundwater chemistry in the study area and special attention is paid to geogenic contaminants such as As and F. Several methods such as hydrogeology, hydrogeochemistry, geochemical modeling including speciation and inverse modeling, and stable isotope and radioactive isotopes are applied to improve existing hydrogeological and hydrogeochemical knowledge and to contribute to better groundwater management in the Sulaimani-Warmawa Sub-basin.

2. Hydrogeochemical and Isotopic Background

2.1 Groundwater investigation in semi-arid regions

The requirement for sustainable management of groundwater resources has increased in recent years due to overexploitation, climate change, and rising population needs. According to the United Nations, by 2025, over two-thirds of the world's population might experience water shortages, with groundwater resources becoming an increasingly vital freshwater supply (UN, 2018).

Countries have enacted rules and standards governing the use of groundwater resources to guarantee effective groundwater management. The Safe Drinking Water Act (SDWA) and the Clean Water Act (CWA) establish a framework for preserving and managing groundwater resources in the United States (EPA, 2022). Similarly, Australia's National Water Initiative (NWI) establishes the principles for the sustainable management of groundwater resources (EPA, 2022).

Several studies were conducted worldwide in semiarid regions including the Middle East. However, a limited number of studies have been done in the Zagros Basin, especially in the Kurdistan Region of Iraq in terms of groundwater management. The most important studies in different areas are discussed below, explaining various methodologies available for better groundwater management.

Gleeson et al. (2010) discussed various sustainable groundwater management strategies, such as aquifer recharge, demand management, and governance reforms. The study highlighted the significance of incorporating social, economic, and environmental factors into groundwater management.

The groundwater chemical constituents and associated hydrochemical processes in the part of Mhlathuze in South Africa were identified by (Elumalai et al., 2023). According to the result of this study, groundwater is significantly undersaturated with respect to sulphate and chloride minerals and saturated concerning carbonate minerals. In addition, hierarchical cluster analysis shows that chemical elements in groundwater in this aquifer come from evaporation, anthropogenic input, silicate and carbonate weathering, and nitrification process.

In National Capital Region (NCR), Delhi, the isotope and hydro-geochemical integrated method was applied to assess groundwater chemical composition processes and mechanisms. Groundwater chemical evolution was examined using flow direction, hydrochemical facies, bivariate plots of ionic ratios, and saturation index. According to the result, the stable isotope demonstrated that quartzite groundwater is largely meteoric and recharges the neighbouring

alluvium aquifer. Tritium data show that western quartzite and alluvium groundwater is older than eastern groundwater. About 13% of groundwater samples are in extremely high contamination zones, mostly in Eastern alluvium aquifers. Human activity affects alluvium aquifer more than quartzite aquifer (high land) (Gupta et al., 2023).

Moreover, managing groundwater resources is much more difficult in semiarid regions worldwide. Several studies have been conducted for better groundwater management in such regions. El-Rawy et al. (2016) conducted a study about assessing groundwater management strategies for sustainable development in a semiarid area, a case study in the Amman-Zarqa basin in Jordan. This study evaluates various groundwater management strategies for the Jordanian Amman-Zarqa Basin, a semiarid region with a water shortage. The numerical groundwater model has been used to simulate and assess the impact of various management scenarios on water availability and quality.

Carpio and Romero, (2018) conducted a study on sustainable water resources management in semiarid in the Altiplano region, Bolivia. This study investigates the challenges and opportunities for sustainable water resources management in the semiarid, water-scarce Altiplano region of Bolivia. A framework for sustainable groundwater management in the area has been proposed, including community participation, the application of appropriate technologies, and the creation of policies and regulations.

Another study was conducted in the Kalahari Desert in Namibia (Uugulu & Wanke, 2020). The chloride mass balance method and environmental isotopes have been used to estimate groundwater recharge in savannah aquifers along a precipitation gradient. The relationship between precipitation and recharge has been investigated to improve the understanding of the hydrogeological processes and to support sustainable groundwater management. The analyses of chloride concentration, stable isotope of ^{2}H and ^{18}O, as well as tritium ^{3}H have been conducted based on the groundwater samples in the area, and the results show that the chloride mass balance method provides a consistent estimate of recharge, which is consistent with the outcomes from the environmental isotopes analysis.

Stadler et al. (2010) investigated the groundwater flow regime, recharge, and regional-scale solute transport in the semiarid Kalahari of Botswana using isotope hydrology and hydrochemistry. The main aim of this study was to improve the understanding of the hydrogeological processes and the factors that impact the quality of groundwater in the region. The major ions, trace elements, and stable hydrogen and oxygen isotopes in the groundwater samples have been analysed. The findings indicate that the quantity and distribution of

precipitation regulate the groundwater recharge in the area, with recharge rates ranging from 1 to 20 mm/year.

Hydrogeochemical and stable Isotope data of the groundwater of a multi-aquifer system in the Maknessy Basin (Mediterranean Area, Central Tunisia) has been investigated (Moussaoui et al., 2023). Chemical, isotopic, and statistical approach has been used to evaluate the quality of water resources. According to the result of this study, the analyzed groundwater is mostly calcium hyper chloride and calcium sulphate. EC and TDS affect water quality, according to multivariate statistical analysis (PCA and HCA) and geochemical methods. In addition, the stable isotopic compositions of the tested fluids vary from −7.53 to −4.90% vs Vienna Standard Mean Ocean Water (VSMOW) for ^{18}O and −53.6 to −32.2% for ^{2}H, indicating groundwater-rock exchange and evaporation. Recent, paleo- and mixed-water isotopic data show groundwater evaporation and interaction, confirming that this aquifer has been refilled by current rains.

Hydrogeochemical and isotopic data analyses have been used in another study to assess groundwater quality and its recharge mechanisms in the Tafilalet plain (south-eastern Morocco) (El Ouali et al., 2023). The results show that the main types of water in the study area are sodium chloride and calcium magnesium chloride facies. The groundwater is mostly degraded and highly mineralized. In addition, increasing concentrations of Cl^{-} and Na^{+} in water have been found as a consequence of the evapotranspiration of irrigation water. Moreover, the isotopic measurements reveal that the average contents of $^{18}O = -6.7‰$ and $^{2}H = -48‰$ respectively, with tritium activity ranging from 3 to 6 TU, recent recharge. Current climate conditions recharged the Quaternary aquifer, according to ^{18}O and ^{2}H data. Thermonuclear tritium and radiocarbon (^{14}C = 94.9 to 107.6 pmC) also indicate current recharge.

Environmental isotope application and hydrochemistry have been investigated to identify groundwater recharge in Wadi Qanunah Basin, Saudi Arabia. The results of the analysis of ionic ratios suggest that the enrichment of groundwater with major constituents such as calcium, sodium, magnesium, sulphate and chloride was influenced significantly by ion exchange, silicate weathering, and evaporation. The relationships between ^{18}O vs D, TDS vs ^{18}O, and ^{18}O vs d-excess indicated that the primary source of groundwater recharge is local precipitation. Meanwhile, certain samples were affected by evaporated rainfall, whereas those with lower salinity levels (<1000 mg/L) were diluted through seepage from the fractured basement aquifer (Masoud et al., 2023).

2.2 Hydrogeology and groundwater management

Hydrogeology is the study of the properties, distribution, and movement of water in the subsurface. It provides the scientific basis for understanding groundwater resources and their interaction with the environment. It is a crucial part of groundwater management and why it plays such an important role. Investigations of the hydrogeology of a region are necessary for several purposes, including the characterization of aquifer systems, the estimation of groundwater recharge and outflow, the evaluation of the effects of human activities on the quality of groundwater, and the development of management plans for the sustainable use of groundwater. In addition, due to the growing demand for groundwater resources globally, hydrogeology has become an essential tool for guaranteeing the responsible use of these resources (Bouwer and Rice, 1976; Freeze and Cherry, 1979; Todd, 1980).

Several applications of hydrogeology can be used for groundwater management in terms of quantity and quality.

For instance, Alley (2018) stated that groundwater monitoring is used as regular monitoring of groundwater levels, and quality is vital for effective management. Hydrogeologists design and implement monitoring networks, assess trends, and provide recommendations for resource management and protection.

Moreover, Managed Aquifer Recharge (MAR) is another tool in hydrogeology to identify suitable locations for managed aquifer recharge, which can help replenish depleted aquifers, mitigate saltwater intrusion, and improve water quality (Dillon, 2005).

2.3 Hydrogeochemistry of groundwater

Hydrogeochemistry is a significant field of study that examines the chemical composition and properties of groundwater. The chemistry of groundwater can provide important information regarding the origin and movement of water, and the geological and hydrological characteristics of aquifers, and it has the potential for water quality issues such as contamination. Analysing the chemical properties of groundwater involves the measurement of major ions, trace metals, and stable isotopes, among other methods. These techniques are crucial for comprehending the physical and chemical processes that occur within aquifers and devising strategies for effectively administering and protecting groundwater resources.

Freeze and Cherry (1979), Todd (1980), Hem (1985), Domenico and Schwartz (1998), and (Maimaiti et al., 2018) are among the authors who have contributed to the knowledge and understanding of groundwater hydrogeochemistry. Covering topics such as the hydrological

cycle, water-rock interactions, geochemical modelling, and contaminant transport and remediation, these authors have provided a comprehensive understanding of the principles and practises of hydrogeochemistry.

In addition, Drever (1997) and Edmunds and Smedley (2000) stated that hydrogeochemistry is the study of the chemical composition of water, particularly groundwater, and its interactions with the surrounding rocks and minerals. This scientific field has several uses for understanding and managing groundwater resources, such as assessing water quality, determining water origin, identifying contamination sources, and guiding remediation efforts.

One important use of hydrogeochemistry is in the assessment of groundwater quality for human consumption and ecological health. This is done through analysing the concentrations of various ions, trace elements, and isotopes in groundwater; water quality can be determined in order to meet the quality standards set by controlling agencies and identify the possible presence of contaminants (Domenico and Schwartz, 1998).

Another application of hydrogeochemistry is to determine the origin of groundwater and its flow paths. This application is done by analysing the isotopic and chemical signatures of the water. Hydrogeochemists can trace its sources, understand its recharge areas, and estimate its residence time (Clark and Fritz, 1997).

Moreover, hydrogeochemistry is also a suitable method for identifying the sources of contamination in groundwater, such as industrial waste, agricultural runoff, or leaking landfills. By comparing the chemical composition of polluted water to the applicable standard for water, contaminants and trace them back to their source can be identified (Appelo and Postma, 2005).

The water cycle is a continuous process in which water moves and changes develop in the atmosphere, surface, and subsurface of the planet, as shown in Figure 1. Evaporation, condensation, precipitation, infiltration, and runoff are the main processes in the water cycle (Dingman, 2015). Fresh water for human use and ecosystem sustainability comes mostly from groundwater, which is located deep below the surface in the pores and cracks of rocks (Fetter, 2001). Discharge occurs when groundwater runs to the surface as springs, seeps into streams, or is extracted via wells. In contrast, recharge occurs when precipitation infiltrates the soil and percolates from the unsaturated zone to the saturated zone (Alley et al., 2002). The water cycle and groundwater are inextricably linked because of their shared importance in maintaining and redistributing the Earth's water supply (Freeze & Cherry, 1979).

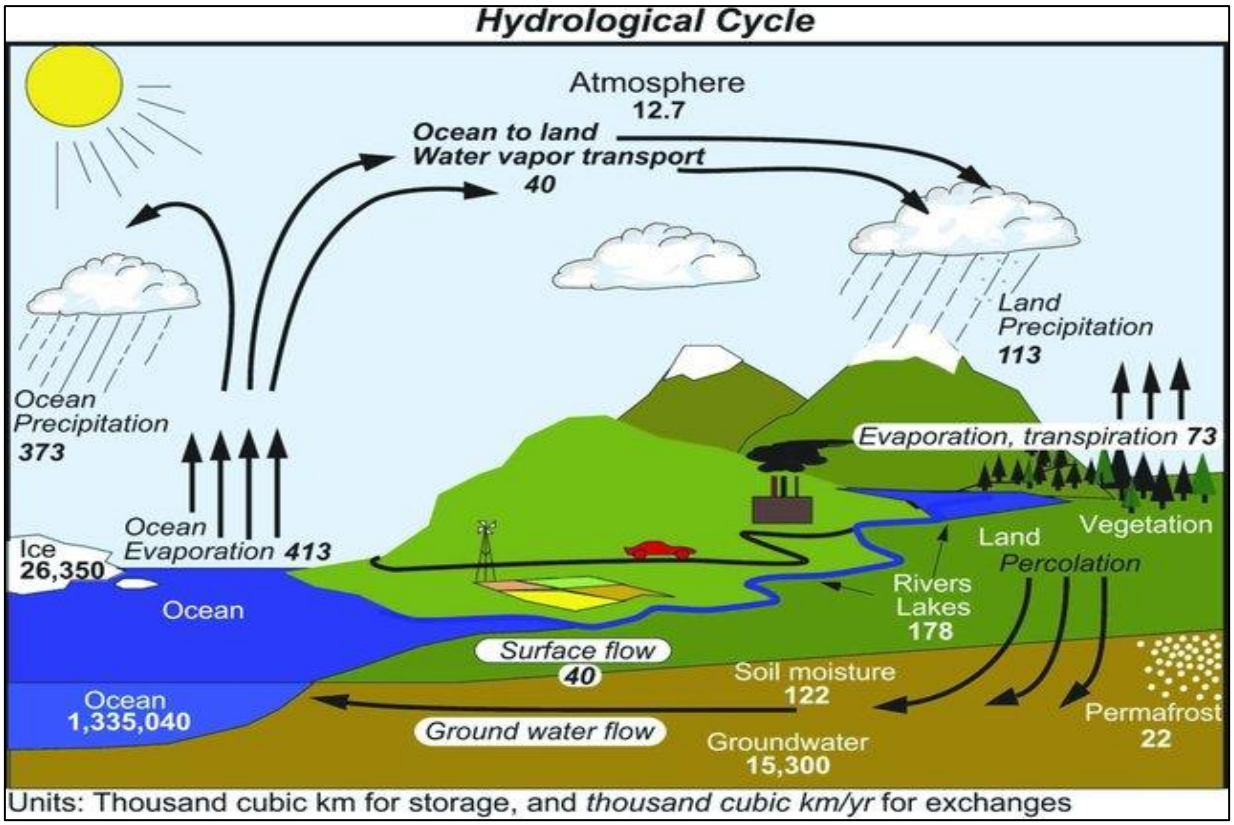

Figure 1 The hydrological cycle (Trenberth et al., 2007).

The fate of precipitation depends on various factors, such as the characteristics of the land surface and the intensity of the rainfall. Some of the precipitation runoff the surface and enters rivers, lakes, and oceans, while the remaining infiltrates the soil and becomes part of the groundwater system (Sophocleous, 2002). Groundwater, in turn, interacts with surface water through baseflow, which maintains river and stream levels during dry periods, and bank storage, where surface water temporarily infiltrates the subsurface during high-flow events (Winter et al., 1998).

The water cycle is also crucial in transporting nutrients, contaminants, and heat across the Earth's systems (Schlesinger and Bernhardt, 2013). Human activities such as deforestation, agriculture, urbanization, and water resource exploitation may disrupt the water cycle and groundwater dynamics, resulting in lower stream baseflow, depleted aquifers, and water pollution (Gleick, 2003; Konikow, 2011). As a result, understanding and managing the water cycle and groundwater supplies is crucial for tackling global water concerns and guaranteeing ecosystem and human society sustainability.

In addition, understanding the geochemistry of water gives evidence to its hydrochemical development and is critical for successful water resource management and preservation (Dragon and Gorski, 2015). The study of hydrochemical differences in groundwater may help

define the flow pattern of aquifers. This understanding is critical in groundwater systems, especially when the hydrogeology of the area is complicated due to the presence of various aquifers. Spatial changes in groundwater chemistry may give insight into the modification of groundwater as it flows across aquifers in multilayer aquifer systems such as the Eastern Dahomey basin (Chukwura et al., 2015; Shin et al., 2017).

Furthermore, groundwater chemistry evolves as a result of hydrogeochemical processes during infiltration and flows in aquifers over space and time (Kalin, 1995; Prasanna et al., 2011; Talabi and Tijani, 2013; Narany et al., 2017; Bodrud-Doza et al., 2019). In watershed and groundwater aquifers, hydrochemical processes, including cation exchange, evaporation, dissolution/precipitation of minerals, seawater intrusion, oxidation-reduction, and biological processes, play essential roles in the hydrochemical evolution of groundwater (Somaratne and Frizenschaf, 2013; Narany et al., 2017 and Adimalla; Kumar, 2020).

2.3.1 Origin of dissolved ions

As groundwater changes from precipitation through infiltration within a soil and rock aquifer, it traps dissolved ions from gas in the atmosphere or minerals within the zones through which it flows. The origin or source of dissolved ions can be either natural or artificial, referred to as geogenic and anthropogenic, respectively. The hydrochemical status of groundwater is determined by several factors, such as mineral solubility, concentration, temperature, redox potential (Eh) and pH, and cation exchange capacity (CEC) (Davis and De West, 1966). The significant dissolved components of groundwater and their common sources are shown in Table 1.

Table 1. Major components of groundwater and their common sources (after Todd, 1980).

Major component	Source in water
Calcium	Primarily from carbonates, gypsum, feldspars
Magnesium	Feldspars, olivine, pyroxene, amphiboles, mica, Mg-calcite
Sodium	Feldspars, evaporite, cation exchange, seawater, industrial waste
Potassium	Feldspar, fertilizer, K-evaporite, glauconite
Silicic acid	Silicates

Ammonia	Pollution, degradation of organic matter, reduced NO_3, cation exchange
Sulphate	Dissolution of gypsum and anhydrite, oxidation of pyrite, seawater, windborne fertilizer salts
Chloride	Windborne rainwater, seawater and brines, evaporite deposits, pollution
Nitrate	Atmospheric deposition, the decay of nitrogen-fixing plants, oxidation of ammonia or organic nitrogen, contamination
Carbonate	soil and atmospheric CO_2, carbonate rocks, oxidation of organic material, volcanic gases
Oxygen	soil gas and atmosphere

The common hydrochemical reactions in groundwater are mineral dissolution and precipitation, redox reactions, ion exchange, and mineralization. These reactions have been explained in the following sections:

A solution of a mineral in water can be frequently described by an equilibrium relationship. When water comes into touch with a mineral, the concentration of dissolved species in the solution rises until it reaches a maximum (for a given physical state), at which point the solution is said to be saturated.

The solubility of a mineral is given by its saturation solution concentration and is affected by environmental conditions such as temperature, pressure, and other chemical variables. Common sedimentary minerals and their corresponding solubilities are listed in Table 2. Minerals are precipitate when ions dissolved in water undergo chemical processes that lead to their formation. This type of response can be observed during the precipitation of iron, which is common in areas where water seeps into the ground surface or springs. In this type of environment, the solid iron hydroxide is formed when iron dissolved in groundwater comes in contact with dissolved oxygen.

Table 2. Selected rock minerals and their solubility (Seidell, 1958).

Mineral	Formula	Solubility at pH 7 (mg/I)
Gibbsite	$Al_2O_3.2H_2O$	0.001
Quartz	SiO_2	12
Fluorite	CaF_2	160
Dolomite	$CaMg(CO_3)_2$	90(at PCO_2 of 10^{-3})
Calcite	$CaCO_3$	100
Gypsum	$CaSO_4.2H_2O$	2,100
Sylvite	KCI	264,000
Epsomite	$MgSO_4.7H_2O$	267,000
Mirabillite	$NaSO_4.10H_2O$	280,000
Halite	NaCl	360,000

Ions released into water by solution reactions result in mineral dissolution. This type of reaction is illustrated by release of calcium (Ca^{2+}) and bicarbonate (HCO_3^-) ions during the dissolution of calcite ($CaCO_3$). Due to the strong solvent properties of water, solution-precipitation reactions with the aquifer matrix are frequently crucial for regulating the chemistry of groundwater.

The majority of silicates that form rocks, with the exception of quartz, dissolve uniformly and produce a secondary solid phase during the dissolution process. For instance, orthoclase, a common mineral found in granites, may dissolve in water and kaolinite is left as a solid phase in an incongruent dissolution reaction:

$$11H_2O + 2KAlSi_3O_8(s) \rightarrow 2K + 2OH + 4Si(OH)_4 + AlSi_2O_5(OH)_3\ (s)$$

(Kaolinite)

The occurrence of incongruent dissolution processes can be observed when multiple minerals, which individually dissolve congruently in pure water, dissolve sequentially. An instance of this phenomenon is the dissolution of gypsum in a solution that is already saturated with respect to calcite. The process of gypsum dissolution results in the release of Ca^{2+} ions:

$$CaSO_4.2H_2O \rightarrow Ca^{2+} + SO_4^{2-} + 2H_2O$$

As indicated by the equation, the increase in Ca^{2+} ion concentration results in a decrease in the solubility of calcite by common ion effect (Freeze and Cherry, 1997; Drever, 1997). In this

scenario, gypsum dissolution is deemed incongruent due to the simultaneous occurrence of calcite precipitation.

In general, some reactions in groundwater involve electrons transfer between dissolved, gaseous, and solid constituents. Electron gain results in a reduction and electron loss results in oxidation. However, since free electrons do not occur in solution, reduction and oxidation coincide and the overall reaction is called a redox reaction, for instance:

$$Fe + 2H^+ \leftrightarrow Fe^{2+} + H_2$$

In this reaction, protons are reduced to hydrogen while Fe is oxidised to Fe^{2+}. It is common practice to express redox reactions in terms of half-reactions, which are afterwards added to cancel out the transferred electrons:

$$Fe0(s) \rightarrow Fe^{2+} + 2e^-$$

$$0.5O_2 + 2H^+ + 2e^- \rightarrow H_2O$$

$$Fe0(s) + 0.5\ O_2 + 2H+ \rightarrow Fe_2+ + H_2O$$

In the Redox reaction, water may participate in the following ways:

- It may be an inactive solvent; in which case it does not appear in the reaction equation.
- It may fulfil an acid-base role, in which case water appears on one side of the equation and H^+ or OH^- on the other side.
- It might be oxidized as; $O^{2-} + 4H+ + 4e^- \rightarrow 2H_2O$
- $H_2O \rightarrow H^+ + OH^-$

This is an instance of a simultaneous acid-base reaction and another reaction. As the reaction continues, the loss of protons as hydrogen causes the solution to become increasingly alkaline. The presence of the products of oxidation-reduction reactions in both groundwater and surface water can be used to infer the dominant oxidation-reduction reactions that have occurred in groundwater.

The groundwater passes through an aquifer, and oxidizing agents in the water are consumed by reaction with reducing agents in the aquifer, beginning with the most effective oxidizing agents (dissolved oxygen (DO), NO_3 reduction, and SO_4 reduction). The presence of oxidizing species may indicate recent recharge of groundwater.

The mineralization and cation exchange processes are critical in groundwater systems, as they play a crucial role in determining the water quality and regulating the dispersion and categorization of diverse ions (Appelo and Postma, 2005). The concept of mineralization

pertains to the process of dissolution and precipitation of minerals in groundwater, which is influenced by various factors such as pH, redox potential, and interactions between water and rock (Drever, 1997). The procedure mentioned above plays a role in the augmentation of dissolved ions' concentration and the formation of secondary minerals, thereby exerting an impact on water hardness and the mobility of pollutants (Freeze and Cherry, 1979). The cation exchange process is characterized by the exchange of ions between a solid surface, such as clay minerals or organic matter, and the surrounding water. This exchange is reversible and governed by surface complexation and electrostatic attraction principles (Stumm and Morgan, 1996). Cation exchange processes are known to have a substantial impact on the modulation of nutrient, pollutant, and trace element transport and fate in groundwater systems (Hem, 1985; Langmuir, 1997; Tossou et al., 2017). Therefore, understanding the mechanisms and dynamics of mineralization and cation exchange is essential for assessing and managing groundwater resources and designing effective water treatment and remediation strategies. Example of mineralization and ion exchanges are shown in Figure 2.

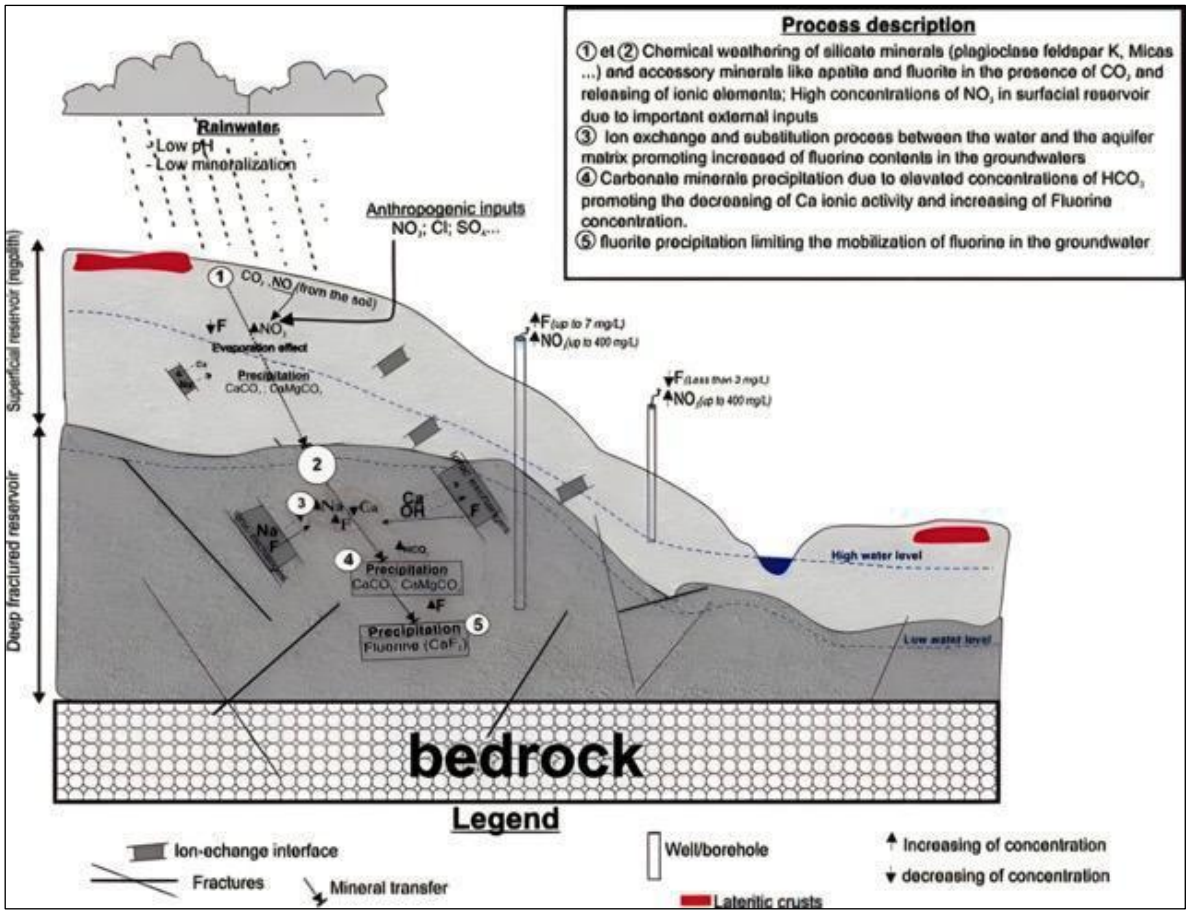

Figure 2. Example of the conceptual scheme of the main processes controlling the groundwater mineralization and occurrence of high fluoride content (Tossou et al., 2017).

2.3.2 Geogenic contaminants

Geogenic contaminants in groundwater constitute significant risks to both human and environmental health, as they originate from natural geological formations and can infiltrate water supplies (Bhattacharya et al., 2017). Geogenic contaminants, such as arsenic, fluoride, uranium, and radon, have been identified as prevalent in various environments (Johnson and Bretzler, 2015). The presence of these contaminants in high concentrations can result in severe health implications, including but not limited to cancer and dental fluorosis (Foster and Chilton, 2016). The release of contaminants is commonly attributed to natural processes such as weathering, oxidation, and dissolution of minerals in rocks and soils (Smedley and Kinniburgh, 2002). The mobility and bioavailability of contaminants in groundwater systems are significantly influenced by geochemical factors such as pH, redox potential, and the existence of competing ions (Nordstrom, 2011). Monitoring and managing geogenic contaminants is crucial for protecting public health and preserving groundwater resources, as stated by Bhattacharya et al. (2017). The Conceptual model of the peri-urban aquifers in semiarid regions northeast of Jaipur, Rajasthan, India is shown in Figure 3. The Quaternary alluvium is overlying the Proterozoic fractured hard rock with a weathered zone at its top. Various anthropogenic and geogenic factors impact groundwater quality and quantity (Frommen et al., 2021).

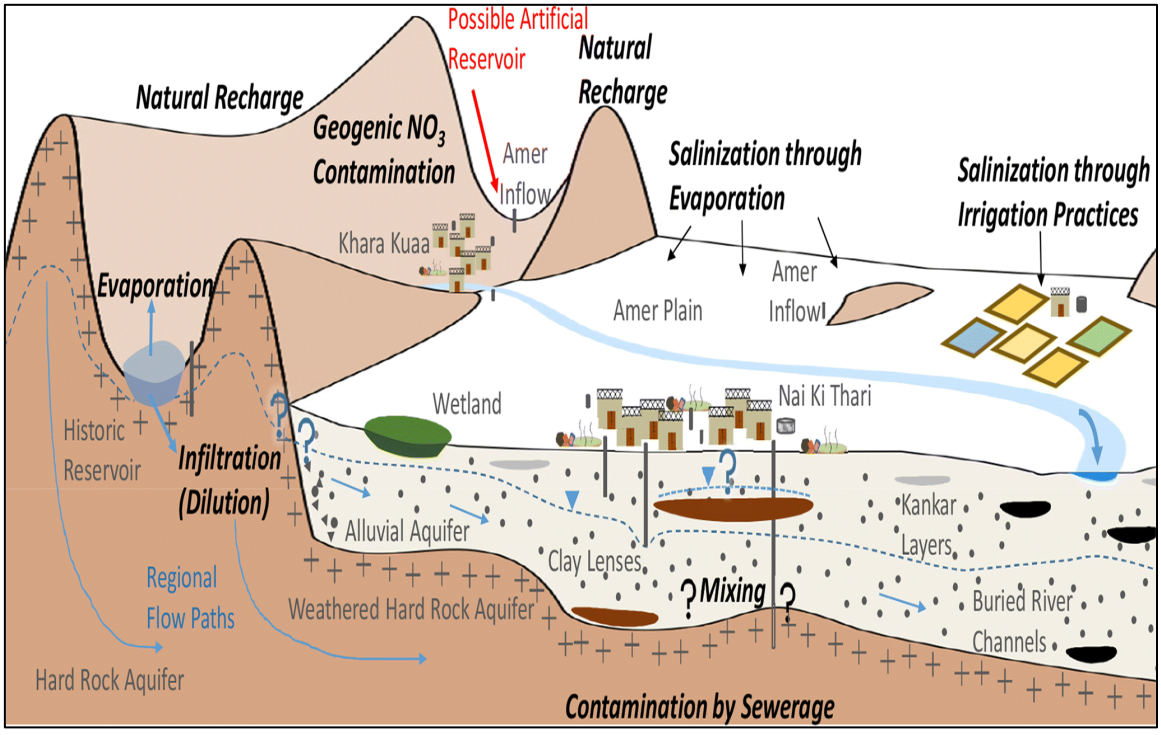

Figure 3. Conceptual model of the peri-urban aquifers in semiarid regions, northeast Jaipur, Rajasthan, India. The Quaternary alluvium is overlying the Proterozoic fractured hard rock with a weathered zone at its top (Frommen et al., 2021).

The distribution of geogenic contaminants in groundwater varies both spatially and temporally, requiring continuous monitoring and comprehensive assessments (Flem et al., 2018). The impact of anthropogenic activities and climate change on hydrological systems can intensify the occurrence of contaminants, resulting in increased mobilization of such substances (Edmunds and Smedley, 2012). According to Rodriguez-Lado et al. (2013), intense groundwater extraction may result in the upwelling of deep, polluted groundwater, while changes in land use can increase soil erosion and, as a result, the release of pollutants.

The contamination of groundwater by geogenic arsenic is a significant concern in semiarid areas, impacting a substantial number of individuals who depend on it as their main source of potable water (Rodríguez-Lado et al., 2013). The mobilization of arsenic in these regions is predominantly influenced by geochemical and hydrogeological factors, including pH, redox potential, and the existence of reactive minerals in the aquifers (Bhattacharya et al., 2017). The concentration of arsenic in shallow aquifers may substantially threaten human health in regions with low precipitation rates and high evaporation (Fendorf et al., 2010) in semiarid areas. Long-term exposure to groundwater contaminated with arsenic has been associated with various health complications such as skin lesions, cancers, and cardiovascular diseases (Smedley and Kinniburgh, 2002 and 2012). Therefore, understanding the factors contributing to arsenic mobilization in groundwater of semiarid regions is crucial for developing effective mitigation strategies and ensuring safe drinking water for affected populations.

The geogenic contamination of arsenic is one of the most serious problems in several places and has been investigated carefully worldwide, especially in semiarid regions. For instance, sources and behaviour of arsenic and trace elements in groundwater and surface water in the Poopó Lake Basin, Bolivian Altiplano (Ramos et al., 2012). According to this study, arsenic in most of the sampled wells exceeded the WHO guideline for drinking water (10 µg/l) because of natural and anthropogenic sources. Natural processes, anthropogenic inputs from mining activities and natural characteristics from reiver and volcanic activities are possible sources of arsenic in the area (Ramos et al., 2012). Moreover, Arsenic (As) and Fluoride (F^-) concentrations in groundwater in northeastern La Pampa province, Chaco-Pampean plain, Argentina, and groundwater quality in two semi-arid La Pampa locations. were investigated. According to the result, the concentrations of As and F^- are high, which is possibly due to the weathering of Andean volcanic ash and loess (rhyolitic glass) is the principal source of As and contaminants (Aullón Alcaine et al., 2020). Geochemistry of thermal waters and arsenic enrichment at Antsirabe, Central Highlands of Madagascar has been examined, despite lower As concentrations than geothermal waters at worldwide tectonic plate borders, Antsirabe may

be a severe environmental issue (Sracek et al., 2019). Additionally, the globally predictable problem of arsenic (As) contamination of water resources and other environments at toxic levels has been informed in all of the 20 Latin American countries (Bundschuh et al., 2020).

In addition, another common geogenic contaminant in groundwater is fluoride contamination which is an issue of serious concern for public health in semiarid regions across the globe (Edmunds and Smedley, 2012). The correlation between elevated levels of fluoride in groundwater and the erosion of fluoride-containing rocks and minerals, including fluorspar, cryolite, and apatite, as well as the dissolution of minerals with high fluoride content in aquifers, has been frequently observed (Chae et al., 2007). Insufficient amounts of precipitation, high evaporation, and low water recharge can all contribute to high fluoride concentrations in groundwater in semiarid regions (Amini et al., 2009). Chronic exposure to high fluoride concentrations can cause dental and skeletal fluorosis, adversely affecting human health and quality of life (Fawell et al., 2006). The groundwater of Ambagarh Chouki, Rajnandgaon, India has been examined and the result shows the elevated levels of F^-, frequently above the WHO guidelines; according to this study, fluoride is present in shallow depths water, perhaps due to the evaporation of water and the subsequent removal of Ca^{2+} via the precipitation of carbonates (Patel et al., 2017). Consequently, understanding the factors contributing to fluoride mobilization in groundwater of semiarid regions is essential for developing effective mitigation strategies and providing safe drinking water to affected populations.

Moreover, Barium (Ba) is an alkaline earth metal that occurs naturally and can potentially serve as a geogenic contaminant in groundwater at high concentrations (Michael-Kordatou et al., 2018). Barium is a principal element found in various minerals, including barite ($BaSO_4$) and witherite ($BaCO_3$). The release of barium into groundwater can occur through the process of weathering and dissolution of these minerals (Han and Liu, 2004). The solubility and mobility of barium in groundwater are subject to various factors, e.g., pH, redox potential, and the existence of competing ions, such as sulphate and carbonate (Gimeno et al., 2016). The presence of high concentrations of barium in drinking water can result in detrimental impacts on human health. While barium is not considered as hazardous as other geogenic pollutants such as arsenic or uranium, its prolonged consumption at elevated levels can lead to gastrointestinal complications, muscular debility, and possible harm to the kidneys, heart, and liver (WHO, 2004). The World Health Organization (WHO) has established a guideline value of 1.0 mg/L for barium in drinking water to minimize health risks (WHO, 2011).

It is crucial to identify and monitor the contamination sources and pathways to manage the presence of barium in groundwater. Michael-Kordatou et al. (2018) stated that geochemical and

hydrogeological assessments could help define the spatial distribution of barium and its controlling factors. In addition, coagulation, precipitation, ion exchange, and membrane filtration can be used to remove barium from drinking water supplies (U.S. EPA, 2005). To develop and implement effective policies and strategies to manage barium contamination in groundwater and ensure public health, public awareness and education initiatives and interdisciplinary collaboration between scientists, policymakers, and stakeholders are necessary (Foster & Chilton, 2003).

2.4. Stable isotopes oxygen-18 (^{18}O), deuterium (^{2}H) and isotope of dissolved inorganic carbon ^{13}C(DIC) in groundwater

Stable isotope analysis has become a crucial tool for understanding and managing groundwater resources. The isotopic composition of water can provide valuable information about the origin of groundwater, flow paths, and age. The most frequently used stable isotopes in groundwater studies are oxygen-18 (^{18}O), deuterium (^{2}H or D), and ^{13}C(DIC).

Stable isotope oxygen-18 (^{18}O) is one of the valuable tools in the study of groundwater, offering insights into recharge processes, flow paths, and residence times (Clark and Fritz, 1997; Kendall and Coplen, 2001). The ^{18}O values in groundwater are influenced by various factors, including the isotopic composition of the original precipitation, temperature, and the degree of evaporation (Kendall and Coplen, 2001; Gat, 2010). The ^{18}O values in groundwater are affected by several factors, including the isotopic composition of the initial precipitation, temperature, altitude, and evaporation rate (Dansgaard, 1964; Rozanski et al., 1993; Kendall and Coplen, 2001; Gat, 2010). Through analyzing the spatial distribution of ^{18}O values, the origin of groundwater sources and the mixing of waters from various sources or migration paths can be determined (Clark and Fritz, 1997). In addition, the combination of ^{18}O with other isotopes, such as deuterium (^{2}H) and tritium (^{3}H), can provide more comprehensive information on the groundwater system, including the rate of recharge, resident time and sources of potential contamination (Cook and Herczeg, 2000; Kendall and Coplen, 2001). For instance, by using ^{18}O with ^{2}H, the local meteoric water line (MWL) can be determined; this relationship allows for the determination of recharge zones, as the isotopic signatures of groundwater reflect the meteoric water line (MWL) in a specific region (Clark and Fritz, 1997). The application of stable isotope ^{18}O in groundwater research has thus significantly advanced our understanding of hydrological processes, contributing to the sustainable management and protection of water resources worldwide.

Deuterium (^{2}H) is another stable isotope that has been frequently used in groundwater system studies to obtain more information about recharge mechanisms, flow pathways, and mixing dynamics (Clark and Fritz, 1997; Kendall and Coplen, 2001). It is a naturally occurring hydrogen isotope, it constitutes approximately 0.015% of all hydrogen atoms and may be utilized as a tracer due to its distinct isotope (Sharp, 2007). In groundwater studies, the ratio of ^{2}H to the more abundant hydrogen isotope (^{1}H) is commonly expressed as ^{2}H, providing valuable information on the origin and history of water molecules (Gat, 2010).

The isotopic composition of groundwater, including ^{2}H values, is determined predominantly by the isotopic signature of precipitation, which varies with latitude, altitude, and temperature (Dansgaard, 1964; Rozanski et al., 1993). Furthermore, the recharge zone, flow paths, resident times, and identifying the mixing of water from different sources can be obtained through ^{2}H values in groundwater samples (Clark and Fritz, 1997). Additionally, the examination of deuterium alongside other isotopes, such as oxygen-18 (^{18}O) and tritium (^{3}H), allows for a more comprehensive understanding of groundwater systems.

The isotopic fractionation of oxygen and hydrogen in water at a location is influenced by factors such as water origin, climate (evaporation, condensation, melting), geology, and surface mixing (Faure, 1986). In systems with no geothermal effect, the ^{2}H and ^{18}O isotopic contents usually remain consistent, as interactions with geologic materials minimally impact their ratios (IAEA, 1983). The isotopic compositions in groundwater can vary due to factors like distance from the ocean, elevation, temperature, and seasonal changes; for instance, high elevation recharge results in lower ^{2}H and ^{18}O contents than lowland areas (Erickson, 1983). recharge of ancient groundwater (palaeowater) under climatic conditions different from the present climate produces isotopic signature of the past climate (Gat and Issar, 1974). The isotopic composition of groundwater may slightly differ from recharging rains because of various modifying processes during or after infiltration (Mazor, 1976). Figure 4 shows the global meteoric water line which when used with a local meteoric water line shows the influences of precipitation in hydrological investigations.

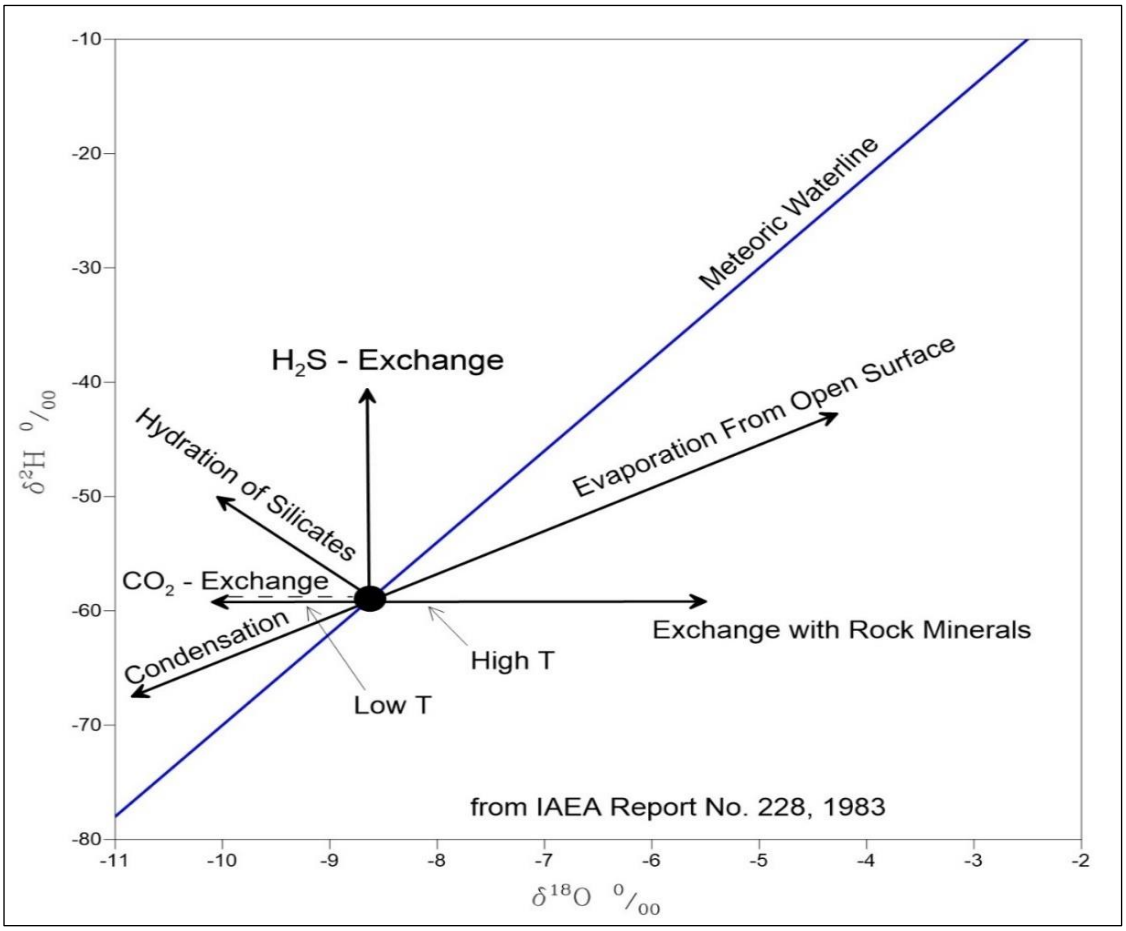

Figure 4. Global meteoric water line which when used with a local meteoric water line shows the influences of precipitation in hydrological investigations (After IAEA, 1983).

Craig (1961) examined ^{2}H and ^{18}O levels in water samples from rivers, lakes, and precipitation sources from different countries to determine a reference line for local groundwater origins and movements. A plot of stable isotopes of $\delta^{2}H$ and $\delta^{18}O$ in water samples from these countries was published by Craig (1961).

The correlation between $\delta^{2}H$ and $\delta^{18}O$ led to a considerable line of data along the best-fit line (Craig, 1961):

$$\delta^{2}H = 8 * \delta^{18}O + 10 \text{ (Global Meteoric Water Line Equation)}$$

The Global Meteoric Water Line (GMWL) includes local variations and is valid worldwide; Thus, the Global Meteoric Water Line may help trace local groundwater sources and flows (Craig, 1961). According to Craig (1961), the isotopic ratios of ^{2}H and ^{18}O in nascent rainwater (i.e., prior to evaporation) vary with temperature-controlled fractionation (i.e. water containing heavier isotopes evaporates and condenses at slightly different fractional rates due to mass differences). Therefore, the inter-relationship between $\delta^{2}H$ and $\delta^{18}O$ in rainwater is practically independent of temperature across the globe and follows a simple linear formula. Consequently,

every hydrochemical study the local meteoric water line has to be established from samples of individual rain events or monthly means of precipitation.

Furthermore, the carbon isotope ratio ^{13}C(DIC) in groundwater is a useful tool for understanding the geochemical processes that impact the dissolved inorganic carbon (DIC) pool. These processes include carbonate dissolution, precipitation, organic matter degradation, and gas exchange with the atmosphere. The ^{13}C(DIC) values can be utilised to trace the origins and transformation processes of dissolved inorganic carbon (DIC) in groundwater systems (Clark and Fritz, 1997). Groundwater that is impacted by the dissolution of carbonates generally shows higher positive values of ^{13}C(DIC). On the other hand, the degradation of organic matter often leads to lower negative values of ^{13}C(DIC) because microbes tend to preferentially use the lighter ^{12}C isotope during respiration (Kendall and McDonnell, 1998). The ^{13}C(DIC) values in groundwater can also help determine the influence of anthropological activities, such as agricultural practices or waste disposal, on groundwater quality (McMahon and Chapelle, 2008). For instance, a noticeable decrease in ^{13}C(DIC) values could indicate contamination from manure, which typically has a lower ^{13}C signature. It could also suggest the oxidation of methane generated from waste decomposition in landfills (Aravena et al., 1993). In addition, when we combine ^{13}C(DIC) data with other isotopic parameters similar to ^{18}O and δD, which can enhance the understanding of different hydrogeological processes. These processes include water-rock interaction, recharge mechanisms, and groundwater flow dynamics (Katz et al., 1997).

The Strontium isotope ratio ($^{87}Sr/^{86}Sr$) is commonly used as a tracer in groundwater studies because it is highly sensitive to geological changes. Additionally, the non-radiogenic nature of ^{86}Sr makes the $^{87}Sr/^{86}Sr$ ratio a reliable indicator of water-rock interaction (Banner, 2004). Using this isotope system can offer valuable insights into the origins and routes of groundwater, as well as how it interacts with the surrounding geological materials. The variations in the $^{87}Sr/^{86}Sr$ ratio can indicate differences in the age and composition of the bedrock that the water has come into contact with. This helps in determining the origin of groundwater and the paths it takes. (Bullen and Kendall, 1998).

2.5. Tritium isotope (^3H)

Tritium (^3H) is a radioactive isotope of hydrogen and has been widely applied in groundwater studies as a valuable tool to examine recharge processes, flow paths, and residence times (Clark and Fritz, 1997; Cook and Herczeg, 2000). The half-life of tritium is approximately 12.3 years; tritium is particularly useful for studying relatively young groundwater systems, as it can provide information on water ages up to several decades (Solomon and Cook, 2000). It is produced naturally in both vaporized and liquid water and its concentration is expressed in tritium units (TU) and decays to produce ^3H. The maximum values in precipitation (> 10000 TU in Northern Hemisphere) were reached in 1963 as a consequence of above-ground nuclear testing (Clark and Fritz, 1997). Annual ^3H releases of about 10 TBq were reported by Son et al. (2013) and Yang et al. (2012) for pressured water reactors in Korea and China, respectively.
Tritium levels in groundwater that are close to detection are commonly found in paleo groundwaters or sub-modern groundwaters that have mixed with modern groundwaters. Both qualitative and quantitative approaches to dating groundwaters with ^3H are possible:

1. Velocity of the 1963 tritium peak — identification of the bomb spike preserved in groundwaters clearly identifies their age.
2. Radioactive decay — calculating the time for decay from a known input level to the measured level.
3. Exponential model for input function — determining the "recharge attenuated" tritium levels for a given groundwater flow system and applying the decay equation.
4. Time series analysis — repeated sampling from specific points over several years allows monitoring of the bomb spike as it passes through the aquifer, indicating mean residence time.
5. Qualitative interpretation — measurable ^3H = component of modern recharge.

According to USGS report (Lindsey et al., 2019), the groundwater age is classified as modern, mixed, and premodern water.

- Modern: water entered the ground since about 1953
- Mixed: water is a mixture of modern and premodern
- Premodern: water entered the ground before 1953

In addition, Davis and Bentley (1982) classified groundwater based on the tritium value as follows:

- <0.8 TU classified as sub-modern water (before the 1950s).
- 0.8 to 5 TU designates a mix of sub-modern and modern water.

- 5 to 15 TU indicates modern water (<5 to 10 years)
- >15 to 30 TU designates s some bomb tritium.
- >30 TU designates recharge to generate in the 1960s to 1970s.

Recently, the ratio of $^{3}He/^{3}H$ has been used for more precise ground water dating (Clark and Fritz, 1997). In such a case, the requirement of tritium input function is eliminated.

3. Study Area Description

3.1 Geography

The studied area Sulaimani-Warmawa Sub-basin (SWSB) is located in the southeast of the Kurdistan Region, northwest of the Zagros basin, Figure 5. Meanwhile, it is located in the High Folded Zone (Buday, 1980; Buday & Jassim, 1987; Jassim & Goff, 2006; Al-Jiburi et al., 2015). The SWSB is mainly in Sulaimani Governorate and Sulaimani City is a part of the study area. The SWSB is placed within longitudes 45° 00' – 46° 00' east and latitudes 35° 00’ – 36° 00’ north. with an elevation range from 500 to more than 1250 meters (m). The SWSB covers an area of approximately 1500 km^2. It is a hydrological sub-basin which is a part Sulaimani-Sharazoor basin.

3.2 Climate

The SWSB in the Kurdistan Region of Iraq. It is a semiarid area characterized by a Mediterranean climate (Csa according to the Köppen climate classification) with relatively cold, humid winters and hot, dry summers. According to Stevanovic and Markovic (2003), most of the precipitation occurs during the winter months spanning from October to May, with the highest amount of precipitation exceeding 100 mm in January. The average annual rainfall is 668.5 mm, the average annual air temperature is 21° C, and the annual evaporation is 2298.8 mm (Mustafa, 2006; Hamamin et al., 2018).

The principal river is the perennial Tanjero River, which is generally dry from August to the beginning of the precipitation season in October.

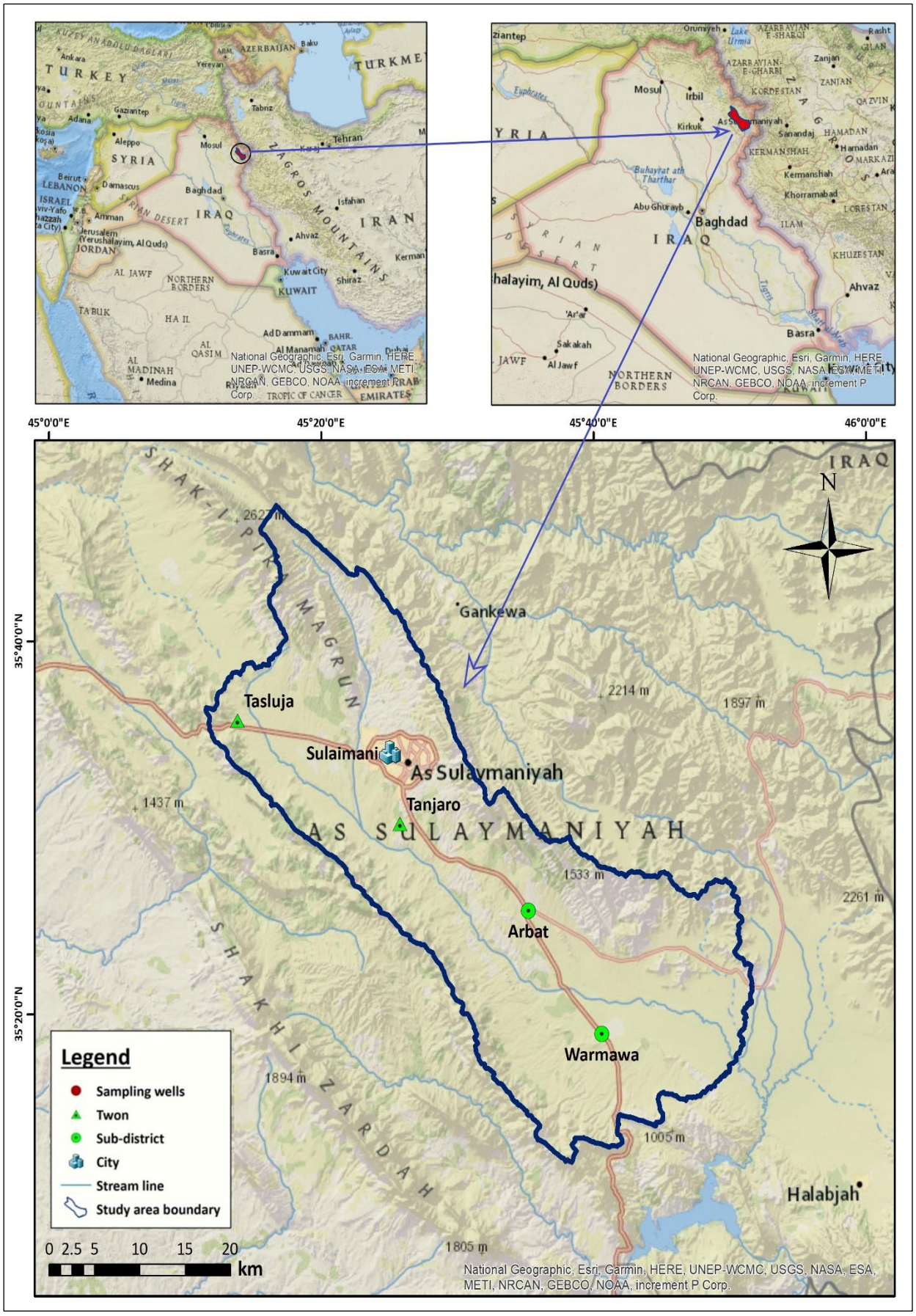

Figure 5. Location of the study area.

3.3 Geological setting of SWSB

The geological formations within the Sulaimani-Warmawa Sub-basin (SWSB) generally include units from the Early Cretaceous to the Tertiary periods and Quaternary deposits (Figures 6 and 7). Hills around the basin are covered by grass and sparse vegetation of pine, Pinus Sylvestris (Figure 8), which are used for sheep and goat grazing.

The Cretaceous units within the research area include the Balambo, Qamchuqa, Kometan, Shiranish, and Tanjero Formations. In the Tertiary units that are visibly protruding in the SWSB, there are the Tanjero, Sinjar, Gercus, and Pila Spi Formations.

Moreover, within the Quaternary deposits, alluvial fans, polygenetic, and floodplain sediments are prominently found, indicating a high degree of geologic activity within the SWSB (Karim & Ali, 2004; Omar et al., 2015; Sissakian, 2015). It is notable that the distribution of these units is not homogeneous. The Cretaceous formations predominantly emerge in the northeast, east, and southeast regions of the SWSB. In contrast, the Tertiary units are generally located in the western and southwestern areas of the studied region.

A particular presence of the Tanjero Formation and Quaternary deposits is observable at the centre of the study area, specifically around Sulaimani City and the Warmawa area. The Tanjero Formation demonstrates a broad presence throughout the Sulaimani-Warmawa Sub-basin, most notably surrounding the city of Sulaimani. The extent of the formation can be traced from the foothills of the Goizha Mountain in the north and northeast, proceeding towards the Tanjero Valley in the south and the Chaqchaq Valley in the northwest (Mustafa, 2006).

The following section will comprehensively characterize each specific geological unit within the SWSB.

3.3.1 Cretaceous units

The early Cretaceous geological units in the SWSB consist of Balambo, Qamchuqa and Kometan formations. Meanwhile, the late Cretaceous units are Shiranish and Tanjero formations.

3.3.1.1 Balambo Formation

The Balambo Formations are primarily observed to outcrop towards the east and southeast. The age of the Balambo Formation has been identified to originate from the Valanginian-Turonian period, which corresponds to the Early to Late Cretaceous age. The characteristic feature of the

Balambo Formations is their composition of thin, well-layered radiolarian limestone (Bellen et al., 1959, Jassim & Goff , 2006; Ali 2007).

The structure of the Balambo Formations is complex and expansive, covering an approximate depth of 762 meters, which is further divided into two distinct units. The upper section, which accounts for about 503 meters, predominantly consists of thin-layered globigerina and radiolarian grey limestone. Conversely, the lower part, which spans around 259 meters, primarily contains thin-layered blue ammonitiferous limestone. This lower portion is punctuated with interspersions of olive-green marl and dark-blue shale (Bellen et al., 1959).

Geographically, the lower part of the Balambo Formations transitions into the Qamchuqa and Sarmord formations in the western and southwest of Sulaimani (Jassim and Goff, 2006). Additionally, the Balambo Formation is overlined by Kometan and Shiranish formations (Bolton, 1958; Al Manmi, 2008).

3.3.1.2 Qamchuqa Formation

The Qamchuqa Formation mostly outcrops in the northern part of the SWSB. The age of the formation was determined as Hauterivian-Albian (Early Cretaceous). In general, stratigraphically, it is divided into three principal units. The upper part is the upper dolomite unit, approximately 192 meters thick. This unit primarily features coarsely crystalline, granular dolomites that have replaced the original neritic, organic limestone, which contained fragments of molluscan shells. In addition, the limestone, which is mainly composed of detrital limestone, locally exhibits argillaceous characteristics or dolomitization.

The middle unit of the formation, spanning around 316 meters, is dominated by coarsely crystalline dolomite with intermittent inclusions of calcite. Below this, the formation exhibits a middle limestone unit that extends for about 147 meters. This section primarily contains a massive and somewhat argillaceous limestone, showing partial signs of dolomitization.

Furthermore, the lower unit is approximately 55 meters thick, mainly composed of very coarse crystalline dolomite. Additionally, a lower limestone unit can be observed, which is roughly 61 meters thickness and is characterized by massive limestone embedded in an argillaceous matrix.

The Qamchuqa Formation overlies unconformably the Kometan Formation, characterized by an erosional surface. The formation evolves laterally into the bathyal globigerina/radiolarian shale, marls, and limestone of the Balambo Formation with noticeable inter-tonguing (Bellen et al., 1959; Ali, 2007).

3.3.1.3 Kometan Formation

The Kometan Formation only outcrops inside the Sulaimani City and originates from the Turonian-Santonian period (Late Cretaceous). The Kometan Formation is described as white-weathering, light grey, thin-bedded, globigerial-oligosteginal limestone, locally silicified (Bellen et al., 1959). It is also described as well-bedded fine crystalline limestone (Sissakian, 2015). In addition, the Kometan Formation is occasionally silicified, extending approximately 36 meters (Bellen et al., 1959) and it is unconformably superseded by the Shiranish Formation.

3.3.1.4 Shiranish Formation

The Shiranish Formation was dated as Campanian-Maastrichtian (Late Cretaceous). It can be found in different parts of the area, outcropped in low thicknesses, and mainly composed of bluish-grey marl and marly limestone (Sissakian, 2015). In addition, the lithology of the Shiranish formation consists of approximately 200 meters of alternating well-bedded bluish-white marl and marly limestone. These sediments were primarily deposited in the offshore region of the Cretaceous Foreland Basin, located in front of the southwest advancing Iranian Plate. The fossil assemblage includes planktonic foraminifera, ammonites, and pelecypods. According to Karim et al. (2008), the Formation is located between the Tanjero Formation at the top and the Kometan Formation at the base and it is conformable with both the overlying Tanjero Formation and underlying the Kometan Formation.

3.3.1.5 Tanjero Formation

The age of the Tanjero Formation has been determined to be Maastrichtian, which corresponds to the Late Cretaceous period. The Tanjero Formation is widespread in the Sulaimani-Warmawa Sub-basin, especially around the city of Sulaimani. It extends from the foothills of Goizha Mountain in the north and northeast towards the Tanjero Valley in the south and the Chaqchaq Valley in the northwest (Mustafa, 2006). It has a thickness ranging from 50 to 600 meters and is characterized by the alternating presence of sandstone and calcareous shale in the slope and basin plain regions. In contrast, the shelf and coastal areas exhibit variations in the form of conglomerate and biogenic limestone. In addition, according to Karim (2004), the Tanjero Formation has been divided into three distinct sections based on its lithological composition: the Lower, Middle, and Upper. The lower section primarily consists of thin sandstone layers intercalated with thick, dark grey calcareous shale. This transitions into a thick layer of boulder and coarse gravel conglomerate beds. The intermediate section is characterized

by bluish marl, while the upper portion comprises a combination of siliciclastic and carbonate strata. These beds are identified by the transformation of biogenic limestone with thick bedding to calcareous shale located on the shelf.

3.3.2 Tertiary units

The Tertiary geological formations in the area are Kolosh, Sinjar, Gercus, and Pila Spi and a detailed description of each is below:

3.3.2.1 Kolosh Formation

The Kolosh Formation, originating from the Paleocene to Lower Eocene period, is characterized by near-shore neritic sediments (Bellen et al., 1959; Buday, 1980). This Formation was deposited in an environment ranging from a shelf to a basin, predominantly composed of shale and fine sandstone interspersed with variously sized fragments of green rock, chert, and radiolarite (Karim, 2004).

The Kolosh Formation is predominantly exposed in the southern and southwestern parts of the studied area, especially within the foothills of Baranan Mountain. It displays interfingering with the Sinjar Formation, particularly in the southern region of the study area, known as the Baranan Homocline. Surdashy (1988) stated that the Kolosh Formation is overlined by the Sinjar Formation, with the transition between them being gradual rather than abrupt.

3.3.2.2 Sinjar Formation

The Sinjar Formation, predominantly exposed in the study area, is comparatively thin and is primarily outcropped in the northwest and southwest. The Sinjar Formation refers to the Upper Paleocene-Lower Eocene. The thickness of the formation is around 120m and has gradational contact with the underlying Kolosh and overlying Gercus Formations. The depositional environment of the Sinjar Formation is a shallow marine (Reefal) environment and is overlain by Gercus Formation (Bellen et al., 1959; Budday, 1980).

The Sinjar Formation is indicative of a shallow marine or reefal depositional environment and is succeeded by the Gercus Formation (Bellen et al., 1959; Buday, 1980). The Sinjar Formation is composed of well-bedded limestone, dolomite, and marly limestone and sandstone (Jassim & Goff, 2006; Sissakian, 2015).

Moreover, the Formation is stratified into four distinct units with a cumulative thickness of approximately 78 meters. According to the classification, it consists of white to grey limestone,

which shows dolomitization in certain parts; skeletal brown to dark grey hard limestone; white, grey limestone embedded with nodules of chert and iron oxide; and the topmost layer featuring dolomitic limestone (Surdashy, 1988).

3.3.2.3 Gercus Formation

The age of the Gercus Formation is referred to Middle Eocene. It is primarily characterized by a series of alternating layers of clastic rocks, including claystone, sandstone, marl, and calcareous shale, interspersed with the occasional conglomerate. Particularly, gypsum lenticels are more prevalent near the top of the formation. Instances of rare lignite have been observed in the sandstone close to the base, while rock salt sporadically emerges throughout the Formation (Bellen et al., 1959; Jassim et al., 1984; Sissakian, 2015). In addition, it has been found that the Gercus Formation represents a significant low-stand system tract within the Tertiary stratigraphic record (Ameen, 2006). Additionally, Jassim and Goff, (2006) described the Gercus Formation as a characteristic red molasse sequence originating from elevated regions in the northern and northeastern areas.

3.3.2.4 Pila Spi Formation

The Pila Spi Formation was dated (Middle–Upper Eocene) and is approximately 100-200 m thick (Buday and Jassim, 1987). The depositional environment of the Pila Spi Formation is described as a carbonate ramp with low topographic patchy reef, back reef, and lagoonal facies (Khanaqa, 2011). It is composed of cyclic claystone deposits, marl, gypsum, and sandstone with occasional limestone (Jassim & Goff, 2006; Sissakian, 2015).

Moreover, the upper part of the formation contains well-bedded, bituminous, chalky, and crystalline limestone, with bands of white, chalky marl and an increase of chert nodules towards the top. The lower part includes well-bedded, hard, porous, or vitreous, bituminous, white, poorly fossiliferous limestone, with algal or shell sections. The additional section consists of dolomitic and chalky limestone with chert nodules (Bellen et al., 1959: Jassim and Goff, 2006).

3.3.3 Quaternary deposits

The Quaternary deposits generally consist of alluvial fans and floodplain sediments. They mainly comprise gravel, sand, silt, mud, sand, and silty clay soil (Mustafa, 2006; Sissakian, 2015). In general, it is composed of floodplain deposits of Tanjero and Qiliasan Rivers grading from course gravels to fine silt and clay and, in some areas, reaches around (10-15) m thickness.

The second major Pleistocene deposits, which cover both sides of the Qiliasan and Tanjero Rivers, are river terraces with (5-10) m thickness.

Alluvial deposits, originating from the foothills of the Goizha, Piramagroon, and Baranan mountains surrounding the study area, present a transition from boulders to sand and clay particles. Particularly, certain parts of Sulaimani City underlying above alluvial fans of the Goizha Mountains.

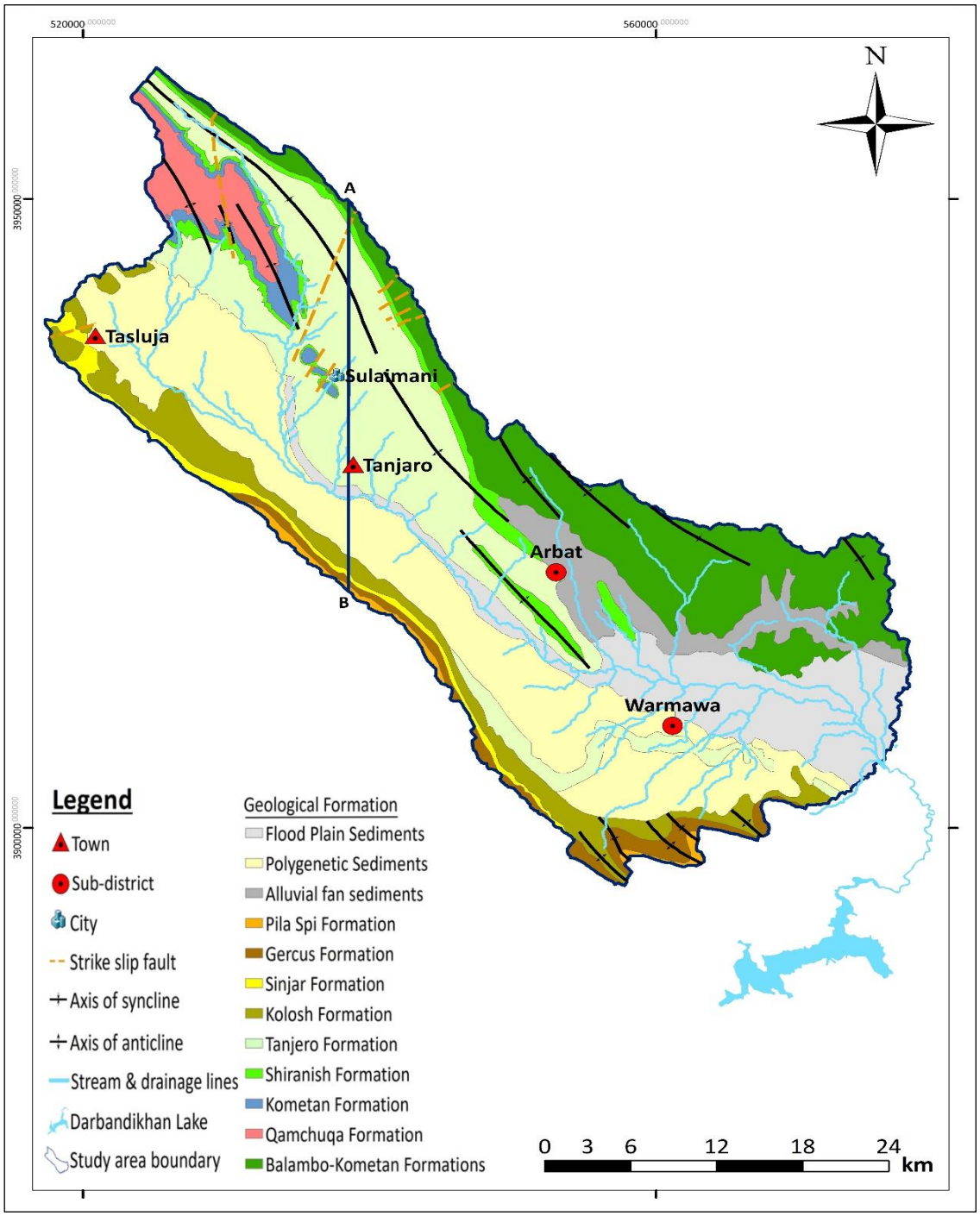

Figure 6. Geological map of the study area (after Karim & Ali, 2004; Omar et al., 2015; Sissakian, 2015).

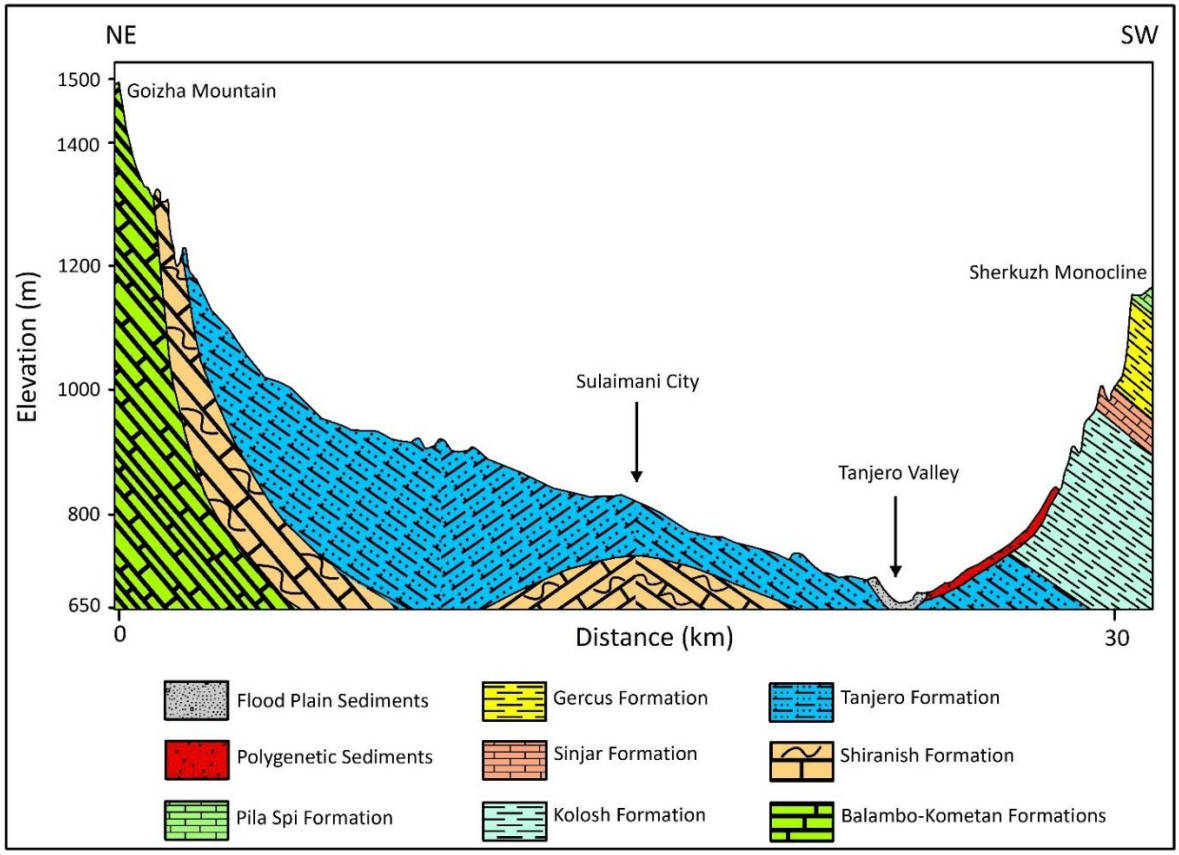

Figure 7. Geological cross-section of the study area (modified after Kareem et al., 2018; Mahmmud et al., 2022).

Figure 8. Slopes in the upper reaches of the basin with typical vegetation cover.

3.4 Hydrogeological setting of SWSB

In general, so far, there were no intensive hydrogeological studies conducted in the study area explaining the hydrogeology of the area in detail. Few studies have been conducted in Iraq and the Kurdistan Region. According to Stevanovic & Markovic (2004), hydrogeological studies conducted on the Kurdistan Region and the Kurdistan Region were divided into several hydrological basins and sub-basins. The Sulaimani Governorate is divided into four main basins and each of them has been divided into several hydrological sub-basin. The division is based on the geology of the area, topography, stream and drainage pattern, the structure of the area and several other criteria. The Sulaimani Governorate is divided into Southeastern Sharazoor, Dukan, Chamchamal-Sangaw, and Penjwin basins. The Sulaimani-Warmawa watershed is part of the Southeastern Sharazoor.

Furthermore, the aquifer system in the Kurdistan Region has been classified into several aquifers due to formation age similarities, lithology, permeability and other hydrogeological characteristics, as follows:

1- Karst aquifer (Bekhme): This type of aquifer is widespread in northern and central northern Iraq, including Qamchuqa, Dokan, Bekhme, Aqra, Sarmord and other Cretaceous/Paleogene age geological formations mainly developed in carbonate facies (limestone, dolomite, and their varieties)
2- Fissured-karstic (Pila Spi) aquifer is primarily located in the central-southern area of the Kurdistan Region and includes Eocene limestone, Sinjar and Khurmala carbonate formations of similar ages.
3- Intergranular Bakhtiari aquifer is mainly located in the southern area of the Kurdistan Region, including overlying Pleistocene terrace and alluvium deposits.
4- The complex aquifer is the combination of two or more aquifers mentioned above and mostly fissured-karstic or karstic type, often over-laid by younger or quaternary deposits.

In addition, Ali (2007) studied the hydrogeology of the Southeastern Sharazoor Basin and according to this study, the aquifer system has been classified into several aquifer types, Table 3. The grouping is based on several factors besides the typical characteristics of porosity, permeability, and lithological properties. The factors are:

1- The capacity of the formations and sediments for water-bearing, i.e., the formations have been classified as aquifer, aquitard and aquiclude.

2- Type of porosity; according to that, aquifers have been divided into Karstic, Karstic-Fissured, Fissured, and Intergranular aquifers.
3- The mineralogical and petrological composition of the aquifer was another factor which was used for aquifer-type classification.
4- The age of geological formations.

Table 3. Aquifer classification in the Southeastern Sahrazoor Basin (Ali, 2007).

Aquifer type	Stratigraphic unit	Mineralogy	Porosity	Hydrogeological group name	Abbreviation
Karstic	Avroman group	Calcite-Dolomite	Fractures, joints caverns	Triassic karstic Aquifer	TKA
	Jurassic Formations	Calcite or Dolomite	Fractures, joints and caverns	Jurassic Karstic Aquifer	JKA
Karstic-Fissured	Cretaceous Formations (Kometan, Balambo & Qamchuqa)	Calcite or Dolomite	Fractures, joints and caverns	Cretaceous Karstic-Fissured Aquifer	CKFA
	Eocene Formations (Sinjar, Pila Spi)	Calcite and Dolomite	Fractures, joints and caverns	Eocene Karstic-Fissured Aquifer	EKFA
Fissured	Cretaceous Qulqula Formation	Quartz or Chalcedony and Calcite	Fracture and joints	Cretaceous Fissured Aquifer	CFA
Intergranular	Recent Sediments, including alluvial fans, flood plains, river deposits, buried valley sediments, river terraces	Polygenetic	Intergranular	Alluvium Intergranular Aquifer	AIA
	Eocene Gercus Formation	Conglomerate of Polygenetic	Intergranular with some fissures	Eocene Intergranular Aquifer	EIA

Complex	Slide debris mainly from (Eocene Sinjar Formation), or Triassic and cretaceous Formations.	Slide debris limestone (Calcite and dolomite	Intergranular and karstic fissured (Fractures or caverns)	Slide Debris Aquifer	SDA
Aquitard	Tanjero Formation	Mainly mixture of sand and clay size silica and calcium	Fissures and joints, occasionally with fault breccias	Tanjero Aquitard	TAT
Aquiclude	Shiranish, Kolosh, Gercus and impervious packages of Qulqula Formation	Mainly mixture of clay minerals and silica	No effective porosity	Aquiclude	–

The aquifer system in the Sulaimani-Warmawa sub-basin has been divided into Karstic-Fissured aquifer (CKFA), including Balambo, Kometan, Qamchuqa, Sinjar and Pila Spi formations. Intergranular aquifer (AIA), including Quaternary deposits, aquitard (TAT), including Tanjero Formation as well as an aquiclude, represented by Shiranish, Kolosh, and Gercus formations.

The groundwater movement in the CKFA aquifer type is mainly controlled by the structural geology of the studied area. The main recharging pathway in this type of aquifer is composed of highly jointed, intensified tectonic ruptures, bedding planes, and tension fractures. The groundwater recharge source is mainly from snow melting on the crest limbs of the Azmer, Goizha, Qaywan, and Piramagroon mountains (Ali, 2007). Most of the groundwater is from the recharge area in these mountains, located in the SWSB and some springs, such as Sarchinar Spring inside Sulaimani City, confirm this flow pattern.

The infiltration in most of the part of the mountain areas inside the SWSB is due to the structural and geomorphological settings. The estimated infiltration rate may reach 50% of the total rainfall (Stevanovic & Markovic, 2004).

Furthermore, the aquifer system in the part of the study was divided into the Quaternary aquifer, including Quaternary deposits; the Kometan aquifer, including Kometan Formation and Tanjero aquifer (Mustafa, 2006).

The hydrogeological map has been created for SWSB (Figure 9) based on a prior Iraq, Kurdistan Region, and Sulaimani Governorate study. In addition to hydrogeological data from (DoGWS), hydrogeological data of 32 water wells in the study region were obtained from 24 to 450 m deep in July and August 2020 (Mahmmud et al., 2022). The hydrostratigraphic units

in the study area have been grouped according to their lithology and hydrogeologic characteristics into the Karstic-fissured aquifer (KFA), the Kometan aquifer (KA), the Tanjero aquifer (TA), an Aquiclude, and a Quaternary intergranular aquifer (QIA) (Stevanovic & Markovic, 2004; Mustafa, 2006; Ali, 2007; SGI, 2011; Mahmmud et al., 2022). The type of aquifers and associated hydrostratigraphic information are summarised in Table 4. According to the hydrogeological data and report from the Directorate of Groundwater of Sulaimani (DoGWS), the main productive aquifers in the study area are the Quaternary Intergranular Aquifer (QIA) and the Tanjero Aquifer (TA) in terms of groundwater quantity and quality (Mustafa, 2006; Kareem et al., 2018; DoGWS, 2020). However, porous karstic formations at basin margins replenish them. The groundwater flow direction is generally from the north and northwest towards Sulaimani and the Tanjero River, which flows into the Darbandikhan Lake out of the basin in the southeast Figure 9.

Table 4. Aquifer types and lithostratigraphy in the study (after Stevanovic & Markovic, 2004; Mustafa, 2006; Ali, 2007; SGI, 2011; Mahmmud et al., 2022).

Aquifer type	**Geological Formation**	**Lithology**	**Hydraulic Conductivity K (m/s)**
Quaternary intergranular aquifer (QIA)	Quaternary deposits	Sand, silt, rock fragments, mud, pebbly, sandy, silty and clayey soil	$9.83 * 10^{-6}$
Tanjero aquifer (TA)	Tanjero	Silty marl, siltstone, shale, sandstone, conglomerate and sandy or silty organic detrital limestone	$1.17 * 10^{-6}$
Aquiclude	Shiranish, Kolosh and Gercus	Claystone, shale, siltstone, sandstone, marl, marly limestone and rare conglomerate	Not available
Kometan aquifer (KA)	Kometan	Limestone	$2.3 * 10^{-5}$
Karstic-fissured aquifer (KFA)	Balambo, Qamchuqa, Pila Spi and Sinjar	Limestone, dolomite and dolomitic limestone and Chalky marl	$6.2 * 10^{-6}$

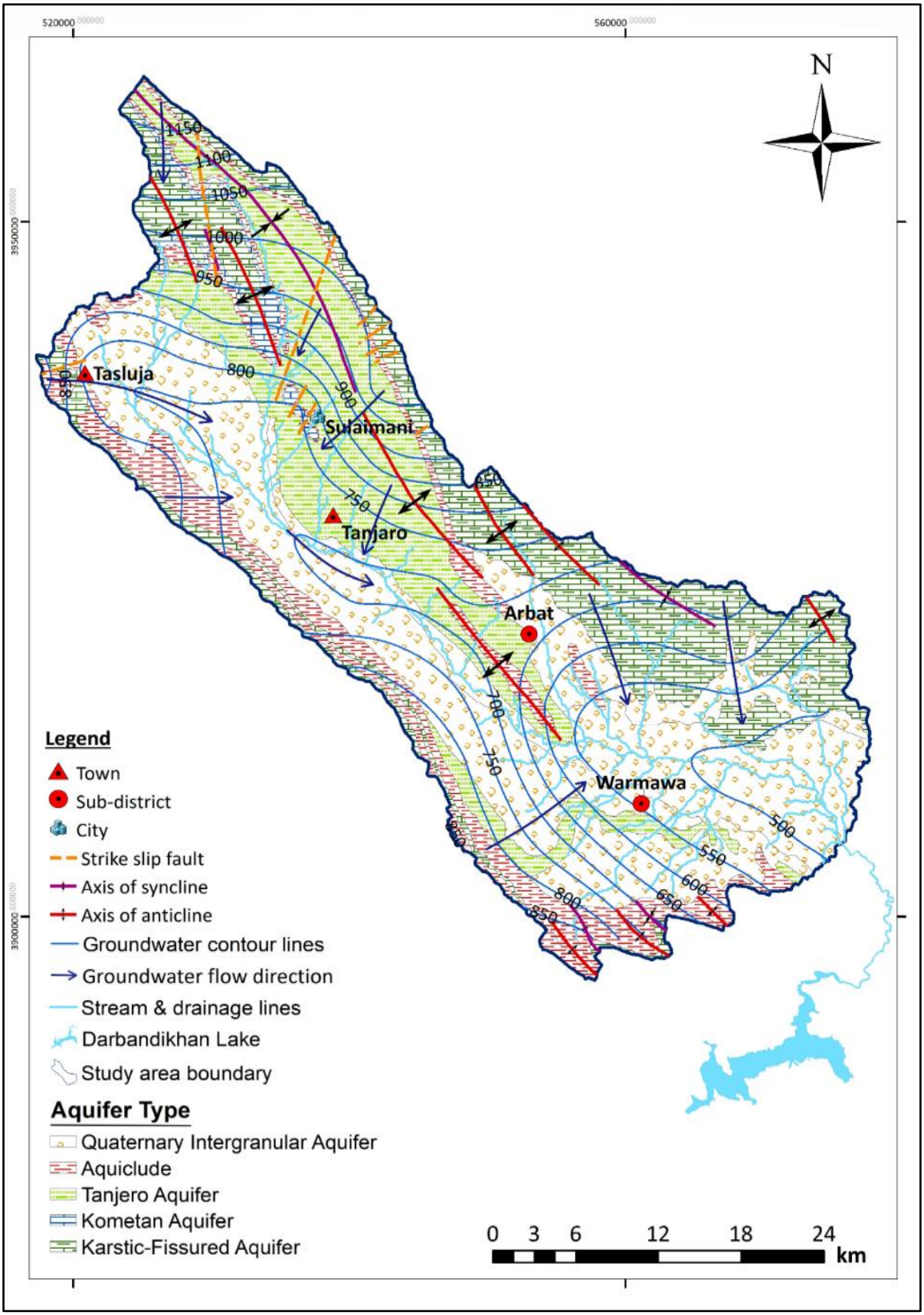

Figure 9. Hydrogeological map and groundwater flow pattern in the study area (Mahmmud et al., 2022).

3.5 Groundwater chemistry of the study area

The groundwater chemistry in the Kurdistan Region, especially in the Sulaimani-Warmawa sub-basin, was not examined in detail. Due to the limited study in the area, there is no comprehensive information about hydrogeochemistry. However, there are some studies which have been conducted in some different parts of the Kurdistan Region.

The impact of sewage wastewater assessment on the Tanjero River and its basin within Sulaimani City has been investigated (Mustafa, 2006). According to the result of this study, the groundwater in the Tanjero area has been classified as (Ca-HCO_3), (Ca-Mg-Cl) and (Ca-Cl) types. The groundwater in the area was polluted with sulfate, nitrate, ammonia, ammonium and heavy metals (Cd, Cu, Ni, Pb and Zn). In addition to that, according to the water quality index (WQI), the groundwater in the area required principal treatment before use for drinking purposes (Mustafa, 2006).

The hydrochemistry study has been conducted for the Sharazoor basin, in which Sulaimani-Warmawa is a hydrological sub-basin belonging to the Sharazoor basin (Ali, 2007). The average pH value of groundwater samples, including water samples from Spring, ranges from 6.6 to 8.4, and the mean pH value was 7.4. Total dissolved solids (TDS) in most of the water samples were less than 1000 ppm which is considered suitable for drinking (WHO, 2017). Ali (2007) discovered that the bicarbonate concentrations in the water samples ranged between 55 to 380 ppm. The highest concentration of bicarbonates was found in the south of Sulaimani City, Arbat and Warmawa area. The highest value of bicarbonate clustered around the main sewage. In addition, bicarbonate ion concentration increased in the groundwater flow direction and due to urbanization impact on the water quality in the area (Ali, 2007).

Mustafa & Ahmad (2008) examined the nitrate pollution in the groundwater of Sulaimani City. According to that, most groundwater samples taken from several boreholes were polluted with nitrate. The possible source of nitrate concentration was sewage and elevated nitrate concentration in the studied area (Mustafa and Ahmad, 2008).

The hazard and risk intensity mapping have been created for the Sulaimani sub-basin, which is a part of the SWSB to assess the risk harmfulness in the area by combining hydrogeological parameters using the DRASTIC system and the hazard factors. The area has been divided into five classes from "no or very low to very high" risk zones. Most parts of the studied site are classified as having very low to low contamination potential according to the low groundwater vulnerabilities and limited impact of hazards (Hamamin et al., 2018).

Geochemical and environmental investigations of the water resources of the Tanjero area have been conducted (Kareem et al., 2018). The Tanjero area is a part of the SWSB near the Tanjero River. Correlation and cluster analysis indicated several sources of contamination. The hydrochemical analysis of water samples identified calcium (Ca^{2+}), sodium (Na^{+}), and magnesium (Mg^{2+}) as the primary ions. The ratios of potassium to rubidium (K/Rb) and sodium to chloride (Na/Cl) suggest interactions between water and various minerals, such as silicates and carbonates. The chemical elements, including strontium (Sr), calcium (Ca^{2+}), magnesium (Mg^{2+}), rubidium (Rb), and potassium (K^{+}), demonstrated concentrations of 1757, 117, 29.8, 7.23, and 10.1 μg/L, respectively, in the water samples. These concentrations correlated with each other and were higher in the wells located near scrape and dump sites in comparison to other wells.

In addition to the ionic composition, the water samples were also classified based on their redox states. Predominantly, they fell into aerobic and intermediate anaerobic categories, as determined by the reduction of dissolved oxygen and manganese (VI) ions with organic matter present in the groundwater. It's noteworthy that the concentration of manganese was found to exceed the acceptable limits for drinking water.

4. Materials and Methods

4.1 Fieldwork and water sampling

Groundwater samples were taken in the study area at different times for data analysis. Sampling was conducted during July, August 2021, and April 2022 from 26 boreholes in the area of interest. In total, 96 samples were obtained including the samples from Erbil area (Mustafa et al., 2023). The samples were used for the examination of cations, anions, and trace elements, providing an understanding of the groundwater chemical constituents, cations, anions and trace element analysis. The samples were also taken for stable isotopes of oxygen-18 (^{18}O) and deuterium (^{2}H) analysis. The collected samples for cations and trace element analyses were filtered in the field with 0.45 mm Millipore filters, acidified with HNO_3^- Suprapur, and stored in 50 mL HDPE bottles. Meanwhile, 15 water samples were taken in March 2022 for Tritium (^{3}H) analysis, including one rain sample and one water sample from Tanjero River. The location sampling wells and inverse geochemical modeling profiles is shown in Figure 10.

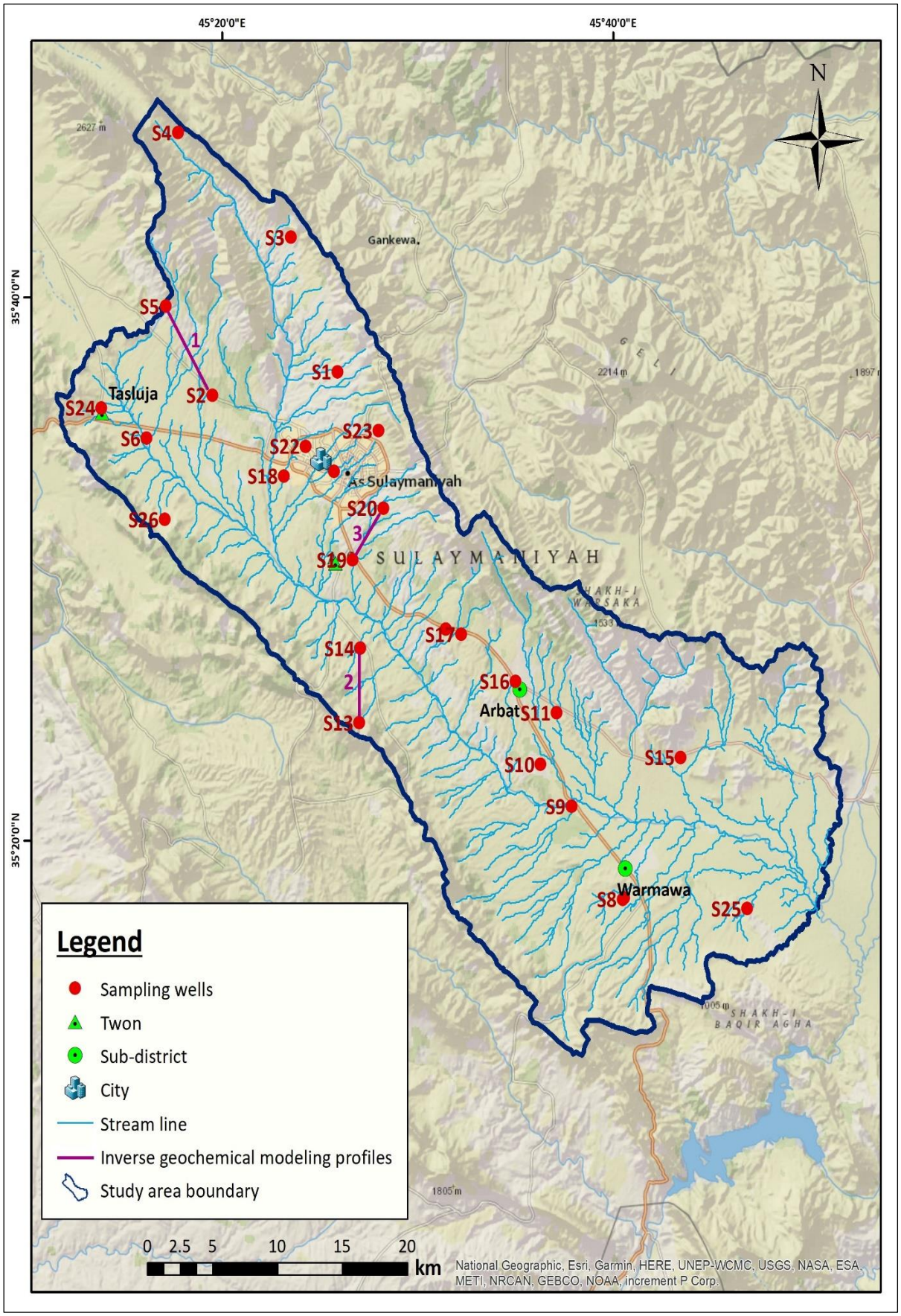

Figure 10. Sampling wells location and inverse geochemical modeling profiles.

4.2 Field and laboratory analyses

The field parameters such as pH, temperature, electrical conductivity (EC) and total dissolved solids (TDS) were measured on-site after pumping several well volumes during data collection. They were measured by the multi-parameter device Cyber Scan PC 300.

The collected groundwater samples have been stored and exported to the Czech Republic and France for laboratory analyses. Cations and trace elements measurements were conducted in the analytical facilities of Charles University in Prague using the ICP-MS technique (Figure 11). The analytical error of each solution analysis was less than 2%. Anions concentrations were measured using HPLC and Dionex ICS (Figure 12). The ferrous iron was determined by titration with potassium dichromate. Alkalinity values were obtained through HCl titration using the Gran plot to determine the endpoint. The QA/QC was carried out according to established protocols. About 10% of the samples were examined twice and obtained results were consistent.

Figure 11. ICP-MS (Inductively Coupled Plasma Mass Spectrometer).

Figure 12. HPLC, Dionex ICS.

The measurements of ^{2}H and ^{18}O isotopes were conducted at the Czech Geological Survey in Prague, Czech Republic, using an LWIA 3000 laser analyzer (LGR), Figure 13. The accuracy of the analysis was 0.4‰ for ^{2}H and 0.12‰ for ^{18}O. The data were standardized in accordance with the international standard (V-SMOW) and presented using standard δ-notation (Clark and Fritz, 1997). For ^{13}C analyses, $BaCl_2$ was added to precipitate DIC as $BaCO_3$. The precipitate was then decomposed in 100% H_3PO_4 under vacuum at 25 °C. The C isotope ratio in the generated CO_2 was determined by a Thermo Delta V mass spectrometer with a precision of ^{13}C values better than ± 0.1‰. Results were expressed using the PDB standard.

Figure 13. LWIA 3000 laser analyzer (LGR).

Strontium (corresponding to at least 2 μg of Sr in solution) was isolated from water samples using exchange chromatography techniques based on Triskem's Sr resin (Pin et al., 1994). The isotopic composition was analyzed using a Neptune Plus instrument (MC-ICP-MC; ThermoFisher Scientific) in the Stable and Radiogenic Isotope Research Laboratory at Charles University in Prague. Analytical mass bias was corrected to $^{88}Sr/^{86}Sr = 8.375209$ (defined as $\delta^{88}/^{86}Sr = 0$ and related to NIST SRM 987, Nier, 1938). The analytical uncertainty was determined by repeated analyses of the SRM 987 standard, with the resulting $^{87}Sr/^{86}Sr$ Sr= 0.7102777 ± 0.0000099 in (2 S.E.M; n = 8).

In addition, 13 groundwater samples were taken for tritium analysis in March 2022, one rainfall sample and one sample from the Tanjero River inside Sulaimani City. The tritium analyses were performed in the Mediterranean Environment and Modelling of Agro-Hydrosystems (EMMAH) of the University of Avignon in France. A Quantulus 1220 ultra-low liquid scintillation spectrometer (Figure 14) was used to measure the amount of tritium present in the water samples after electrolytic enrichment by low-level liquid scintillation counting with the detection level of 1 TU.

Figure 14. Quantulus 1220 ultra-low liquid scintillation spectrometer, University of Avignon in France.

4.3 Software and data management

The ArcGIS has been used to prepare the maps and cross-sections for the study area. Statistica 13.3 were used for statistical analysis and for creating graphs. The USGS program PHREEQC (Parkhurst & Appelo, 1999) with the minteq.dat database was used to calculate speciation and saturation indices and to determine mass transfer between selected mineral phases and groundwater using the inverse geochemical modeling module. The program Geochemist Workbench was used to prepare the Piper diagram and Eh–pH diagram. The PAST program (Hammer et al., 2001) was used to prepare hierarchical cluster analysis (HCA), where samples and wells were grouped in the Ward's mode based on their similarity.

5. Results and Discussion

In this chapter, the results of principal ions, trace elements, stable isotope, geogenic contaminants, geochemical modelling, and tritium analysis for groundwater samples as well as a discussion are presented.

5.1 Results

5.1.1 Principal ions and trace elements

The statistical parameters of the water chemistry in the studied areas are given in Table 5. The Piper plot for the groundwater chemistry data is presented in Figure 15. The overall trend along the flow path is the evolution from Ca-HCO_3 groundwater type towards Mg-Ca-HCO_3 groundwater type with rising EC. However, there are some exceptions. Mainly, anomalous sample S14 presents a Na-Cl water type, and sample S24 is a complex mix of Na-Ca-HCO_3-SO_4-Cl type groundwater. Sample S18 is Ca-HCO_3-SO_4 groundwater type with elevated EC located close to the Tanjero River (Figure 10).

The values of electrical conductivity range from 328 to 2460 μS/cm; the average is 757.28 μS/cm. The pH values in the area of interest are in the range from 7.02 to 8.75 and the average pH value is 7.56. The average value of Ca^{2+} is 72.14 mg/L with concentrations from 6.07 to 174 mg/L. Concentrations of Mg^{2+} range from 2.33 to 79 mg/L, with the average being 26.29 mg/L. Concentrations of Na^{+} are from 2.66 to 480 mg/L, with the average being 37.87 mg/L. The concentration of K^{+} ranges from 0.26 to 3.1 mg/L, and the average is 1.14 mg/L. Concentrations of HCO_3^{-} range from 140 to 320 mg/L, with an average of 222.76 mg/L. The concentration of SO_4^{2-} ranges from 7.34 to 200.7 mg/L, with an average of 52.1 mg/L. The concentration of Cl^{-} ranges from 1.88 to 462.37 mg/L; the average is 39.06 mg/L. The average value of NO_3^{-} is 34.28 mg/L with concentrations from 1.63 to 207.11 mg/L.

Table 5. Water chemistry parameters of the groundwater samples in the SWSB.

Sample code	Unit	S1	S2	S3	S4	S5	S6	S7	S8	S9	S10	S11	S12	S13
pH		8.13	7.55	7.54	7.5	7.53	7.18	7.37	7.54	7.03	7.07	7.86	8.02	7.84
Temperature	°C	29.1	24.9	21.8	26	25.5	31.5	23.3	25	23.5	23	22.9	27	23.3
EC	µS/cm	504	475	450	522	565	841	450	807	692	963	602	496	467
TDS	ppm	132	236	234	276	283	421	223	416	348	491	275	248	238
HCO_3^-		190	190	180	260	180	220	240	180	220	300	220	200	240
Ca^{2+}		62.00	52.20	47.30	23.60	45.60	72.00	37.80	64.00	94.47	88.00	57.00	56.00	45.60
K^+		4.60	0.39	0.67	0.61	0.71	1.20	0.65	3.10	0.90	1.10	0.43	1.30	0.65
Mg^{2+}		N/A	8.35	8.64	5.68	10.30	70.00	8.71	61.00	19.08	79.00	12.10	53.00	26.50
Na^+		14.20	4.32	14.70	2.66	16.40	4.50	41.90	39.00	30.00	7.50	3.98	16.80	4.79
Si		N/A	6.52	7.77	4.00	7.22	N/A	8.18	N/A	N/A	N/A	6.35	N/A	7.23
Cl^-		36.00	3.47	2.38	N/A	4.24	30.00	5.77	25.00	35.00	14.00	4.46	13.00	2.81
$SO4^-$		20.00	30.91	19.03	N/A	31.81	41.00	27.05	38.00	31.00	55.00	7.34	14.00	23.59
F^-		N/A	<0.2	<0.2	N/A	<0.2	0.57	<0.2	0.37	<1	0.63	<0.2	0.33	0.20
$NO3^-$		N/A	23.16	8.96	N/A	26.75	28.46	6.75	23.93	1.63	37.04	17.27	27.90	2.64
Li	µg/L	N/A	2.63	4.27	1.03	7.05	5.34	4.93	7.39	4.80	6.80	4.70	3.89	4.09
Al		N/A	19.31	18.15	18.80	17.33	<0,05	16.32	<0,05	<0,05	<0,05	18.21	<0,05	16.29
Ti		N/A	204.64	183.35	92.97	168.21	N/A	142.87	N/A	N/A	N/A	214.39	N/A	177.95
V		N/A	3.85	1.90	0.86	1.27	5.78	4.01	5.09	5.57	4.75	3.11	4.73	2.27
Cr		N/A	3.13	0.91	0.08	0.72	4.26	1.19	7.29	2.29	2.32	1.75	2.41	1.88
Mn		N/A	0.46	BDL	BDL	2.51	1.08	8.28	2.39	3.47	0.91	1.22	0.39	BDL
Fe		N/A	347.05	312.18	151.37	278.36	<0,005	234.54	<0,005	<0,005	<0,005	372.90	<0,005	307.51
Co		N/A	0.16	0.12	0.05	0.11	0.33	0.21	0.15	0.50	0.11	0.16	0.10	0.10
Ni		N/A	1.13	0.97	0.54	1.83	2.86	0.84	1.27	3.01	0.83	1.40	1.71	1.79

Cu		N/A	0.37	0.47	0.08	0.19	1.92	0.61	0.69	4.11	4.95	12.80	17.45	2.36
Zn		N/A	0.38	BDL	0.21	3.62	17.69	289.67	62.48	70.02	372.73	339.68	120.41	27.11
As		N/A	BDL	BDL	BDL	BDL	0.65	0.15	0.47	1.03	0.46	BDL	0.41	BDL
Rb		N/A	0.40	0.51	0.35	0.56	0.27	0.92	0.46	0.87	0.54	0.24	0.46	0.32
Sr		N/A	1002.10	1663.85	166.08	1286.81	763.47	900.03	931.89	788.72	1118.18	1181.95	617.27	866.83
Cd		N/A	0.10	0.04	0.02	0.02	0.06	0.02	0.06	0.06	0.06	0.02	0.05	0.05
Ba		N/A	32.72	51.85	12.15	74.77	72.37	24.11	100.67	112.99	52.03	383.38	32.47	21.96
Ce		N/A	0.03	0.03	0.03	0.03	0.01	0.03	0.12	0.01	0.04	0.04	0.02	0.02
Pb		N/A	0.03	0.01	0.08	0.04	0.88	0.64	0.55	0.81	0.63	0.53	0.90	0.37
Bi		N/A	0.87	0.86	0.80	0.77	N/A	0.73	N/A	N/A	N/A	0.72	N/A	0.69
U		N/A	0.85	0.46	0.39	0.30	0.84	0.49	1.07	0.70	1.32	0.59	0.73	1.14
Sc		N/A	N/A	N/A	N/A	N/A	3.79	N/A	3.72	3.44	3.46	N/A	3.24	N/A
Y		N/A	N/A	N/A	N/A	N/A	0.02	N/A	0.08	0.02	0.02	N/A	0.01	N/A
Sn		N/A	N/A	N/A	N/A	N/A	0.03	N/A	0.07	0.05	0.04	N/A	0.03	N/A
Sb		N/A	N/A	N/A	N/A	N/A	4.40	N/A	1.10	6.97	5.95	N/A	2.98	N/A
Cs		N/A	N/A	N/A	N/A	N/A	0.00	N/A	0.01	0.01	0.02	N/A	0.01	N/A
La		N/A	N/A	N/A	N/A	N/A	0.01	N/A	0.08	0.01	0.02	N/A	0.01	N/A
Th		N/A	N/A	N/A	N/A	N/A	0.00	N/A	0.01	0.00	0.00	N/A	0.00	N/A
Br	mg/l	N/A	N/A	N/A	N/A	N/A	<0,4	N/A	<0,4	<1	<0,4	N/A	<0,2	N/A
PO4		N/A	N/A	N/A	N/A	N/A	<0,8	N/A	<0,8	<2	<0,8	N/A	<0,4	N/A

Sample code	Unit	S14	S15	S16	S17	S18	S19	S20	S21	S22	S23	S24	S25	S26
pH		8.55	7.22	7.32	7.4	7.02	7.03	7.65	7.2	7.16	8.57	8.75	7.46	7.53
Temperature	°C	22.3	22.4	20.6	26.8	26.3	23	24.9	31	25	26.7	25.5	19	23.5
EC	µS/cm	2460	408	469	401	935	642	328	841	483	486	792	1123	1217
TDS	ppm	0.00000121	187	232	204	460	321	164	421	237	243	398	N/A	N/A
HCO_3^-		140	220	160	180	320	200	240	180	210	240	230	345	307
Ca^{2+}		19.10	63.20	80.00	55.00	113.00	84.10	47.60	104.00	69.50	25.50	6.07	159.00	174.00
K^+		1.84	0.26	1.30	2.66	0.47	0.39	0.35	1.20	0.52	0.64	2.30	0.86	1.79
Mg^{2+}		2.33	5.05	70.00	10.70	40.40	19.30	7.27	70.00	9.58	6.62	2.45	20.32	30.93
Na^+		480.00	2.67	8.30	4.80	19.40	10.60	3.52	8.20	8.15	61.50	157.00	9.19	10.46
Si		6.21	5.36	N/A	7.69	12.08	9.97	8.09	N/A	6.61	7.54	17.46	N/A	N/A
Cl^-		462.37	1.88	23.00	5.31	43.51	43.55	6.63	29.00	11.37	8.73	44.07	54.06	66.80
$SO4^-$		200.70	7.65	27.00	16.00	84.32	44.74	7.97	152.00	34.73	53.15	121.10	52.96	161.49
F^-		0.54	<0.2	0.63	<0.2	<0.2	<0.2	<0.2	<1	<0.2	0.29	<0.2	0.39	<1
$NO3^-$		<0.2	14.16	1.79	25.05	18.48	35.96	27.30	35.37	20.39	4.01	<0.2	160.00	207.11
Li		13.48	2.09	13.20	4.34	8.67	5.22	2.21	4.69	3.54	30.84	2.14	9.06	6.85
Al		17.01	17.33	<0,05	6.07	5.35	5.87	6.03	<0,05	5.80	6.16	6.04	<0,05	<0,05
Ti		81.62	225.31	N/A	198.72	394.34	293.79	172.75	N/A	256.94	94.53	26.34	N/A	N/A
V		16.71	3.45	0.81	4.98	8.98	7.10	4.21	4.28	2.12	0.86	1.79	3.64	2.40
Cr		0.65	1.31	1.86	1.63	3.25	1.06	2.89	2.89	0.98	2.98	0.53	3.64	4.55
Mn	µg/L	1.89	0.08	13.39	BDL	4.43	BDL	BDL	2.02	0.03	6.93	2.01	6.22	2.04
Fe		130.89	395.96	<0,005	335.10	689.54	506.00	292.43	<0,005	445.98	147.93	27.59	<0,005	<0,005
Co		0.07	0.13	0.27	0.12	0.31	0.18	0.09	0.25	0.15	0.04	-0.01	0.39	0.27
Ni		0.73	1.65	1.12	0.97	3.44	1.46	0.85	1.56	1.46	0.57	0.57	3.37	2.88
Cu		7.20	0.65	2.09	BDL	0.42	0.01	BDL	0.89	BDL	0.60	1.95	19.57	0.89
Zn		2.31	140.45	16.24	7.10	127.63	0.17	BDL	15.80	1.37	28.71	25.10	57.35	15.13

As		4.27	0.20	0.48	0.10	0.34	0.06	BDL	0.43	BDL	BDL	0.12	0.69	0.35
Rb		0.84	0.21	1.43	0.99	0.69	0.41	0.33	0.57	0.33	0.42	4.17	0.40	1.08
Sr		556.71	332.45	3447.96	952.67	2682.28	1768.78	547.64	1643.19	970.35	1108.00	171.86	1034.42	839.40
Cd		0.09	0.02	0.06	0.02	0.02	0.00	0.02	0.05	0.02	0.01	0.02	0.07	0.04
Ba		12.00	214.11	654.52	46.04	144.29	165.96	63.44	74.71	173.70	101.71	7.46	142.41	78.58
Ce		0.03	0.03	0.12	0.01	0.01	0.01	0.01	0.01	0.01	0.01	0.01	0.10	0.02
Pb		1.59	0.97	2.10	0.46	0.39	0.41	0.25	0.26	0.15	0.09	0.18	1.75	0.28
Bi		0.86	0.68	N/A	0.67	0.66	0.66	0.64	N/A	0.65	0.64	0.64	N/A	N/A
U		0.08	0.46	0.22	0.58	1.94	1.28	0.46	1.27	0.54	0.32	0.01	1.93	1.18
Sc		N/A	N/A	3.02	N/A	3.99	N/A	N/A	3.52	N/A	N/A	N/A	3.66	3.60
Y		N/A	N/A	0.09	N/A	0.03	N/A	N/A	0.03	N/A	N/A	N/A	0.12	0.02
Sn		N/A	N/A	0.04	N/A	0.03	N/A	N/A	0.04	N/A	N/A	N/A	0.24	0.03
Sb		N/A	N/A	1.04	N/A	1.15	N/A	N/A	12.11	N/A	N/A	N/A	1.80	1.51
Cs		N/A	N/A	0.06	N/A	0.02	N/A	N/A	0.03	N/A	N/A	N/A	0.01	0.01
La		N/A	N/A	0.09	N/A	0.01	N/A	N/A	0.01	N/A	N/A	N/A	0.06	0.02
Th		N/A	N/A	0.00	N/A	0.00	N/A	N/A	0.00	N/A	N/A	N/A	0.01	0.00
Br	mg/l	N/A	N/A	<0,4	N/A	<1	N/A	N/A	<1	N/A	N/A	N/A	<0,4	<1
PO4		N/A	N/A	<0,8	N/A	<2	N/A	N/A	<2	N/A	N/A	N/A	<0,8	<2
BDL= Below detection limit, N/A= Not available														

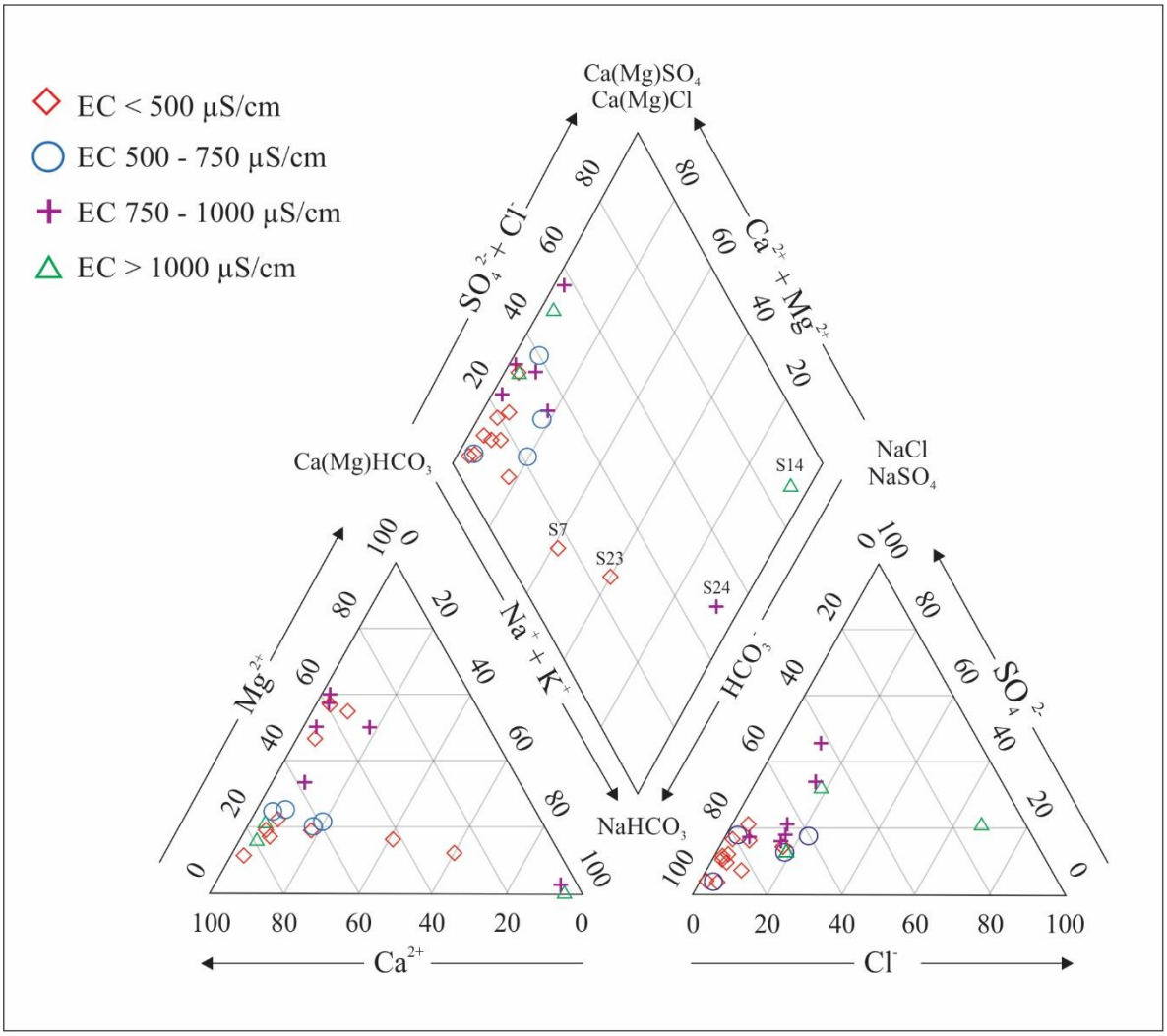

Figure 15. Piper diagram; samples are sorted based on their EC values, outliers S7, S23, S24, and S14 are marked.

The average concentration of Al is 12.5 µg/L with a range from 5.35 to 19.31 µg/L. Concentrations of Cr range from 0.08 to 7.29 µg/L, with an average of 2.26 µg/L. The average value of Fe is 310.96 µg/L with concentrations from 27.59 to 689.54 µg/L Concentrations of Cr range from 0.08 to 7.29 µg/L, with the average being 2.26 µg/L.

Generally, the quality of water has been influenced by redox processes in addition to the mobility status of the toxic elements can be affected by redox processes that are naturally present in aquifer materials, along with organic and inorganic components. These processes in the aquifer contribute to the breakdown or preservation of anthropogenic contaminants (McMahon & Chapelle, 2008).

Regarding redox indicators, NO_3^- are from 1.63 to 207.11 mg/L, average 34.28 mg/L; concentrations of Fe are from 0.027 0.68 mg/L, average 0.31 mg/L; and concentrations of Mn generally in half of the groundwater samples was below the detection limit and maximum concentration reaches only 13.39 µg/L. Moreover, the concentration of Cl^- in rain collected in the studied area out of Sulaimani was 2.2 mg/L.

5.1.2 Geogenic contaminants

Regarding the geogenic contaminants in the study area, fluoride, arsenic and barium are the most common in the semi-arid area, including the area of interest. The concentrations of Ba range from 7.46 to 654.52 µg/L, with the average being 114 µg/L. Furthermore, the Concentrations of F^- range from 0.2 to 0.63 mg/L, with an average of 0.44 mg/L. The average value of As is 0.64 µg/L with concentrations from 0.06 to 4.27 µg/L.

The available groundwater data were used to make a geostatistical interpolation and construction of predictive maps for Ba, F and As concentrations in groundwater. The maps for Ba, F^- and As (Figure 16 A, B & C) indicate vulnerable areas. This can help authorities to become aware of potentially contaminated groundwater. The spatial distribution of As and F in the studied area is patchy, and different concentration hotspots are present. This may suggest the existence of local sources (Parrone et al., 2020).

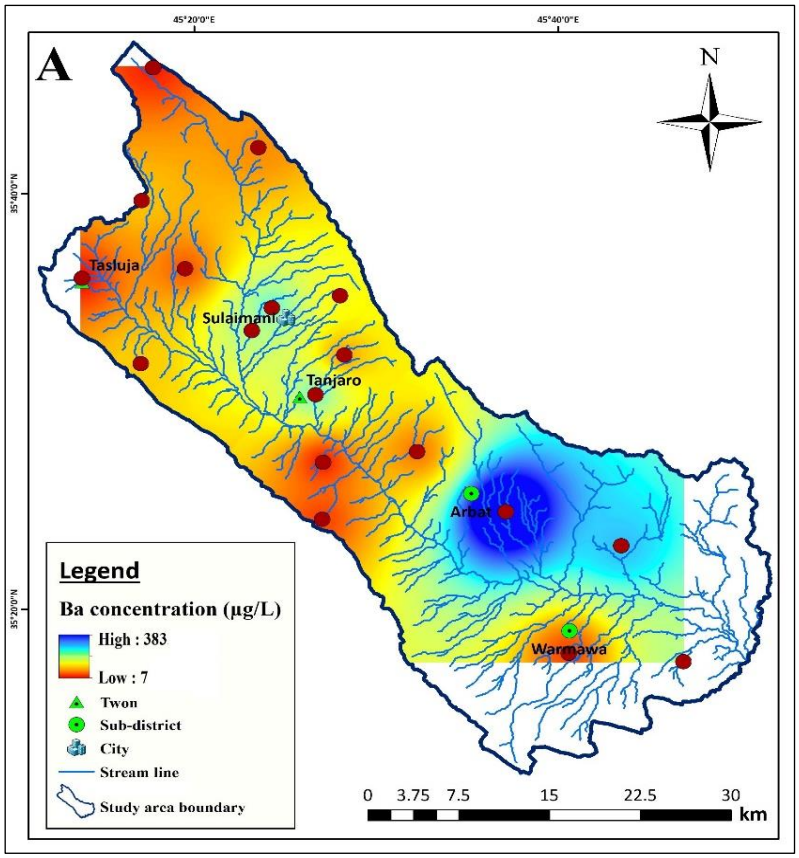
A
45°20'0"E
45°40'0"E
35°40'0"N
35°20'0"N
N
Tasluja
Sulaimani
Tanjaro
Arbat
Warmawa
Legend
Ba concentration (µg/L)
High : 383
Low : 7
Twon
Sub-district
City
Stream line
Study area boundary
0 3.75 7.5 15 22.5 30
km

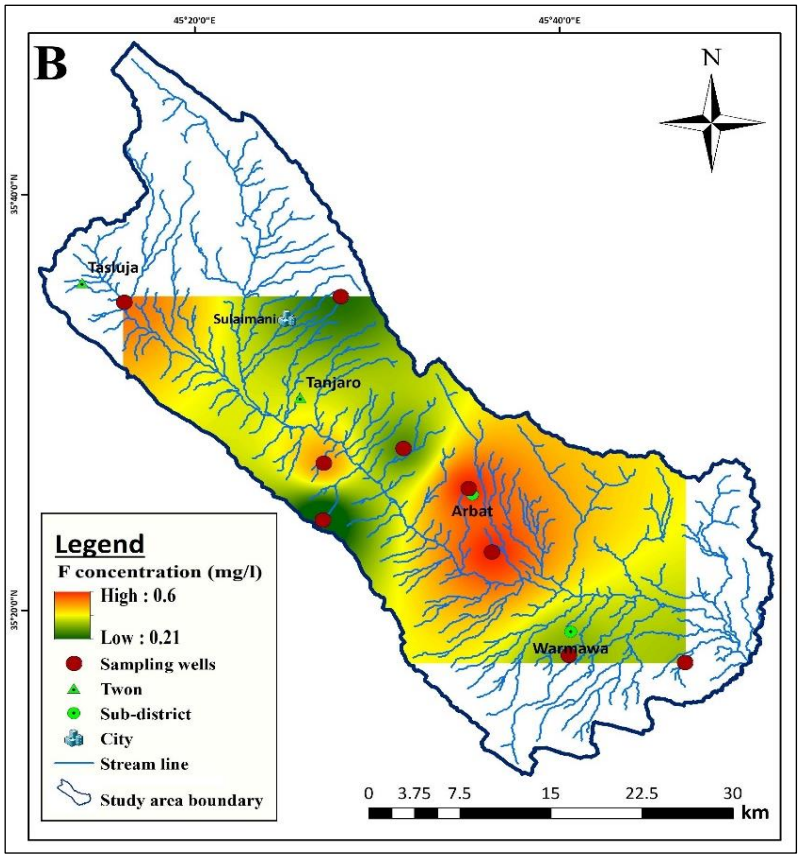
B
45°20'0"E
45°40'0"E
35°40'0"N
35°20'0"N
N
Tasluja
Sulaimani
Tanjaro
Arbat
Warmawa
Legend
F concentration (mg/l)
High : 0.6
Low : 0.21
Sampling wells
Twon
Sub-district
City
Stream line
Study area boundary
0 3.75 7.5 15 22.5 30
km

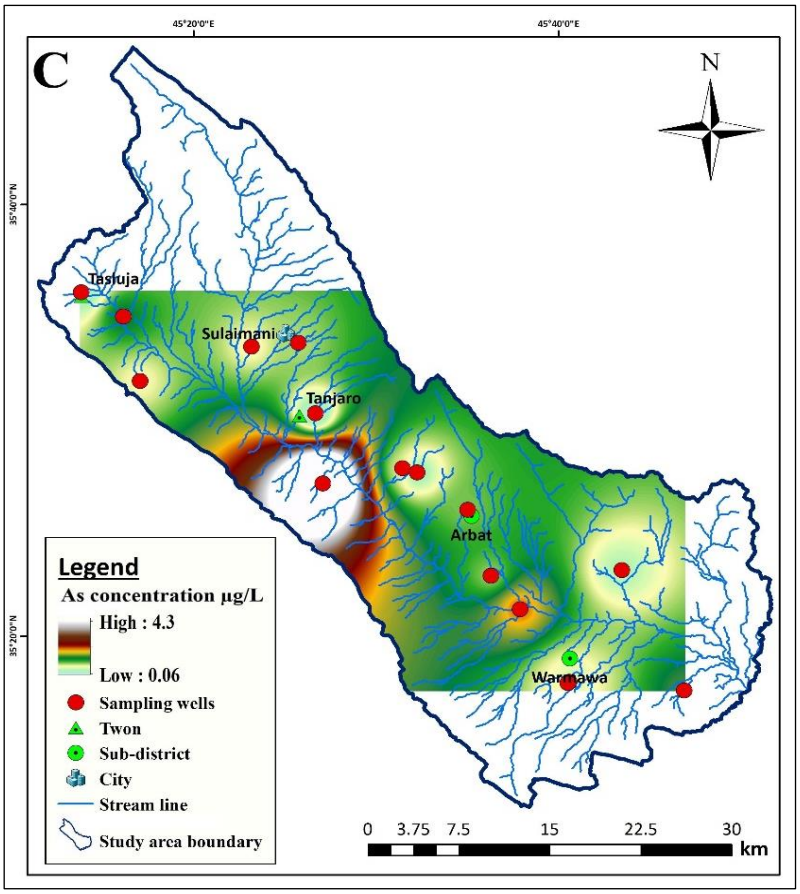

Figure 16. Spatial distribution of (A) Ba, (B) F and (C) As.

5.1.3 Stable isotopes

The groundwater samples from the Sulaimani-Warmawa Sub-basin reveal their stable isotopic compositions through the δ-notation, representing per mil deviation from the globally recognized standard, V-SMOW (Vienna Standard Mean Ocean Water). This data is outlined in Table 6 and visualized in Figure 17.

Table 6. Isotopes in groundwater samples from the Sulaimani-Warmawa Sub-basin, Kurdistan Region, during the period July–August 2020 and March-April 2022.

Sample No.	$\delta^{2}H$ (‰)	$\delta^{18}O$ (‰)	Deuterium excess	$\delta^{13}C$(DIC) (‰)	$^{87}Sr/^{86}Sr$
S1	-28.5	-6.1	20.0	−2.4	N/A
S2	-25.5	-5.6	19.2	−1.6	0.7082
S3	-32.9	-6.6	19.6	−1.5	0.7078
S4	-34.7	-7.0	21.7	−1.8	N/A
S5	-30.3	-6.3	20.4	−1.7	0.7079
S6	-26.2	-5.4	17.1	N/A	N/A
S7	-26.2	-5.5	18.0	−2.5	0.708
S8	-24.0	-4.9	15.6	N/A	N/A
S9	-24.4	-4.6	12.6	N/A	N/A
S10	-27.0	-5.0	13.4	N/A	N/A
S11	-28.7	-5.7	16.9	−3.4	0.7082
S12	-27.5	-5.1	12.9	N/A	N/A
S13	-33.7	-6.5	18.4	−1.7	0.7081
S14	-39.5	-6.7	13.9	−4.3	0.7076
S15	-29.8	-6.5	22.1	−1.3	0.7081
S16	-38.2	-6.7	15.2	N/A	0.7082
S17	-29.1	-5.6	16.0	−1.6	N/A
S18	-30.2	-5.5	13.6	N/A	N/A
S19	-28.5	-5.5	15.2	−1.6	0.7082
S20	-27.5	-6.2	22.1	−1.5	0.7082
S21	-30.7	-5.4	12.6	N/A	N/A
S22	-29.9	-6.2	19.3	−1.2	0.7081
S23	-36.9	-6.9	18.4	−1.4	0.7078
S24	-36.9	-6.9	18.1	−2.3	0.7077
S25	-24.0	-4.5	11.6	N/A	N/A
S26	-27.4	-5.6	17.7	N/A	N/A
N/A= Not available					

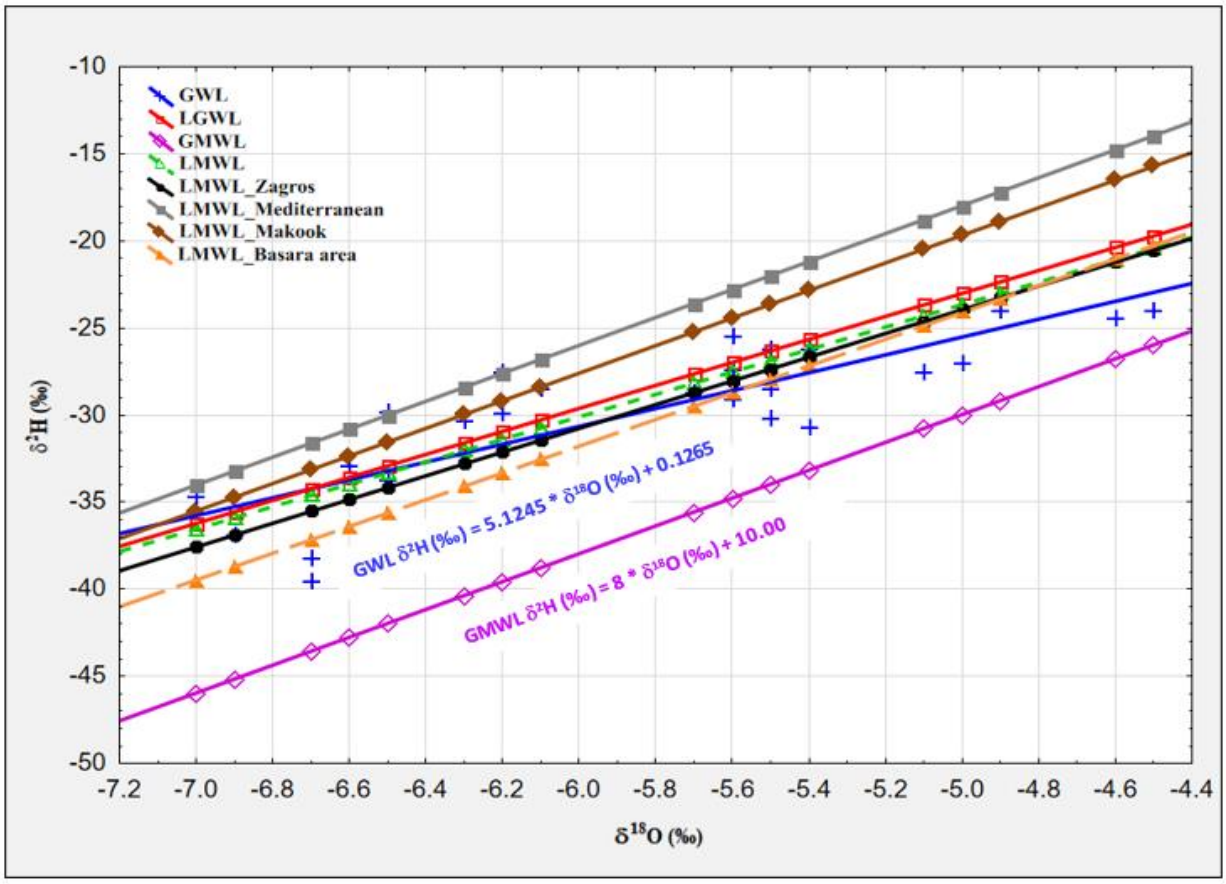

Figure 17. Diagram of ^{2}H vs ^{18}O, GWL is groundwater line for the study area, LGWL is the local groundwater line for the study area (Mahmmud et al., 2022), LMWL (Total) is average local meteoric water line for Zagros, LMWL (Zagros) is local meteoric water line for winter precipitation in Zagros, LMWL (Mediterranean) is local meteoric water line for precipitation in Mediterranean Sea, LMWL (Makook) is local meteoric water line for precipitation in Makook anticline area (Mustafa et al., 2015)., LMWL (Basara) is the local meteoric water line for precipitation, springs, wells and streams in Basara (Hamamin and Ali, 2013), and GMWL is the world global meteoric water line.

The value of ^{18}O ranges from (−7.0‰) to (−4.5‰) and the value of ^{2}H ranges from (−39.5‰) to (−24 ‰). Values of deuterium excess are high, in some samples more than 20‰. The local rainfall isotopic composition can be influenced by several factors such as humidity, surface air temperature, geographic location (longitude and latitude) and altitude (Mook, 2001; Mazor,

2004; Al-Charideh, 2011). According to the results of the isotopic composition of the groundwater samples in the area of interest, the most negative value ($^{18}O = -7.0‰$) was measured for the highest altitude sample, which is 1224 m above sea level (Mahmmud et al., 2022). The sample collected in the Alan village near Warmawa sub-district (altitude 527 m) had more positive value of ^{18}O, which was (−4.5‰). The groundwater line (GWL) for the study area is (δ^2H (‰) = 5.1245*$\delta^{18}O$ (‰) + 0.1265). The global meteoric water line (GMWL) has a higher slope and intercept than the local groundwater line (GWL) for the collected sample in the SWSB (Craig, 1961; Gat & Carmi, 1970) (Figure 17). Th local GWL for the groundwater samples in the studied area has a higher slope and intercepts the local meteoric water lines (LMWL Zagros) developed for the Zagros by Osati et al. (2014).

The local GWL for groundwater samples in the research area shows slope and intercept between local meteoric water lines (LMWL) calculated for the Zagros by Osati et al. (2014) (δ^2H = 6.80*^{18}O + 10.1) and Mohammadzadeh et al., 2020 (δ^2H = 6.44*^{18}O + 8.514). Nevertheless, there is a strong concurrence between the local GWL and the Local Meteoric Water Line (LMWL) in relation to winter precipitation, as indicated by the equation δ^2H = 6.67*$\delta^{18}O$ + 9.766 (Mohammadzadeh et al., 2020).

The result of stable isotope data shows that the groundwater in the study region was nearly entirely recharged by winter rainfall, with little evaporation impact during infiltration. This contrasts with groundwater data from western Iraq, where there was a strong evaporation effect with a slope of the groundwater line 5.19 (Ali et al., 2015).

The values of carbon isotope composition of dissolved inorganic carbon ^{13}C (DIC) are in Table 6. Additionally, the relationship between ^{13}C(DIC) and bicarbonate (HCO_3) is in Figure 18. The majority of ^{13}C(DIC) values fall within the range of -3.0 to -1.0‰. The samples S10 and S13 show exceptional values of -3.4 and -4.3‰, respectively. The presence of high values suggests that there is a state of equilibrium with carbonate rocks in a closed-system environment. This is further supported by the high saturation index (SI) values for calcite, particularly in wells located near Sulaimani (as shown in Table 8). The primary plant species found in the recharge areas surrounding Sulaimani are grasses, specifically C4 plants, as shown in Figure 7. These grasses show high ^{13}C values, approximately -12‰, as reported by Clark and Fritz (1997). These plants serve as the source of CO_2 that interacts with Cretaceous carbonate rocks, which typically possess ^{13}C values ranging from -1 to -2‰, (Razmjooei et al., 2020).

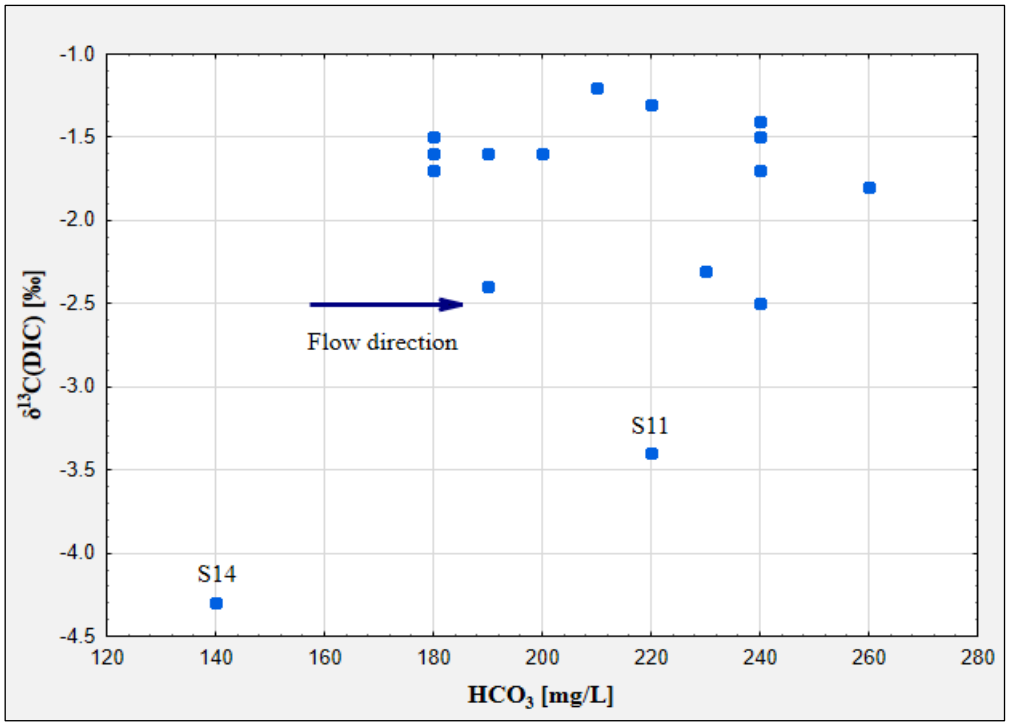

Figure 18. The ^{13}C(DIC) vs HCO_3 concentration, outliers are marked.

The values of $^{87}Sr/^{86}Sr$ ratios in groundwater are in Table 6, while a relationship between $^{87}Sr/^{86}Sr$ and Sr concentration is provided in Figure 19. The majority of $^{87}Sr/^{86}Sr$ ratios fall within the range of 0.7081 to 0.7082. Samples S3, S5, S23, and S24 obtained from wells in proximity to recharge areas near the groundwater divide (Figure 10) show values slightly below 0.708. The groundwater from well S14 shows anomalous water chemistry, as indicated by its lowest recorded value of 0.7076. Nevertheless, the aforementioned values are representative of groundwater that has come into contact with Cretaceous carbonates (Veizer, 1989).

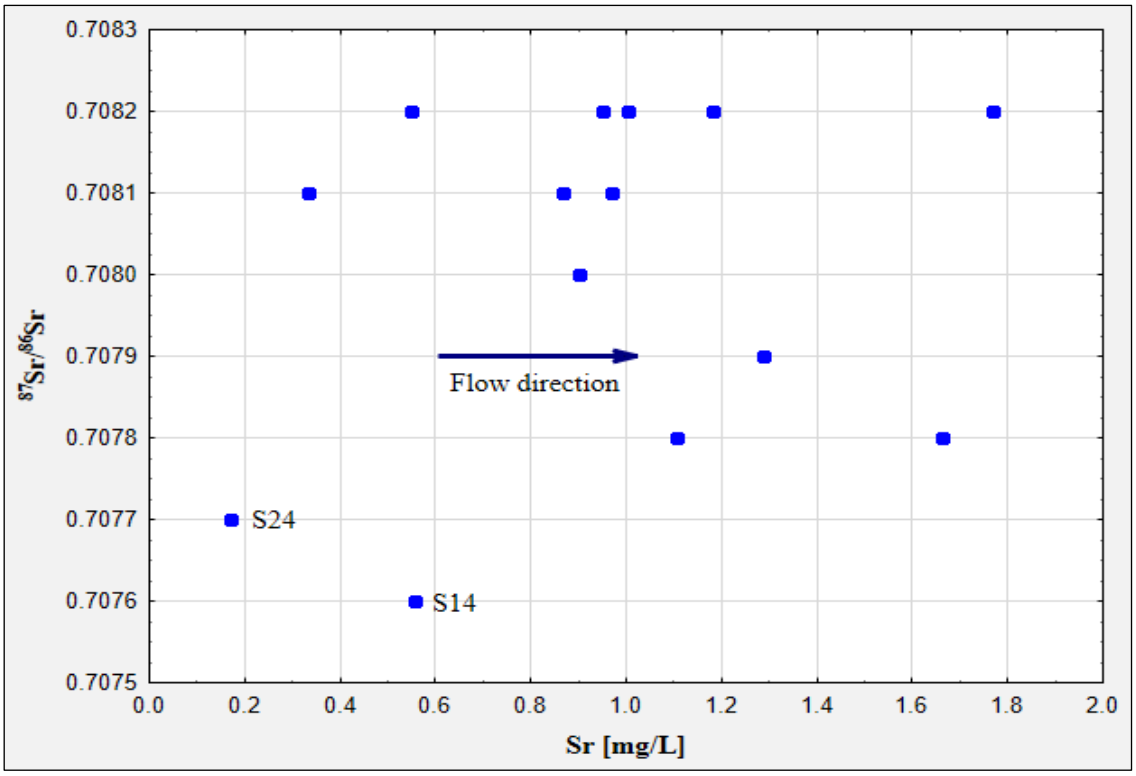

Figure 19. The $^{87}Sr/^{86}Sr$ ratio vs. Sr concentration, outliers are marked.

5.1.4 Tritium (^{3}H)

The result of tritium analysis for groundwater samples, one rainfall sample and one water sample from Tanjero River near Sulaimani City are in Table 7.

Table 7. Tritium analysis result of water samples in the SWSB.

No.	Samples	pH	EC (µS/cm)	Activity (TU)	Aquifer type
1	S1	7.5	350	3.5	Tanjero Aquifer
2	S3	6.3	560	4.1	Tanjero Aquifer
3	S4	8	550	3.9	Tanjero Aquifer
4	S5	7.8	340	2.6	Tanjero Aquifer
5	S11	8.3	350	3.2	Quaternary Intergranular Aquifer
6	S12	7.9	440	2.7	Karstic-Fissured Aquifer
7	S13	8.4	2980	≤ 0.8	Quaternary Intergranular Aquifer
8	S14	7.5	370	3.2	Quaternary Intergranular Aquifer
9	S17	7.8	990	3.4	Tanjero Aquifer
10	S18	7.4	650	4.3	Tanjero Aquifer
11	S21	7.4	890	4.9	Tanjero Aquifer
12	S22	6.03	490	1.7	Tanjero Aquifer
13	S23	8.5	870	0.7	Aquiclude
14	Rainfall	N/A	N/A	7.3	N/A
15	Tanjero River	5.4	540	4.4	N/A
N/A= Not available					

The tritium value of the rain sample was 7.3 TU, the tritium value of the river sample was 4.4 TU and the mean values of the groundwater samples were 3.2 TU for Quaternary Intergranular Aquifer, 3.55 TU for Tanjero aquifer, 2.7 and 0.7 TU for Karstic-Fissured Aquifer and Aquiclude, respectively, Table 8. The tritium concentration in the groundwater samples was from less than 0.8 to 4.9 TU. In general, there were higher values close to the catchment boundaries (except for wells S22 and S23) and lower values in the lowlands.

5.1.5 Speciation modeling

The selected results of speciation modelling are in Table 8. The Eh values in the range of 0.122 to +0.114 V, determined using the Fe(II)/Fe(III) pair, indicate post-oxic, mildly reducing conditions. These values suggest the presence of post-oxic conditions with a moderate level of reduction. The values of total carbon C expressed as carbon dioxide CO_2 in millimoles per kilogramme of water (mmol/kgw) generally exhibit an increase from 2.2 to 6.81 along the flow path. Recharge zones in proximity to the groundwater divide show low values, as observed in wells S5 and S24.

Conversely, high values are concentrated along the axis of the valley, as exemplified by wells S18 and S20. The log P_{CO2} values in recharge zones near the basin boundaries tend to be low, with a recorded value of -3.43 in S24. In contrast, these values are higher in the central axis of the valley, with a value of -1.54 in S18. Nevertheless, the S14 well shows anomalous Na-Cl groundwater with the lowest recorded values for both total carbon (C) and partial pressure of carbon dioxide (log P_{CO2}), as shown in Table 8. Most wells contain groundwater that is either supersaturated with calcite or in a state of equilibrium with it. Supersaturation or equilibrium with dolomite is observed in certain wells, particularly those located along the valley axis.

In contrast, it can be observed that all samples exhibit undersaturation with respect to gypsum and strontianite, $SrCO_3$, indicating conservative behaviour of both sulphate and strontium in groundwater. In general, the saturation indices for ferrihydrite are below saturation levels, while for more crystalline goethite exceed saturation levels. Groundwater shows undersaturation with respect to all manganese minerals and typically demonstrates undersaturation with respect to barite. Moreover, all samples show undersaturation in relation to amorphous silica while generally exhibiting supersaturation concerning quartz.

Furthermore, supersaturation with respect to kaolinite is observed, but calculated values are uncertain because of the possible presence of colloidal aluminium in some samples.

Table 8. Selected results of speciation modelling.

Sample	Total CO_2	Log P_{CO2}	Eh	Barite	Calcite	Dolomite(o)	Ferrihydrite	Goethite	Gypsum	Kaolinite	Manganite	Rhodochrosite	SiO_2(a)	Strontianite
	mmol/kgw													
S2	3.27	-2.28	0.033	-0.65	0.1	-0.24	4.71	5.71	-2.16	2.5	-10.52	-2.5	-1.25	-1.15
S3	3.12	-2.31	0.051	-0.61	-0.01	-0.44	0	5.78	-2.39	3	N/A	N/A	-1.15	-0.99
S5	3.11	-2.28	0.039	-0.28	0.01	-0.28	-0.21	5.69	-2.2	2.46	-9.74	-1.88	-1.21	-1.09
S7	4.26	-1.99	0.071	-0.84	-0.11	-0.51	-0.25	5.66	-2.35	2.83	-9.17	-1.41	-1.16	-1.29
S11	3.67	-2.55	-0.01	-0.18	0.48	0.61	-0.03	5.79	-2.75	2.05	-9.98	-1.91	-1.25	-0.74
S13	4.01	-2.49	-0.02	-0.96	0.39	0.87	-0.05	5.78	-2.38	2.07	N/A	N/A	-1.2	-0.87
S14	2.22	-3.48	-0.1	-0.53	0.3	0	-0.04	5.75	-2.01	0.59	-9.42	-1.53	-1.27	-0.77
S15	4.05	-1.9	0.094	-0.4	-0.11	-0.99	-0.12	5.68	-2.67	3.18	-11.17	-3.58	-1.32	-1.92
S17	3.17	-2.14	0.049	-0.8	-0.02	-0.37	-0.31	5.64	-2.42	1.71	N/A	N/A	-1.2	-1.34
S18	6.18	-1.54	0.099	0.2	0.06	0.03	-0.41	5.53	-1.59	2.74	N/A	N/A	-0.99	-1.12
S19	3.89	-1.76	0.115	0.14	-0.25	-0.83	-0.23	5.59	-1.88	3.04	N/A	N/A	-1.05	-1.47
S20	4.09	-2.28	0.022	-0.92	0.27	0.07	-0.16	5.73	-2.77	1.48	N/A	N/A	-1.16	-1.22
S22	3.91	-1.85	0.089	0.09	-0.13	-0.78	-0.28	5.61	-2.02	2.2	-11.97	-4.17	-1.25	-1.54
S23	3.8	-3.22	-0.12	0.04	0.87	1.53	-0.33	5.62	-2.26	-0.66	-9.41	-0.8	-1.23	-0.04
S24	3.6	-3.43	-0.1	-0.8	0.33	0.62	-0.31	5.6	-2.58	-0.2	-9.19	-1.32	-0.87	-0.76

5.2 Discussion

The groundwater flow system in the SWSB is a gravity-driven flow system in the terminology used by Tóth (2009). In such flow systems, mineralization expressed as EC and pH increase along the flow path, and values of Eh decrease (Tóth, 1999). Based on the values of ^{2}H and ^{18}O (Table 6) and only small Cl^{-} enrichment compared to rain in the assumed recharge area, evaporation of infiltrating precipitation is limited. In terrains with carbonate lithology, equilibrium with carbonates and high mineralization can occur already in recharge areas or even in epikarst, especially when infiltration is slow and contact time with carbonates is long (Frost & Toner, 2004; Ford & Williams, 2007; Faimon et al., 2012). Dissolution of evaporate minerals locally present in carbonates contribute Na^{+}, Ca^{2+}, Cl^{-}, and SO_4^{2-} and may result in precipitation of carbonate minerals such as calcite due to the common ion effect (Appelo & Postma, 2005; Khosravi et al., 2020). Hierarchical cluster analysis (HCA) was applied, which divides groundwater samples or groundwater parameters into different clusters based on their similarity, i.e., similar wells and parameters are in identical clusters (Davies, 2002). The results of the HCA performed in Ward's mode are in Figure 20. Sample S14 with high concentrations of Na^{+} and Cl^{-} and samples S24 and S18 with high sulfate concentration are clearly separated from other samples in different clusters.

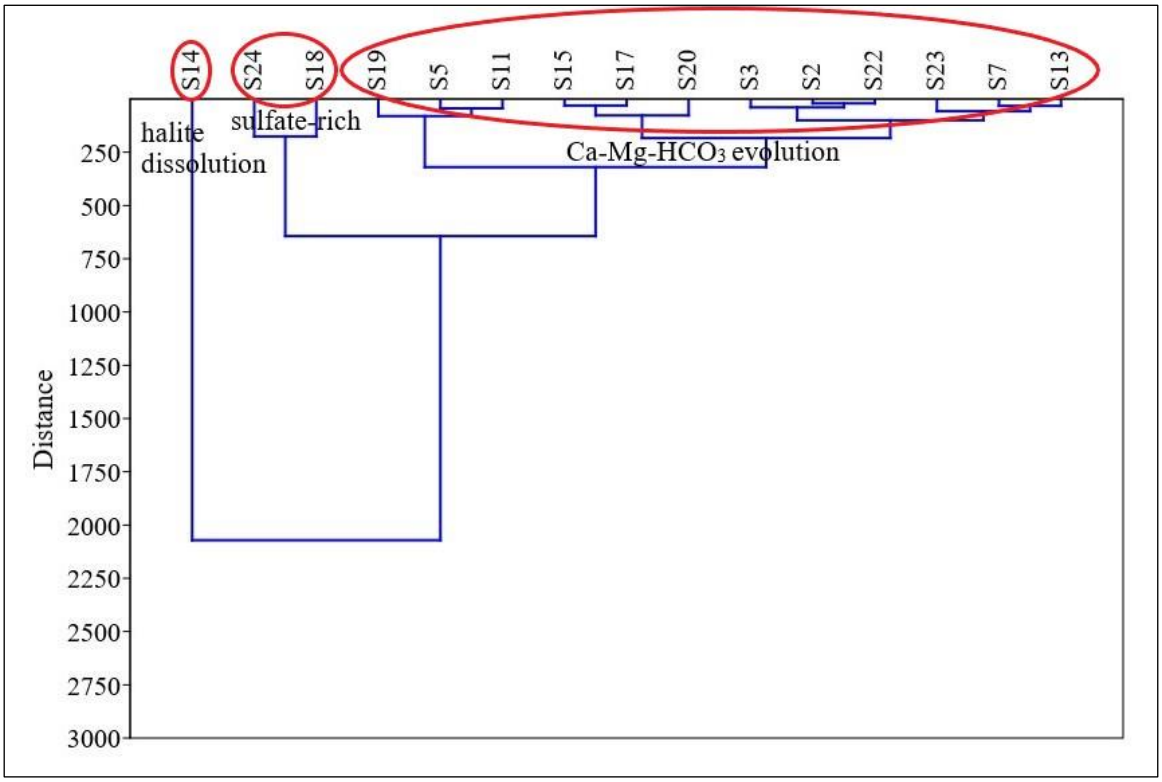

Figure 20. Hierarchical cluster analysis (HCA) of sampled wells; different groups of wells are marked.

In contrast, other samples with Ca-Mg-HCO_3 chemistry are in the right part of the HCA plot. This is consistent with the Piper diagram in Figure 15 and with almost constant ratios of $^{87}Sr/^{86}Sr$ between 0.7076 and 0.7082, consistent with the interaction of groundwater with carbonates. Interactions with clastic non-carbonate material would have resulted in significantly higher ratios (Frost & Toner, 2004). Also, the $^{87}Sr/^{86}Sr$ ratios in groundwater samples are close to the $^{87}Sr/^{86}Sr$ ratios in precipitation in the Kurdistan Region (mean = 0.7083) as reported by Mustafa et al. (2016).

Results of the HCA for groundwater parameters again in Ward's mode are shown in Figure 21. In this diagram, Na^+ and Cl^-, as well as Ca^{2+} and SO_4^{2-}, are in separate clusters, suggesting their common origin in the dissolution of evaporates. Bicarbonate and EC are linked to all parameters as they represent groundwater mineralization. Then, T, pH, Si, Mg^{2+} and NO_3^- are in a distinct cluster at the right, as Si and Mg are linked to high pH values and most other parameters are in the large central cluster.

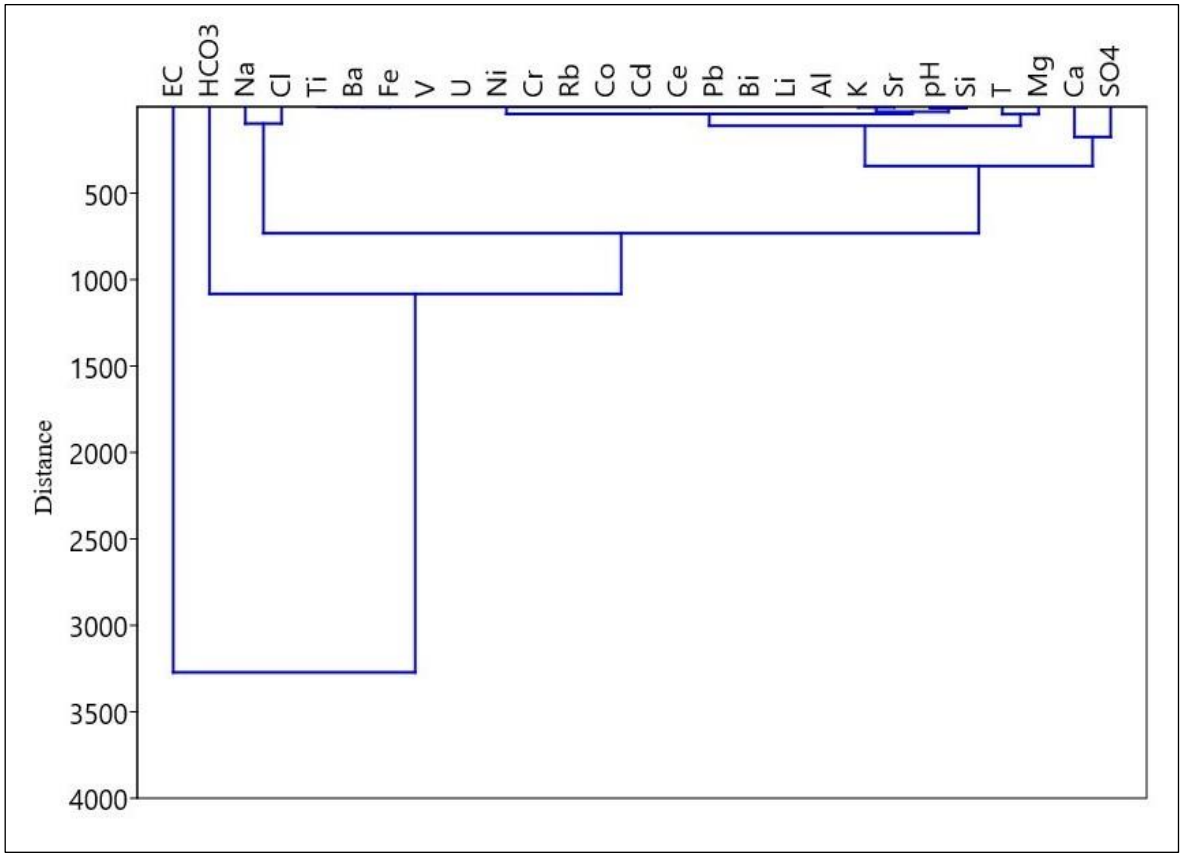

Figure 21. Hierarchical cluster analysis (HCA) of sampled wells.

Inverse geochemical modeling has been performed to interpret groundwater chemistry evolution on selected profiles (Figure 10). The modeled profiles were as follows, Profile 1: S2-S5 (profile close to the recharge zone); Profile 2: S13-S14 (profile affected by the dissolution of evaporites); and Profile 3: S19-S20 (profile in the axis of the valley, also with some impact of evaporite dissolution). The modeling was calibrated using values of ^{13}C(DIC) because interaction with carbonates is important in all modeled profiles. The ^{13}C value for carbonate rocks was set to −2‰ (Razmjooei et al., 2020), and a value of ^{13}C for organic matter CH_2O linked to C4 plants was set to −14‰ (Clark & Fritz, 1997).

The results of inverse geochemical modeling are in Table 9. On Profile 1 (S2-5), close to the recharge zone, there are only minor mass transfers because groundwater chemistry does not change very much along the flow path. Small amounts of calcite dissolve and only very minor amounts of Na-silicate dissolution (here albite) account for increasing Na^+ because Cl^- concentrations on the profile remain almost constant. On the other hand, on the Profile 2 (S13-14), a very high amount of halite and some gypsum dissolve to account for large changes in Cl^- and SO_4^{2-} concentrations and some dolomite precipitates due to the common ion effect. Finally, changes on the Profile 3 (S19-20) are less significant than on the Profile 2, but small amounts of halite and gypsum dissolve and a minor amount of calcite precipitates. Also, small amounts of organic matter CH_2O are introduced to account for changes in redox state, also indicated by slightly increasing dissolved iron concentrations downgradient. Amorphous quartz precipitates on Profiles 2 and 3 and cation exchange operates on all profiles. There is an excellent agreement between calculated and measured values of ^{13}C, confirming realistic values of mass transfer in groundwater interaction with carbonates. The modeling results are also consistent with Pearson's correlation coefficients in Table 10.

Table 9.Transfer of phases calculated by inverse geochemical modeling. Mass transfer coefficients in mmol/L.

Profile	Calcite	Dolomite	Halite	Albite	Gypsum	$Fe(OH)_3$	CH_2O	$SiO_2(a)$	NaX	CaX2	MgX2	$\delta^{13}C$	$\delta^{13}C$
												calc.	meas.
1	+0.104	-	-	+0.001	-0.009	+0.001	+0.0003	-	+0.67	−0.1	−0.24	−1.6	−1.6
2	-	−1.286	+12.96	+3.40	+1.84	+0.027	-	−6.84	+1.85	−1.22	+0.29	−4.1	−4.3
3	−0.03	-	+1.11	-	+0.382	+0.004	+0.001	+0.31	−0.79	+0.07	+0.34	−1.6	−1.6

+ dissolution, − precipitation, X cation exchange

Table 10. Pearson correlation matrix.

Chemical Variables	pH	EC	Ca^{2+}	K^{+}	Mg^{2+}	Na^{+}	Cl^{-}	HCO_3^{-}	SO_4^{2-}	F^{-}	NO_3^{-}
pH	1.00										
EC	0.43	1.00									
Ca^{2+}	-0.85	-0.23	1.00								
K^{+}	0.47	0.37	-0.48	1.00							
Mg^{2+}	-0.48	-0.09	0.75	-0.30	1.00						
Na^{+}	0.63	0.95	-0.51	0.50	-0.34	1.00					
Cl^{-}	0.44	0.98	-0.30	0.38	-0.21	0.96	1.00				
HCO_3^{-}	-0.21	-0.34	0.45	-0.36	0.65	-0.43	-0.45	1.00			
SO_4^{2-}	0.57	0.91	-0.34	0.50	-0.10	0.92	0.87	-0.19	1.00		
F^{-}	0.55	0.91	-0.41	0.33	-0.30	0.94	0.95	-0.45	0.80	1.00	
NO_3^{-}	-0.70	-0.38	0.63	-0.30	0.21	-0.53	-0.36	-0.05	-0.48	-0.44	1.00

There is no Eh data collected, but the redox state of aquifers can be determined on the basis of redox indicators, i.e., O_2, NO_3^{-}, Mn(II), Fe(II), SO_4^{2-}, and CH_4, and the redox state gradually decreases in the sequence (Appelo and Postma, 2005; McMahon and Chapelle, 2008). In some wells, the value of Eh calculated using the iron couple indicates a moderately reducing environment (Table 8). Concentrations of NO_3^{-} were elevated in several wells, reaching up to 36 mg/L in S19 (Table 5). Nitrate pollution from grazing in hills and from sewage at the valley bottom could be a possible source for observed elevated NO_3^{-} concentrations (Mustafa & Ahmad, 2008). Samples from some wells, e.g., S18, has elevated both iron and NO_3^{-} concentrations, probably indicating an overlap of nitrate reduction and dissolution of Fe(III) mineral zones or mixing in long-screen pumping wells (Sracek et al., 2018). The Eh–pH diagram for the Fe-S system is in Figure 22. The points in the diagram are aligned along $Fe(OH)_3$(ppd) and Fe^{2+} boundary, suggesting that precipitation of amorphous $Fe(OH)_3$(ppd) controls dissolved iron concentration. More stable crystalline phases, such as goethite, FeOOH, crystalize later from the unstable amorphous phase (Appelo and Postma, 2005).

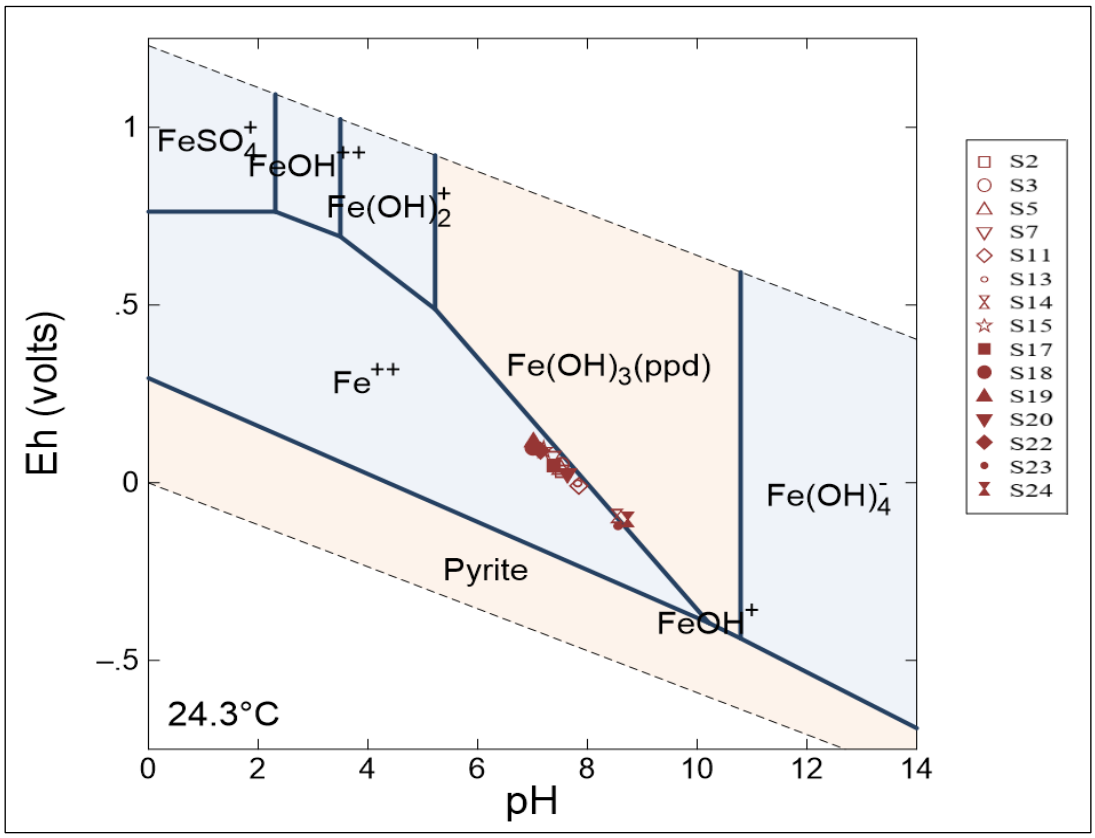

Figure 22. Eh–pH diagram for system Fe-S, ppd-precipitated, FeT= 1 × 10− 5 mol/L, ST = 5 × 10− 4 mol/L.

The principal geogenic contaminant in the study area is Ba with concentrations up to 0.383 mg/L in well S11, but it is still much less compared to the WHO limit of 0.7 mg/L (WHO, 2017). Even in this well, the S1 value for barite is negative (Table 8); thus, precipitation of the mineral cannot control Ba concentrations. The presence of barite impurities in carbonate rocks of the area was reported and represents a possible geogenic source for Ba (Mustafa & Merkel, 2015; Mustafa et al., 2015). The maximum concentration of F^-, 0.54 mg/L is in well S14 and is below the WHO limit of 1.5 mg/L, and concentrations in most wells are below the detection limit. This is expected in carbonate-dominated systems with high dissolved Ca^{2+} concentrations where precipitation of fluorite, CaF_2, keeps F^- at low concentrations (Alarcón-Herrera et al., 2013; Sracek et al., 2015). The results from SWSB vary; some samples reached more than 2 mg/L. Increased F^- concentration contributed to the removal of Ca^{2+} by cation exchange and, thus, the lack of fluorite precipitation control (Mustafa et al., 2023).

The maximum concentration of As is 4.27 µg/L, below the WHO limit of 10 µg/L. The maximum concentration of Cr is 3.25 µg/L in well S18, also below the WHO limit of 50 µg/L. Both contaminants form oxyanionic species and are desorbed at high pH (Appelo and

Postma, 2005; Sracek et al., 2018). However, they remain adsorbed and immobile at a slightly alkaline pH in the studied system. Concentrations of dissolved Mn are only up to 8.28 μg/L in well S7 and in most wells are below the detection limit. However, Kareem et al. (2018) found concentrations of Mn up to 911 μg/L south of Sulaimani, downgradient from the municipal waste landfill located close to the Tanjero River. It seems that most of the dissolved Mn is from the waste material and is mobilized under reducing conditions. Concentrations far from the landfill were much lower and like those found in the study. In Erbil area, concentrations of As were consistently below the WHO limit of 10 μg/ (Mustafa et al., 2023).

Analysis of the interaction of groundwater with surface water in the hyporheic zone of the Tanjero River was beyond the scope of the study. The river is extremely contaminated (Mustafa, 2006) and dries out in late summer and fall, and water flow re-appears in early October in the early precipitation period. Cyclic drying and flooding may induce redox changes with the re-mobilization of contaminants like Mn (Sengupta et al., 2018). The waste landfill, with a resulting increased Mn concentration downgradient, is located close to the river, already contaminated by municipal sewage discharge. In that case, the behavior of Mn and other redox-sensitive contaminants should be investigated in detailed piezometric profiles close to the Tanjero River.

The difference in isotopic data of precipitation in the Kurdistan regions of Iraq in comparison to the global meteoric water line (GMWL), can be attributed to the combination of air masses originating from the Eastern Mediterranean with high deuterium excess, and those from the Persian Gulf. The influence of the Persian Gulf becomes more significant during the autumn season, leading to a decrease in the slope of the Kurdistan local meteoric water line (LMWL) to 6.08 (Mohammadzadeh et al., 2020). During the autumn season, there is a potential for the impact on precipitation by the air masses originating from the very evaporated Caspian Sea (Mohammadzadeh & Heydarizad, 2019). According to Mustafa et al. (2015), a partial evaporation impact is possible in the Tanjero Formation due to slow infiltration penetration into low permeability marly limestone, but the evaporation has generally only limited impact.

In general, there were higher values close to the catchment boundaries (except for wells S22 and S23) and lower values in the lowlands.

Motzer (2007) suggested the below classification based on tritium value in groundwater:

1. < 0.8 TU—water is old/sub-modern (originating from before 1950),

2. 0.8–4 TU indicating mixing of modern and old/sub-modern waters,
3. 5–15 TU modern waters (< 5 to 10 years),
4. 15–30 TU indicating waters affected by the higher activity concentrations of tritium in the atmosphere during bomb testing and/or nuclear accidents,
5. > 30 TU indicating groundwater recharge in about 1963 during the tritium peak caused by above-ground nuclear testing.

In reference to this classification, only samples S13 and S23 belong show old age originating before 1950 and the others are a mix of modern and old groundwaters. Samples S13 are from the Quaternary intergranular aquifer and S23 is from aquitard. Tritium concentration increases with depth down to 125 m (4.9 TU) and then decreases with depth until it reaches the concentration of 1.7 TU at a depth of 450 m. There are several possibilities for the age of groundwater for most of the groundwater samples, from young around 10 years old up to 70 years. Groundwater samples that are classified as modern are relatively shallow groundwaters (S3, S4, S14, S18, and S21) and they are assumed to be from unconfined aquifer. On the other hand, samples from higher depths show older ages and they are supposed to be from confined aquifer, similar to the finding of Lindsey et al. (2019). The presence of higher tritium concentration at shallower depths suggests that the groundwater was recharged by recent precipitation compared to the mixing with the older groundwater in the deeper parts of the flow system (Kashiwaya et al., 2017).

Groundwater samples that are classified as modern are relatively shallow (Figure 23). Samples of modern groundwater ages are in the nearest 20% of the distance from the outcrop area and the shallowest 10% of the aquifer system. The groundwater samples with mixed ages, most sites were relatively shallow and near the outcrop area. The two mixed samples that are farthest from the outcrop are from relatively shallow wells. Some wells near the outcrop are classified as premodern, but groundwater ages can be premodern near the outcrop if the aquifer is confined.

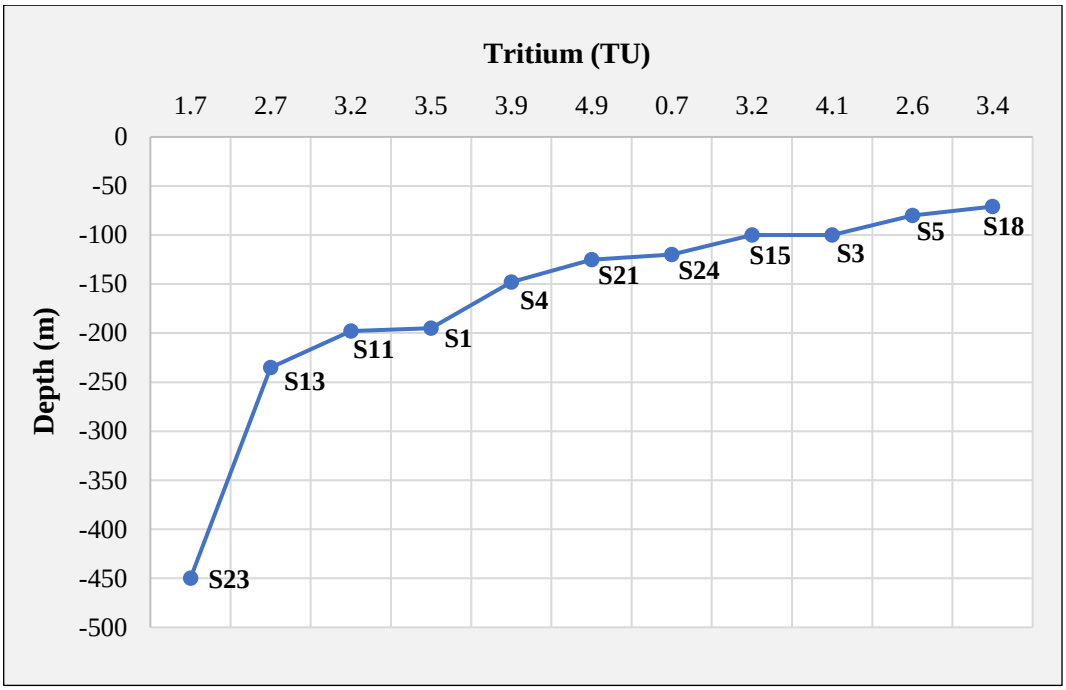

Figure 23. Tritium vs depth of water wells

The older waters sample (S13), with the minimum tritium concentration of ≤ 0.8 TU is characterized by very high mineralization (2,980 µS/cm) (Figure 24), which can be interpreted as a consequence of limited flushing in stagnating zone of relatively low permeability.

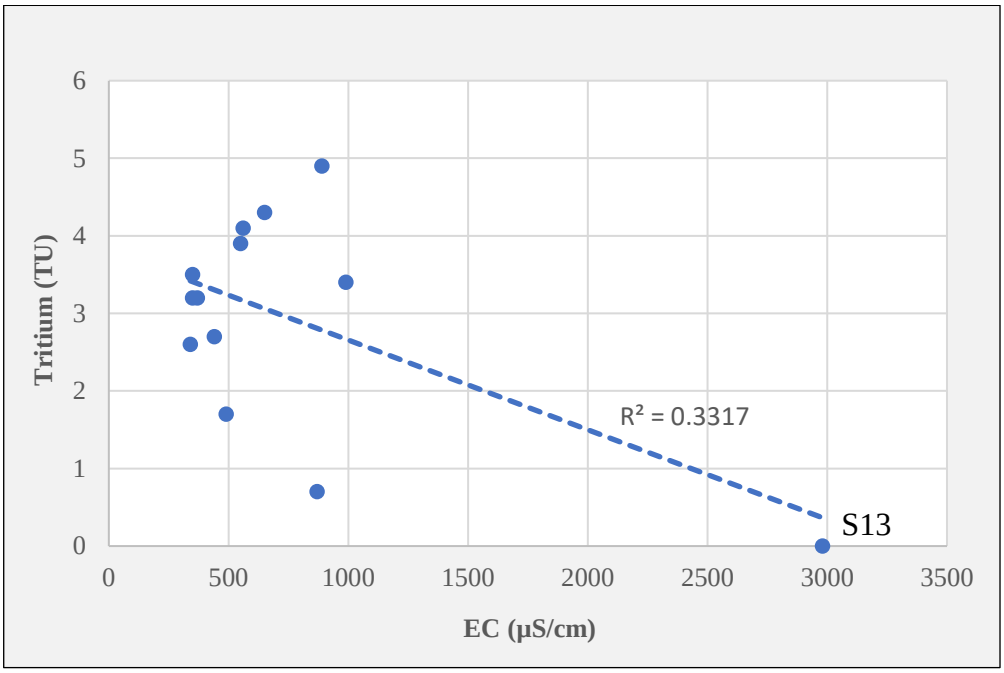

Figure 24. Relations between tritium and EC.

Furthermore, the correlation between tritium and ^{18}O in various groundwaters is limited, as shown in Figure 25. Enriched waters, in terms of ^{18}O, correspond to modern waters that have higher concentrations of tritium. The presence of the aquifer outcrop in certain areas (Mustafa, 2007; Kareem et al., 2018) can result in the evaporation of recharged water and the subsequent isotopic enrichment of the groundwater (Habi Hamani et al., 2022). The water samples can be categorised into two main groups: Group I, which is composed of samples recharged by recent infiltrations of precipitation (> 1 TU), and Group II, which consists of samples recharged by older water. The majority of the measured samples belong to group I, with the exception of samples S13 and S23, which belong to group II. Sample S23 is derived from an aquitard and is indicative of previous recharge that occurred through fractures caused by tectonic stress in the region (Mustafa, 2007).

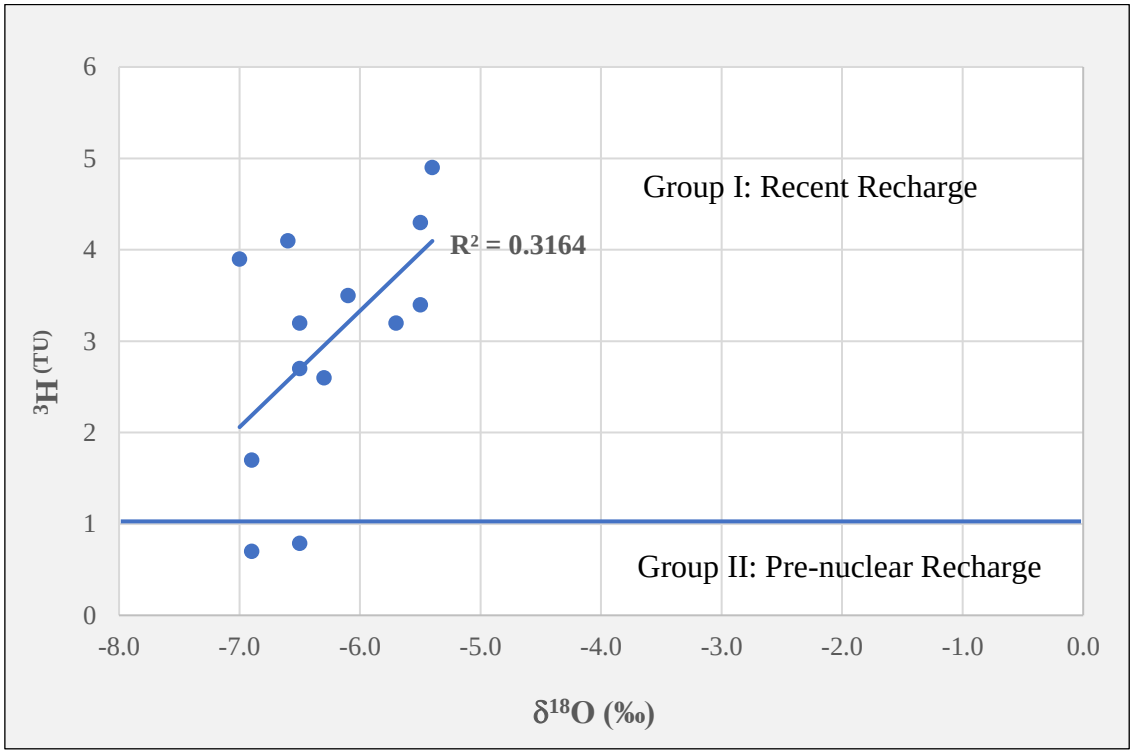

Figure 25. Relations between ^3H and ^{18}O.

6. Conclusions

Investigation of groundwater in the Sulaimani-Warmawa Sub-basin in the Kurdistan Region of Iraq was conducted using hydrogeology and geochemistry tools provided data for developing a conceptual model of groundwater chemistry evolution, groundwater recharge amount and timing as well as groundwater age determination. The area of interest is in the Kurdistan Region of Iraq, located in the Zagros Basin. It is a semi-arid region with seasonal precipitation, with a maximum in January. The hydrogeological map has been prepared for the SWSB indicating the groundwater flow direction from north and northeast towards south and southwest, i.e., the groundwater flows from the recharge area in the mountains towards the Tanjero River and then the Darbandikhan Lake. In general, the evolution of water chemistry is characterised by a transition from Ca-HCO_3 groundwater type close to the recharge area in the basin boundaries towards Ca-Mg-HCO_3 groundwater type close to the Tanjero River in the axis of the basin. The dissolution of carbonates takes place in recharge area close to the groundwater divide. In some wells, higher concentrations of sodium (Na^+), chloride (Cl^-), and sulphate (SO_4^{2-}) have been produced by the dissolution of halite and gypsum minerals embedded in carbonate rocks. This dissolution process leads to a reduction in bicarbonate concentration due to the common ion effect. The pH values are slightly alkaline or alkaline; in addition, redox parameters indicate a moderately reducing environment. The simultaneous existence of iron (Fe) and nitrate (NO_3^-) in certain samples is possibly due to groundwater mixing in long-screen pumping wells.

The concentrations of Ba can reach up to 0.383 mg/L. The concentrations of other geogenic contaminants, such as Mn, As, F^-, and Cr, are either low or below the detection limit. Speciation modeling was conducted and showed that the Fe(II)/Fe(III) pair's Eh values ranged from 0.122 to +0.114 V, consistent with moderately reducing conditions. Along the flow path, total carbon content increases from 2.2 to 6.81 mmol/kgw. Wells near the groundwater divide show relatively low concentrations, while those along the valley axis show higher values and reach either calcite and dolomite supersaturation or equilibrium.

Furthermore, inverse geochemical modelling was conducted on selected profiles, and the mass transfer coefficients in geochemical reactions were calibrated using the measured ^{13}C values. The mass transfer coefficients for interactions with carbonates are relatively low compared to much higher values observed for halite and gypsum. The isotopes ^{2}H and ^{18}O indicated recharge from winter precipitation with no or limited evaporation. The values of dissolved ^{13}C (DIC) suggest that there has been an interaction with carbonates and the source

of CO_2 is likely C4 plants. The values of $^{87}Sr/^{86}Sr$ ratio in groundwater show limited variability and are in a good agreement with carbonate dissolution as a primary process.

In general, the tritium concentration in the groundwater samples was from less than 0.8 to 4.9 TU. There were higher values close to the catchment boundaries (except for wells S22 and S23) and lower values in the lowlands. The water samples have been categorised into two main groups: Group I, which is composed of samples recharged by recent infiltrations of precipitation (> 2 TU), and Group II, which consists of water samples which contain older water.

7. Recommendations

Based on the results of the study, the following recommendations are proposed for future studies for establishing better management plan of groundwater resources:

1. A comprehensive hydrogeological study should be conducted to determine the depth and boundary of each aquifer.

2. More detailed hydrogeochemical and isotopic studies should be conducted in the area for a better understanding of geochemical processes.

3. Well monitoring system plan should be prepared to obtain continuous hydrogeological and hydrogeochemical data.

4. Future work should focus on interactions in the hyporheic zone of the Tanjero River and the impact of seasonal cyclic drying and flooding of river sediments.

5. Comprehensive monitoring of geogenic contaminants of Ba, F and As is needed to consider potential contamination sources.

Probably, the most severe threat to groundwater quality are interactions of the studied aquifers with the heavily contaminated Tanjero River. Treatment of water in the river is very important and a water treatment plant should be built in Sulaimani.

References

Adimalla, N. and Taloor, A.K., 2020. Introductory editorial for 'Applied Water Science'special issue:"Groundwater contamination and risk assessment with an application of GIS". Applied Water Science, 10, pp.1-2.

Al Manmi D A, (2008). Water resources management in Rania area, Sulaimaniyah NE-Iraq. Ph.D. Thesis, University of Baghdad, Baghdad, Iraq.

Alarcón-Herrera, M. T., Bundschuh, J., Nath, B., Nicolli, H. B., Gutierrez, M., Martín-Dominguez, I. R., Reyes-Gomez, V. M., Nuñez, D., Martín-Domínguez, A., & Sracek, O. (2013). Co-occurrence of arsenic and fluoride in groundwater of semi-arid regions in Latin America: Genesis, mobility and remediation. Journal of Hazardous Materials, 262, 960–969.

Al-Charideh, A. R. (2011). Environmental isotope study of groundwater discharge from the large karst springs in the west Syria. Environment and Earth Science, 63, 1–10.

Ali, K. K., Al-Kubaisi, Q. Y., & Al-Paruany, K. B. (2015). 'Isotopic study of water resources in a semi-arid region, western Iraq. Environmental Earth Sciences, 74(2), 1671–1686. https:// doi. org/ 10. 1007/ s12665- 015- 4172-6.

Ali, S. S., (2007). Geology and hydrogeology of Sharazoor - Piramagroon Basin in Sulaimani Area, Northeastern Iraq. Unpublished Ph.D. Thesis, Faculty of Mining and Geology, University of Belgrade, Serbia, 330 p.

Al-Jiburi, H. K. et al. (2015). Hydrogeological map of Iraq, scale 1: 1000 000, 2013. Iraqi Bulletin of Geology and Mining, 11(1):17–26. Available at: https:// www. iasj. net/ iasj/ downl oad/69d0e c38d8 54102b.

Alley WM, Healy RW, LaBaugh JW et al (2002) Flow and storage in groundwater systems. Science 296:1985–1990.

Alley, K. D., Maurya, N. and Das, S. (2018) 'Parameters of Successful Wastewater Reuse in Urban India', Indian Politics & Policy, 1(2). doi: 10.18278/inpp.1.2.4.

Al-Surdashy, A.M., 1988: Study of facies and depositional environments of Sinjar Formation in Sulaimaniya sections, Northeastern Iraq. Unpublished M.Sc. thesis, Salahaddin University, 164p.

Ameen B. M., 2006: Sequence stratigraphy of Gercus Formation (Middle Eocene) In Sulaimanyia area, Northeast Iraq. Iraqi Jour. of earth science, Vol.6, No.2, 23-32.

Amini M, Johnson A, Abbaspour KC, Mueller K (2009) Modeling large scale geogenic contamination of groundwater, combination of geochemical expertise and statistical techniques. 18th World IMACS/MODSIM Congress, Cairns, pp 4100–4106.

Appelo, C. A. J., & Postma, D. (2005). Geochemistry, groundwater and pollution (2nd ed.). CRC Press.

Aravena, R. and Wassenaar, L.I., 1993. Dissolved organic carbon and methane in a regional confined aquifer, southern Ontario, Canada: Carbon isotope evidence for associated subsurface sources. Applied Geochemistry, 8(5), pp.483-493.

Aullón Alcaine, A. et al. (2020) 'Hydrogeochemical controls on the mobility of arsenic, fluoride and other geogenic co-contaminants in the shallow aquifers of northeastern La Pampa Province in Argentina', Science of the Total Environment. Elsevier B.V., 715, p. 136671. doi: 10.1016/j.scitotenv.2020.136671.

Banner, J. L., 2004, Radiogenic isotopes: systematics and applications to earth surface processes and chemical stratigraphy, Earth Science Reviews, 65, 141–94.

Bhattacharya, P., Lesafi, F., Filemon, R., Ligate, F., Ijumulana, J. and Mtalo, F., 2016, April. Geogenic fluoride and arsenic contamination in the groundwater environments in Tanzania. In EGU General Assembly Conference Abstracts (pp. EPSC2016-16677).

Bellen, R. C., Dunnington, H. V., Wetzel, R., & Morton, D. (1959). Lexique Stratigraphique International, Iraq. Vol. III, Asie, Fasc. 10a, Paris. 336 p.

Bentley, H.W., Phillips, F.M., Davis, S.N., Gifford, S., Elmore, D., Tubbs, L.E. and Gove, H.E., 1982. Thermonuclear 36Cl pulse in natural water. Nature, 300(5894), pp.737-740.

Bodrud-Doza, M., Islam, S.D.U., Hasan, M.T., Alam, F., Haque, M.M., Rakib, M.A., Asad, M.A. and Rahman, M.A., 2019. Groundwater pollution by trace metals and human health risk assessment in central west part of Bangladesh. Groundwater for sustainable development, 9, p.100219.

Bolton, C.M.G., 1958. The Geology of Ranyia area. Site Inv. Co., Unpubl. Report, GEOSURV Library, Baghdad.

Bouwer H, Rice RC. 1976. A slug test for determining hydraulic conductivity of unconfined aquifers with completely or partially penetrating wells. Water Resources Research 12: 423–428.

Bresciani, E., Cranswick, R.H., Banks, E.W., Batlle-Aguilar, J., Cook, P.G. and Batelaan, O., 2018. Using hydraulic head, chloride and electrical conductivity data to distinguish between mountain-front and mountain-block recharge to basin aquifers. Hydrology and Earth System Sciences, 22(2), pp.1629-1648.

Bretzler, A. and Johnson, C.A., 2015. The Geogenic Contamination Handbook: Addressing arsenic and fluoride in drinking water. Applied Geochemistry, 63, pp.642-646.

Buday, T. (1980). Regional geology of Iraq: Vol. 1, Stratigraphy, I. I. Kassab & S. Z. Jassim (Eds.) D. G. Geo Survey. Min. Invest. Publication. 445 p.

Buday, T., & Jassim, S. Z. (1987). The regional geology of Iraq: Tectonics, magmatism, and metamorphism. I. I. Kassab & M. J. Abbas (Eds.), Baghdad, 445 p.

Bullen, T.D. and Kendall, C., 1998. Tracing of weathering reactions and water flowpaths: a multi-isotope approach. In Isotope tracers in catchment hydrology (pp. 611-646). Elsevier.

Bundschuh, J. et al. (2020) 'Arsenic in Latin America: New findings on source, mobilization and mobility in human environments in 20 countries based on decadal research 2010-2020', Critical Reviews in Environmental Science and Technology. Taylor & Francis, 51(16), pp. 1–139. doi: 10.1080/10643389.2020.1770527.

Chae, G. T., Yun, S. T., Mayer, B., Kim, K. H., Kim, S. Y., Kwon, J. S., et al. (2007). Fluorine geochemistry in bedrock groundwater of South Korea. Science of the Total Environment, 385, 272–283.

Chukwura UO, Udom GJ, Cuthbert SJ, Hursthouse AS (2015) Evaluation of hydrochemical characteristics and flow directions of groundwater quality in Udi Local Government Area Enugu State, Nigeria. Environ Earth Sci 73:4541–4555.

C Kendall, JJ McDonnell (eds). 1998. Isotope Tracers in Catchment Hydrology. Elsevier: Amsterdam.

Clark, I., & Fritz, P. (1997). Environmental isotopes in hydrogeology, Lewis, 328 p.

Cook P, Herczeg AL (2000) Environmental tracers in subsurface hydrology. Kluwer, Boston.

Craig, H. (1961). Isotopic variations in meteoric waters. Science, 133, 1702–1703. https:// doi. org/ 10. 1126/ scien ce. 133. 3465. 1702.

Dansgaard, W., 1964. Stable isotopes in precipitation. tellus, 16(4), pp.436-468.

Davies, J. C. (2002). Statistics and data analysis in geology (3rd ed.). John Wiley & Sons.

Davis, S.N. and BENTLEY, H.W., 1982. Dating groundwater: A short review.

Davis S. N, De Wiest RJM: 1966. Hydrogeology. Wiley, New York

Dillon, P., 2005. Future management of aquifer recharge. Hydrogeology journal, 13(1), pp.313-316.

Dingman LS (2015) Physical hydrology. Waveland Press Inc.

Directorate of Groundwater of Sulaimani, DoGWS. (2020). Ministry of Agriculture and Water Resourcses, Kurdistan Regional Government, Kurdistan Region, Iraq. https:// gov. krd/ moawr.

Domenico, P. A., F. W. Schwartz, Physical and Chemical Hydrogeology 2, 506, John Wiley, New York, 1998.

Dragon, K. and Gorski, J., 2015. Identification of groundwater chemistry origins in a regional aquifer system (Wielkopolska region, Poland). Environmental Earth Sciences, 73, pp.2153-2167.

Drever JI (1997) The geochemistry of natural waters, 3rd edn. Prentice Hall, New Jersey, 436 pp.

Edmunds WM, Smedley PL (1996). Groundwater geochemistry and health: An overview. In: Appleton JD, Fuge R, McCall GJH (eds.) Environmental geochemistry and health with special reference to developing countries. Geological Society Special Publication No.113, pp. 91-105.

Edmunds, W.M. and Smedley, P.L., 2000. Residence time indicators in groundwater: the East Midlands Triassic sandstone aquifer. Applied Geochemistry, 15(6), pp.737-752.

Edmunds, W.M. and Smedley, P.L., 2012. Fluoride in natural waters. In Essentials of medical geology: Revised Edition (pp. 311-336). Dordrecht: Springer Netherlands.

El Ouali, A., Roubil, A., Lahrach, A., Moudden, F., Ouzerbane, Z., Hammani, O. and El Hmaidi, A., 2023. Assessment of groundwater quality and its recharge mechanisms using hydrogeochemical and isotopic data in the Tafilalet plain (south-eastern Morocco). Mediterranean Geoscience Reviews, 5(1), pp.1-14.

El-Rawy, M., Zlotnik, V.A., Al-Raggad, M., Al-Maktoumi, A., Kacimov, A. and Abdalla, O., 2016. Conjunctive use of groundwater and surface water resources with aquifer recharge

by treated wastewater: evaluation of management scenarios in the Zarqa River Basin, Jordan. Environmental Earth Sciences, 75, pp.1-21.

Elumalai, V., Rajmohan, N., Sithole, B., Li, P., Uthandi, S. and van Tol, J., 2023. Geochemical evolution and the processes controlling groundwater chemistry using ionic ratios, geochemical modelling and chemometric analysis in uMhlathuze catchment, KwaZulu-Natal, South Africa. Chemosphere, 312, p.137179.

Environmental Protection Agency, EPA, 2022 (Department of Agriculture, Water and the Environment, 2022).

EPA (U.S. Environmental Protection Agency). (2005). Toxicological review of barium and compounds. Washington, DC: US Environmental Protection Agency. Resource document. http://www.epa.gov/iris/toxreviews/0010tr.pdf.

Eriksson, E. (1983). Stable isotopes and tritium in precipitation. Guidebook on Nuclear Techniques in Hydrology. 1983 Technical Report Series No. 91 International Atomic Energy Agency, Vienna.

Faimon, J., Ličbinská, M., Zajíček, P., & Sracek, O. (2012). Partial pressures of CO2 in epikarstic zone deduced from hydrogeochemistry of permanent drips, the Moravian Karst. Czech Republic, Acta Carsologica, 41(1), 47–57.

Faure, G. (1986). "Principles of Isotope Geology," John Wiley and Sons, New York.

Fawell J, Bailey K, Chilton J, Dahi E, Fewtrell L, Magara Y (2006) Fluoride in drinking water. IWA, London.

Fendorf, S., Michael, H.A. and van Geen, A., 2010. Spatial and temporal variations of groundwater arsenic in South and Southeast Asia. Science, 328(5982), pp.1123-1127.

Fetter CW (2001). Historical Knowledge and Use of Groundwater.www.appliedhydrogeology.info/History_files.

Flem, B. et al. (2018) 'Graphical statistics to explore the natural and anthropogenic processes influencing the inorganic quality of drinking water, ground water and surface water', Applied Geochemistry. Elsevier Ltd, 88, pp. 133–148. doi: 10.1016/j.apgeochem.2017.09.006.

Ford, D., & Williams, D. (2007). Karst hydrogeology and geomorphology, 2nd Edition, John Wiley & Sons, Ltd.

Foster, S.S.D. and Chilton, P.J., 2003. Groundwater: the processes and global significance of aquifer degradation. Philosophical Transactions of the Royal Society of London. Series B: Biological Sciences, 358(1440), pp.1957-1972.

Freeze RA, Cherry JA (1979) Groundwater. Printice-Hall, New Jersey.

Frommen, T., Groeschke, M., Nölscher, M., Koeniger, P. and Schneider, M., 2021. Anthropogenic and geogenic influences on peri-urban aquifers in semi-arid regions: insights from a case study in northeast Jaipur, Rajasthan, India. Hydrogeology Journal, 29, pp.1261-1278.

Frost, C. D., & Toner, R. (2004). Strontium isotopic identification of water-rock interaction and ground water mixing. Ground Water, 42(3), 418–432.

Gat JR (2010) Isotope hydrology: A study of the water cycle. Series on environmental science and management. Vol 6. Imperial College Press, London.

Gat, J. R., & Carmi, I. (1970). Evolution of the isotopic composition of atmospheric waters in the Mediterranean Sea area. Journal of Geophysical Research, 75, 3039–3048.https:// doi. org/ 10. 1029/ JC075 i015p 03039.

Gat, J. R., & Issar, A. (1974). Desert isotopes hydrology: water resources of the Sinai desert, Geochim. Cosmochim. Acta. 38:1117-31.

Gleeson, T., VanderSteen, J., Sophocleous, M. et al. Groundwater sustainability strategies. Nature Geosci 3, 378–379 (2010). https://doi.org/10.1038/ngeo881.

Gleick, P.H., 2003. Global freshwater resources: soft-path solutions for the 21st century. Science, 302(5650), pp.1524-1528.

Goldscheider, N., 2005. Karst groundwater vulnerability mapping: application of a new method in the Swabian Alb, Germany. Hydrogeology Journal, 13, pp.555-564.

Goldscheider, N., Meiman, J., Pronk, M. and Smart, C., 2008. Tracer tests in karst hydrogeology and speleology. International Journal of speleology, 37(1), p.3.

Gupta, S., Nandimandalam, J.R., Pant, D., Chatterjee, S. and Ram, P., 2023. Environmental isotope constraints and hydrogeochemical evolution of groundwater in the semi-arid national capital environs of Delhi, India. Urban Climate, 49, p.101481.

Halm, D., Gaiser, T., & Stahr, K. (2002). Seepage and groundwater recharge in sandy soils of the semi-arid region of Picos, Northeast Brazil. Neues Jahrbuch Fur Geologie Und Palaontologie-Abhandlungen, 225, 85–101.

Hamamin, D. F., et al. (2018). 'Hazard and risk intensity maps for water-bearing units: A case study', International. Journal of Environmental Science and Technology, 15(1), 173–184. https:// doi. org/ 10. 1007/ s13762- 017- 1376-1.

Hamamin, D.F. and Ali, S.S., 2013. Hydrodynamic study of karstic and intergranular aquifers using isotope geochemistry in Basara basin, Sulaimani, North-Eastern Iraq. Arabian Journal of Geosciences, 6, pp.2933-2940.

Hamani, A.H.H., Adamou, M.M., Sandao, I. and Hado, H.A., 2022. Physico-Chemical and Isotopic (18O, 2H and 3H) Characterization of the Upper Dallol Maouri Watershed (Niger). Open Journal of Geology, 12(8), pp.613-639.

Hammer, Ø., Harper, D. A. T., & Ryan, P. D. (2001). PAST: Paleontological software for education and data analysis. Paleontological Association. https:// palaeo- elect ronica. org/ 2001_1/ past/ issue1_ 01. htm.

Han, G. and Liu, C.Q., 2004. Water geochemistry controlled by carbonate dissolution: a study of the river waters draining karst-dominated terrain, Guizhou Province, China. Chemical Geology, 204(1-2), pp.1-21.

Harrington, G. A., Cook, P. G., & Herczeg, A. L. (2002). Spatial and temporal variability of groundwater recharge in central Australia: A tracer approach. Ground Water, 40, 518–527.

Hem, J.D., 1985. Study and interpretation of the chemical characteristics of natural water (Vol. 2254). Department of the Interior, US Geological Survey.

Hunt, R.J., Bullen, T.D., Krabbenhoft, D.P. and Kendall, C., 1998. Using stable isotopes of water and strontium to investigate the hydrology of a natural and a constructed wetland. Groundwater, 36(3), pp.434-443.

International Atomic Energy Agency (IAEA). (1983). "Guidebook on Nuclear Techniques in Hydrology 1983 edition Technical Report Series No. 91 IAEA, Vienna, 1983.

Jassim, S.Z., Karim, S.A., Basi, M.A., Al-Mubarak, M.A. and Munir, J.,1984. Final Report of the Regional Geological Survey of Iraq. Vol.3, Stratigraphy. GEOSURV, int. rep. no. 1447.

Jassim, S. Z., & Goff, J. C. (2006). Geology of Iraq. Jassim (Eds.) D. G. Geo Survey. Min. Invest. Publication. 445 p.

Kalin, R.M., Murphy Jr, C.E. and Hall, G., 1995. Reconstruction of tritium release history from contaminated groundwater using tree ring analysis. Fusion Technology, 28(3P1), pp.883-887.

Kareem, A., Mustafa, O., & Merkel, B. (2018). Geochemical and environmental investigation of thae water resources of the Tanjero area, Kuristan region, Iraq. Arabian Journal of Geosciences, 11, 461.

Karim, K. H. (2004) Basin analysis of Tanjero Formation in Sulaimaniya area, NE-Iraq. PhD Thesis, University of Sulaimani, Iraq.

Karim, K., & Ali, S. S. (2004). Origin of dislocated limestone blocks on the slope side of Baranan (Zirgoez) Homocline: An attempt to outlook the development of western part of Sharazoor Plain. (JZS) Journal of Zankoy Sulaimani, 3(1), 5–21.

Karim, K.H., Khalid, M.I. and Bakhtiar, M.A., 2008. Lithostratigraphic study of the contact between Kometan and Shiranish formations (Cretaceous) from Sulaimaniyah Governorate, Kurdistan Region, NE Iraq. Iraqi Bull. Geol. Min., Vol.4, No.2, p. 16 – 27.

Kashiwaya, K., Muto, Y., Kubo, T., Ikawa, R., Nakaya, S., Koike, K. and Marui, A., 2017. Spatial variations of tritium concentrations in groundwater collected in the southern coastal region of Fukushima, Japan, after the nuclear accident. Scientific reports, 7(1), p.12578.

Katz, B.G., Coplen, T.B., Bullen, T.D. and Davis, J.H., 1997. Use of chemical and isotopic tracers to characterize the interactions between ground water and surface water in mantled karst. Groundwater, 35(6), pp.1014-1028.

Kendall, C., & Coplen, T. B. (2001). Distribution of oxygen-18 and deuterium in river waters across the United States. Hydrological Processes, 15(7), 1363–1393.

Khanaqa, P.A. and Al-Manmi, D.A., 2011. Hydrogeochemistry and geomicrobiology of Darzila spring in Sangaw, Sulaimaniyah, NE Iraq. Iraqi Bulletin of Geology and Mining, 7(3), pp.63-79.

Khosravi, R., Zarei, M., & Sracek, O. (2020). Hydraulic and geochemical interactions between surface water and sediment pore water in seasonal hypersaline Maharlu Lake, Iran. Hydrological Processes, 34, 3358–3369.

Konikow, L.F., 2011. Contribution of global groundwater depletion since 1900 to sea-level rise. Geophysical Research Letters, 38(17).

Langmuir, D., 1997. Aqueous environmental. Geochemistry Prentice Hall: Upper Saddle River, NJ, 600.

Lee, E., Shin, D., Hyun, S.P., Ko, K.S., Moon, H.S., Koh, D.C., Ha, K. and Kim, B.Y., 2017. Periodic change in coastal microbial community structure associated with submarine groundwater discharge and tidal fluctuation. Limnology and Oceanography, 62(2), pp.437-451.

Lindsey, B. D., Jurgens, B. C. and Belitz, K. (2019) 'Tritium as an Indicator of Modern, Mixed, and Premodern Groundwater Age, USGS Scientific Investigations Report 2019-5090'.

Mahmmud, R., Sracek, O., Mustafa, O., Čejková, B., Jačková, I. and Vondrovicová, L., 2022. Groundwater geochemistry evolution and geogenic contaminants in the Sulaimani-Warmawa Sub-basin, Sulaimani, Kurdistan Region, Iraq. Environmental Monitoring and Assessment, 194(5), p.352.

Maimaiti, A., Deng, S., Meng, P., Wang, W., Wang, B., Huang, J., Wang, Y. and Yu, G., 2018. Competitive adsorption of perfluoroalkyl substances on anion exchange resins in simulated AFFF-impacted groundwater. Chemical Engineering Journal, 348, pp.494-502.

Markovich, K. H., Manning, A. H., Condon, L. E., & McIntosh, J. C. (2019). Mountain-block recharge: A review of current understanding. Water Resources Research, 55(11), 8278–8304.

Masoud, M., El Osta, M., Alqarawy, A. and Ezzeldin, H., 2023. Application of Environmental Isotopes and Hydrochemistry to Identify the Groundwater Recharge in Wadi Qanunah Basin, Saudi Arabia. Sustainability, 15(3), p.2648.

Mazor, E. (1976). Multitracing and multisampling in hydrological studies. Interpretation of environmental isotopes and hydrochemical data in groundwater hydrology. Proceedings of an advisory group meeting. Vienna 27-31 January, 1975. IAEA, Vienna.

Mazor, E. (2004). Chemical and isotopic groundwater hydrology (3rd ed., p. 465p). Weizmann Institute of Science Rehovot.

McMahon, P. B., & Chapelle, F. (2008). Redox processes and water quality of selected principal aquifer systems. Groundwater, 46, 259–271.

Mickler, P.J., Banner, J.L., Stern, L., Asmerom, Y., Edwards, R.L. and Ito, E., 2004. Stable isotope variations in modern tropical speleothems: evaluating equilibrium vs. kinetic isotope effects. Geochimica et Cosmochimica Acta, 68(21), pp.4381-4393.

Michael-Kordatou, I., Karaolia, P. and Fatta-Kassinos, D., 2018. The role of operating parameters and oxidative damage mechanisms of advanced chemical oxidation processes in the combat against antibiotic-resistant bacteria and resistance genes present in urban wastewater. Water Research, 129, pp.208-230.

Mohammadzadeh, H., & Heydarizad, M. (2019). δ18O and δ2H characteristics of moisture sources and their role in surface water recharge in the north-east of Iran. Isotopes in Environmental and Health Studies, 55(6), 550–565. https:// doi. org/ 10. 1080/ 10256 016. 2019. 16805 52

Mohammadzadeh, H., Eskandari Mayvan, J., & Heydarizad, M. (2020). The effects of moisture sources and local parameters on the 18O and 2H contents of precipitation in the west of Iran and the east of Iraq. Tellus, Series B: Chemical and Physical Meteorology, 72(1), 25–39. https:// doi. org/ 10. 1080/ 16000 889. 2020. 17212 24.

Molina Carpio, Jorge & Espinoza Romero, Daniel & Caloir, Beatriz & F, Rodolfo & Pacheco, Paula & Lima, Wilson & Uría Arraya, Alvaro & Cornejojo, Coraly & Hernandez, Daniel & Carrasco, Carlos & Castel, Ana Paola. (2018). Water resources management under climate change scenarios: Case studies in Bolivia. 10.13140/RG.2.2.26092.26243.

Mook, W. G. (2001) 'Environmental isotopes in the hydrological cycle: Principles and applications, Volume I: Introduction: Theory, Methods, Review', International Hydrological Programme IHP-V, 1, pp. 1–165. Available at: http:// wwwna web. iaea. org/ napc/ ih/ docum ents/ global_ cycle/ Envir onmen tal% 20Iso topes% 20in% 20the% 20Hyd rolog ical% 20Cyc le% 20Vol% 201. pdf.

Motzer, W., 2007. Tritium age dating of groundwater. Hydro visions, 16(2).

Moussaoui, I., Rosa, E., Cloutier, V., Neculita, C.M. and Dassi, L., 2023. Chemical and isotopic evaluation of groundwater salinization processes in the Djebeniana coastal aquifer, Tunisia. Applied Geochemistry, 149, p.105555.

Mustafa, O. (2006). Impact of sewage wastewater on the environment of Tanjero River and its basin with Sulaimani City/NE-Iraq, M.Sc. Thesis, University of Sulaimani-College of Science, Dep. of Geology.

Mustafa, O., & Ahmad, H. (2008). Nitrate pollution in groundwater of Sulaimaniyah City, Kurdistan Region, NE Iraq. Iraqi Bulletin of Geology and Mining, 4(2), 73–82.

Mustafa, O., & Merkel, B. (2015). Geochemical evolution and water–rock interactions in Makook Karst aquifers, Kurdistan Region, Iraq. Topical issues of rational use of natural resources, April 22–24, 2015a, St. Petersburg, Russia, National Mineral Resources University, p. 12–14.

Mustafa, O., Mahmmud, R., Sracek, O. and Seeyan, S., 2023. Geogenic Sources of Arsenic and Fluoride in Groundwater: Examples from the Zagros Basin, the Kurdistan Region of Iraq. Water, 15(11), p.1981.

Mustafa, O., Merkel, B., & Weise, S. (2015). Assessment of hydrogeochemistry and environmental isotopes in karst springs of Makook Anticline, Kurdistan Region, Iraq. Hydrology, 2, 48–68.

Mustafa, O., Tichomirowa, M., Kummer, N. A., & Merkel, B. (2016). Assessment of water-rock interaction processes in the karst springs of Makook anticline (Kurdistan Region, Iraq) using Sr-isotopes, rare earth, and trace elements. Arabian Journal of Geosciences, 9, 368. https:// doi. org/10. 1007/ s12517- 016- 2344-7.

Narany, T.S., Aris, A.Z., Sefie, A. and Keesstra, S., 2017. Detecting and predicting the impact of land use changes on groundwater quality, a case study in Northern Kelantan, Malaysia. Science of the Total Environment, 599, pp.844-853.

Nier, A. O. (1938). The isotopic constitution of strontium, barium, bismuth, thallium and mercury. Physical Review, 5, 275–279.

Nordstrom, D.K., 2011. Hydrogeochemical processes governing the origin, transport and fate of major and trace elements from mine wastes and mineralized rock to surface waters. Applied geochemistry, 26(11), pp.1777-1791.

Omar, A. A., Lawa, F. A., & Sulaiman, S. H. (2015). Tectonostratigraphic and structural imprints from balanced sections across the north-western Zagros fold-thrust belt, Kurdistan region, NE Iraq. Arabian Journal of Geosciences, 8(10), 8107–8129. https:// doi. org/ 10. 1007/ s12517- 014-1682-6.

Osati, K., et al. (2014). Spatiotemporal patterns of stable isotopes and hydrochemistry in springs and river flow of the upper Karkheh River Basin, Iran. Isotopes in Environmental and Health Studies, 50(2), 169–183. https:// doi. org/ 10.1080/ 10256 016. 2014. 857317.

Parkhurst, D. L., & Appelo, C. A. J. (1999). Guide to PHREEQC (Version 2)-a computer program for speciation, batchreaction, one-dimensional transport, and inverse geochemical calculations. Water-Resources Investigations Report 99–4259, U.S. Geological Survey.

Parrone, D., Ghergo, S., Frollini, E., Rossi, D. and Preziosi, E., 2020. Arsenic-fluoride co-contamination in groundwater: Background and anomalies in a volcanic-sedimentary aquifer in central Italy. Journal of Geochemical Exploration, 217, p.106590.

Patel, K. S. et al. (2017) 'Groundwater arsenic and fluoride in Rajnandgaon District, Chhattisgarh, northeastern India', Applied Water Science. Springer Berlin Heidelberg, 7(4), pp. 1817–1826. doi: 10.1007/s13201-015-0355-2.

Pérez-Gimeno, A., Navarro-Pedreño, J., Almendro-Candel, M.B., Gómez, I. and Jordán, M.M., 2016. Environmental consequences of the use of sewage sludge compost and limestone outcrop residue for soil restoration: salinity and trace elements pollution. Journal of soils and sediments, 16, pp.1012-1021.

Pin, C., Briot, D., Bassin, C., & Poitrasson, F. (1994). Concomitant separation of strontium and samarium-neodymium for isotopic analysis in silicate samples, based on specific extraction chromatography. Analytica Chimica Acta, 298(2), 209–217.

Prasanna, M.V., Chidambaram, S., Hameed, A.S. and Srinivasamoorthy, K., 2011. Hydrogeochemical analysis and evaluation of groundwater quality in the Gadilam river basin, Tamil Nadu, India. Journal of earth system science, 120(1), pp.85-98.

Ramos Ramos, O.E., Cáceres, L.F., Ormachea Muñoz, M.R., Bhattacharya, P., Quino, I., Quintanilla, J., Sracek, O., Thunvik, R., Bundschuh, J. and García, M.E., 2012. Sources and behavior of arsenic and trace elements in groundwater and surface water in the Poopó Lake Basin, Bolivian Altiplano. Environmental earth sciences, 66, pp.793-807.

Razmjooei, M. J., Thibault, N., Kani, A., Ullman, C. V., & Jani, A. M. (2020). Santonian-Maastrichtian carbon-isotope stratigraphy and calcareous nannofossil biostratigraphy of the Zagros Basin: Long-range correlation, similarities and differences of carbon-isotope trends at global scale. Global and Planetary Change, 184, 103075.

Rodríguez-Lado, L., Sun, G., Berg, M., Zhang, Q., Xue, H., Zheng, Q. and Johnson, C.A., 2013. Groundwater arsenic contamination throughout China. Science, 341(6148), pp.866-868.

Rozanski, K., Araguás-Araguás, L. and Gonfiantini, R., 1993. Isotopic patterns in modern global precipitation. Climate change in continental isotopic records, 78, pp.1-36.

Scanlon, B. R., Keese, K. E., Flint, A. L., Flint, L. E., Gaye, B. C., Esmunds, W. M., & Simmers, I. (2006). Global synthesis of groundwater recharge in semiarid and arid regions. Hydrological Processes, 20, 3335–3370.

Seidell, A., 1958. Solubility of Inorganic and Metal organic compounds 4th ed. Am. Chem. Soc., 964.

Sengupta, S., Sracek, O., Jean, J. -S., Yang, H. -J., Wang, C. -H., Kar, S., Babek, O., Lee, C. -Y., & Das, S. (2018). Difference in attenuation among Mn, As, and Fe in riverbed sediments. Journal of Hazardous Materials, 341, 277–289.

Schlesinger WH, Bernhardt ES (2013) Biogeochemistry: An Analysis of Global Change (3rd edn). Academic Press, Elsevier, New York.

Sharp Z (2007) Principles of stable isotope geochemistry. Prentice-Hall, New Jersey.

Sissakian, V. K. (2015). Geological map of Sulaimaniyah, Scale 1:250000', (October). https:// doi. org/ 10. 13140/ RG.2. 1. 5109.0642.

Smedley, P.L. and Kinniburgh, D.G., 2002. A review of the source, behaviour and distribution of arsenic in natural waters. Applied geochemistry, 17(5), pp.517-568.

Smedley, P.L. and Kinniburgh, D.G., 2012. Arsenic in groundwater and the environment. In Essentials of Medical Geology: Revised Edition (pp. 279-310). Dordrecht: Springer Netherlands.

Solomon, D.K., 2000. 3H and 3He, chapter 13, pp 397–424. Environmental tracers in subsurface hydrology, p.529.

Somaratne, N. and Frizenschaf, J., 2013. Geological control upon groundwater flow and major ion chemistry with influence on basin management in a coastal aquifer, South Australia. Journal of Water Resource and Protection, 2013.

Son, J.K., Kim, H.G., Kong, T.Y., Ko, J.H., Lee, G.J., 2013. Radiological effluents released and public doses from nuclear power plants in Korea. Radiat. Prot. Dosimetry 155, 517e521.

Sophocleous, M., 2002. Interactions between groundwater and surface water: the state of the science. Hydrogeology Journal, 10, pp.52-67.

Sracek, O. et al. (2019) ‘Geochemistry of thermal waters and arsenic enrichment at Antsirabe, Central Highlands of Madagascar’, Journal of Hydrology. Elsevier, 577(April), p. 123895. doi: 10.1016/j.jhydrol.2019.06.067.

Sracek, O., Kříbek, B., Mihaljevič, M., Ettler, V., Vaněk, A., Penížek, V., Filip, J., Veselovský, F. and Bagai, Z.B., 2018. Geochemistry and pH control of seepage from Ni-Cu rich mine tailings at Selebi Phikwe, Botswana. Environmental monitoring and assessment, 190, pp.1-12.

Sracek, O., Wanke, H., Ndakunda, N. N., Mihaljevič, M., & Buzek, F. (2015). Geochemistry and fluoride levels of geothermal springs in Namibia. Journal of Geochemical Exploration, 148, 96–104.

Stadler, S., Osenbrück, K., Suckow, A. O., Himmelbach, T., & Hötzl, H. (2010). Groundwater flow regime, recharge and regional-scale solute transport in the semi-arid Kalahari of Botswana derived from isotope hydrology and hydrochemistry. Journal of Hydrology, 388(3–4), 291–303.

Stevanovic, Z., & Markovic, M. (2003). Hydrogeology of northern Iraq, climate, hydrology, geomorphology, Geology. Ed. Filed documents, Vol. 1.

Stevanovic, Z., & Markovic, M. (2004). Hydrogeology of Northern Iraq, Vol.2, General Hydrogeology and Aquifer Systems. Food and Agriculture Organization of the United Nations, Rome P 264.

Studio Galli Ingegneria (SGI). (2011). Hydrogeological study for the governorate of around the center of the city, Final Report, January, 2011, Kurdistan Region, Iraq. 200p.

Stumm and Morgan, 1996 W. Stumm, J.J. Morgan Aquatic chemistry: chemical equilibria and rates in natural waters (3rd ed.), Wiley Interscience, New York (1996), pp. 672-725.

Talabi, A.O. and Tijani, M.N., 2013. Hydrochemical and stable isotopic characterization of shallow groundwater system in the crystalline basement terrain of Ekiti area, southwestern Nigeria. Applied Water Science, 3, pp.229-245.

Tirkey, P., Bhattacharya, T., Chakraborty, S. and Baraik, S., 2017. Assessment of groundwater quality and associated health risks: a case study of Ranchi city, Jharkhand, India. Groundwater for sustainable development, 5, pp.85-100.

Todd, K.D. (1980). Ground water hydrology. 2nd ed. New York: John Wiley and Sons.

Todd, D.K. and Mays, L.W., 2004. Groundwater hydrology. John Wiley & Sons.

Tossou, Y.Y.J., Orban, P., Gesels, J., Otten, J., Yessoufou, S., Boukari, M. and Brouyère, S., 2017. Hydrogeochemical mechanisms governing the mineralization and elevated fluoride\left (F^-\right) F-contents in Precambrian crystalline aquifer groundwater in central Benin, Western Africa. Environmental Earth Sciences, 76, pp.1-14.

Tóth, J. (1999). Groundwater as a geological agent: An overview of the causes, processes, and manifestations. Hydrogeology J., 7, 1–14.

Tóth, J. (2009). Gravitational systems of groundwater flow. Cambridge University Press.

Trenberth, K.E. and Dai, A., 2007. Effects of Mount Pinatubo volcanic eruption on the hydrological cycle as an analog of geoengineering. Geophysical Research Letters, 34(15).

UN World Water Development Report (2018), Nature-based Solutions for Water.

United Nations Development Programme (UNDP), (2017). Sustainable Development Goals Report.

Uugulu, S., & Wanke, H. (2020). Estimation of groundwater recharge in savannah aquifers along a precipitation gradient using chloride mass balance method and environmental isotopes, Namibia. Physics and Chemistry of the Earth, Parts a/b/c, 116, 102844.

Veizer, J. (1989). Strontium isotopes in seawater through time. Annual Review of Earth and Planetary Sciences, 17, 141–167.

WHO (2011) Guidelines for drinking water quality, 4th edn. World Health Organization, Geneva.

WHO. (2017). Guidelines for Drinking-water Quality. https://www. who. int/ publi catio ns/i/ item/ 97892 41550 017.

Winter, T.C., J.W. Harvey, O.L. Franke, and W.M. Alley. 1998. Groundwater and surface water: A single resource. USGS Circular 1139.

World Health Organisation (WHO) (2004) Guidelines for drinking water quality, 3rd edn, vol 1, Recommendations, Geneva, Switzerland.

Yang, D.J., Chen, X.Q., Li, B., 2012. Tritium release during nuclear power operation in China. J. Radiol. Protect. 32, 167e173.

Appendices

Appendix 1: Table S1: Water wells information

Well Code	Governorate	District	Subdistrict	Site/Village	Longitude	Latitude	Elevation (m)	Depth (m)
S1	Sulaimani	Centre	Centre	Hawari Shar Park	539010	3941941	966	195
S2	Sulaimani	Centre	Centre	Kobany city	529355	3940350	830	180
S3	Sulaimani	Centre	Bakrajo	Qulqula Village	535422	3951104	1050	100
S4	Sulaimani	Centre	Bakrajo	Qzlar Village	526716	3958232	1224	148
S5	Sulaimani	Centre	Bakrajo	Qamartly Village	525764	3946404	985	80
S6	Sulaimani	Centre	Bakrajo	Sardarawa area	524297	3937421	767	53
S7	Sulaimani	Centre	Warmawa	Baiyzawa	561080	3906142	603	140
S8	Sulaimani	Centre	Halabjay Taza	Halabjay Taza	560968	3906026	600	170
S9	Sulaimani	Centre	Warmawa	Qaragol Village	557030	3912358	555	24
S10	Sulaimani	Centre	Arbat	Barika Residential	554625	3915225	608	85
S11	Sulaimani	Centre	Arbat	Ashty camp	555874	3918729	638	198
S12	Sulaimani	Centre	Arbat	Damrkan Village	547326	3924423	753	171
S13	Sulaimani	Centre	Arbat	Zrgwez Village	540677	3918058	970	235
S14	Sulaimani	Centre	Arbat	Bardakar Village	540758	3923131	719	100
S15	Sulaimani	Saidsadq	Saidsadq	Kani Panka area	565412	3915692	557	100
S16	Sulaimani	Centre	Tanjero	Weladar Village	552716	3920876	717	130
S17	Sulaimani	Centre	Arbat	Koza Raqa Village	548534	3924063	766	160
S18	Sulaimani	Centre	Centre	Industrial area of Sulaimani	534865	3934849	745	71

S19	Sulaimani	Centre	Tanjero	Industrial area of Tanjero	540156	3929141	756	100
S20	Sulaimani	Centre	Centre	Qrga Quarter	542525	3932662	908	120
S21	Sulaimani	Centre	Centre	Shorsh Quarter	538727	3935168	854	125
S22	Sulaimani	Centre	Centre	Bakhtiary Quarter	536543	3936871	800	142
S23	Sulaimani	Centre	Centre	Goizha	542166	3937935	1060	450
S24	Sulaimani	Centre	Tasluja	Tasluja	520818	3939491	796	120
S25	Sulaimani	Centre	Warmawa	Alan Village	570554	3905391	527	66
S26	Sulaimani	Centre	Bakrajo	Qazan Village	525682	3931889	850	90

Appendix 2: First published article

Environ Monit Assess (2022) 194:352
https://doi.org/10.1007/s10661-022-09933-6

Groundwater geochemistry evolution and geogenic contaminants in the Sulaimani-Warmawa Sub-basin, Sulaimani, Kurdistan Region, Iraq

Rebar Mahmmud · Ondra Sracek · Omed Mustafa · Bohuslava Čejková · Ivana Jačková · Lenka Vondrovicová

Received: 7 July 2021 / Accepted: 5 March 2022

Abstract Evolution of groundwater geochemistry in the Sulaimani-Warmawa Sub-basin in the Kurdistan Region of Iraq has been investigated using hydrogeochemical and isotopic methods. This is a semiarid region with seasonal precipitation in winter. Water chemistry generally evolves from Ca-HCO_3 groundwater type close to the basin boundaries towards Ca-Mg-HCO_3 groundwater type close to the Tanjero River along the axis of the basin. Some samples have increased concentrations of Na, Cl, and SO_4 as a consequence of dissolution of halite and gypsum embedded in carbonates. Values of pH are slightly alkaline or alkaline, and redox parameters indicate a moderately reducing environment. Isotopes δ^2H and $\delta^{18}O$ indicate recharge from winter precipitation with no evaporation. Values of dissolved ^{13}C(DIC) correspond to equilibrium with carbonates and C4 plants as the source of CO_2. Values of $^{87}Sr/^{86}Sr$ in groundwater are in a good agreement with carbonate dissolution as a principal process. The principal geogenic contaminant is Ba with concentrations up to 0.383 mg/L. Dissolved concentrations of other geogenic contaminants such as As, F, Mn, and Cr are low or below the detection limit as expected based on their low contents in carbonate rocks. Inverse geochemical modeling on selected profiles calibrated using $\delta^{13}C$ values provided mass transfer coefficients for possible geochemical reactions. Future work should focus on interactions in the hyporheic zone of the Tanjero River.

Keywords Clastic aquifer · Environmental isotopes · Geochemical modeling · Kurdistan Region of Iraq

Supplementary information The online version contains supplementary material available at https://doi.org/10.1007/s10661-022-09933-6.

R. Mahmmud (✉) · O. Sracek
Department of Geology, Faculty of Science, Palacky University, 17. listopadu 12, 771 46 Olomouc, Czech Republic
e-mail: rebar.mahmmud@gmail.com; rebar.mahmmud@upol.cz

O. Mustafa
College of Education & Natural Sciences, Charmo University, 46023 Chamchamal, Sulaimani, Kurdistan Region, Iraq

O. Mustafa
Groundwater Protection and Restoration Group, Department of Civil and Structural Engineering, University of Sheffield Broad Lane, S3 7HQ Sheffield, UK

B. Čejková · I. Jačková
Czech Geological Survey, Geologická 6, 152 00 Prague 5, Czech Republic

L. Vondrovicová
Institute of Geochemistry, Mineralogy and Natural Resources, Faculty of Science, Charles University, Albertov 6, 128 00 Prague 2, Czech Republic

Published online: 11 April 2022

Introduction

Groundwater is an important and sometimes the only source of water in semiarid regions. Several studies of groundwater have been carried out in such regions,

e.g., in the Kalahari Desert in Namibia (Uugulu & Wanke, 2020) and Botswana (Stadler et al., 2010), northeast of Brazil (Halm et al., 2002), and central Australia (Harrington et al., 2002). It was found that groundwater quality is generally influenced by strong evaporation and depends on the type of recharge (diffuse vs. focused), land use, and land cover (Scanlon et al., 2006). Mountain front recharge is frequently observed when the principal aquifer recharge zones occur in mountain areas with higher precipitation and then groundwater flows towards lowlands, where principal exploitation takes place (Markovich et al., 2019).

Geogenic contaminants are present in groundwater even when there is no source of anthropogenic contamination. Typical contaminants are As, F, Mn, and Ba (Johnson & Bretzler, 2015; Bondu et al., 2020). Natural processes releasing As are reductive dissolution of ferric minerals and release of adsorbed As, and high pH values in oxidizing environments when negatively charged As species are released. High concentrations of F are linked to groundwater low in calcium when F is released from minerals such as fluorite (CaF_2). Mobility of Mn depends on redox conditions, i.e., Mn becomes mobile under moderately reducing conditions, and concentration of Ba is controlled by sulfate when Ba precipitates as barite ($BaSO_4$) in high sulfate water. High natural concentrations have also been observed for other contaminants, e.g., Cr in Sao Paulo state in Brazil, where Cr is mobile under oxic and high pH conditions (Bertolo et al., 2011).

The study area is in the Iraqi Kurdistan Region around the city of Sulaimani (Fig. 1a); it is a hydrologic Sub-basin which is a part of the Sulaimani-Sharazoor basin (Stevanovic & Markovic, 2004). It is a semiarid region with a Mediterranean-type climate and precipitation occurs mostly in winter. Groundwater is a very important resource because local streams are generally perennial and dry out during late summer. The region is economically important because of its huge oil reserves and several towns are booming due to the oil industry. Sulaimani is the principal city in the study area with 740,000 inhabitants, mostly dependent on groundwater for water supply in the surrounding area.

The purpose of this study was (1) to identify groundwater chemistry evolution processes at the basin scale in the aquifers composed of carbonate and evaporate rocks, and (2) to determine potential geogenic contaminants limiting groundwater use. The working hypothesis was that groundwater chemistry is formed in carbonate rocks in recharge areas and changes due to common ion effect along flow path where evaporitic minerals dissolve (Ford & Williams, 2007). Also, expected concentrations of geogenic contaminants should be low because they are generally low in carbonate source rocks (Ravenscroft et al., 2009).

Physio-geographical, geological, and hydrogeological framework

The study area encompasses an area of about 1500 km^2 and is located in the Sulaimani governorate in the Iraqi Kurdistan Region in the foothills of the Zagros Mountains (Fig. 1a) roughly between altitudes of 700 m and 1200 m. The region is characterized by a Mediterranean climate (Csa according to the Köppen climate classification) with relatively cold humid winters and hot dry summers. Most precipitation falls in winter between October and May with a maximum of more than 100 mm in January (Stevanovic & Markovic, 2003). Mean annual precipitation is 668.5 mm, mean annual air temperature is 21° C, and mean annual evaporation is 2298.8 mm (Mustafa, 2006; Hamamin et al., 2018). Hills around the basin are covered by grass and sparse vegetation of pine, *Pinus Sylvestris* (Fig. 1d), which are used for sheep and goat grazing. The principal river is the perennial Tanjero River, which is generally dry from August to the beginning of the precipitation season in October. The principal city is Sulaimani in the west of the study area, which is a source of municipal waste disposed at a waste dump southwest of the city (Rashid et al., 2018). The impact of the waste dump on groundwater quality in the proximity of Sulaimani was studied by Kareem et al. (2018) who identified increased concentrations of manganese as a principal problem.

The Sulaimani-Warmawa Sub-basin is located in the High Folded Zone (Buday, 1980; Buday & Jassim, 1987; Jassim & Goff, 2006; Al-Jiburi et al., 2015), (Fig. 1b). The study area consists of geological formations from early Cretaceous to Quaternary age (Karim & Ali, 2004; Omar et al., 2015; Sissakian, 2015) (cross section in Figs. 1c and 2). The lower Cretaceous Formations in the area are Balambo, Qamchuqa, and Kometan. The Balambo Formations mostly outcrop east and southeast of the study area and are composed

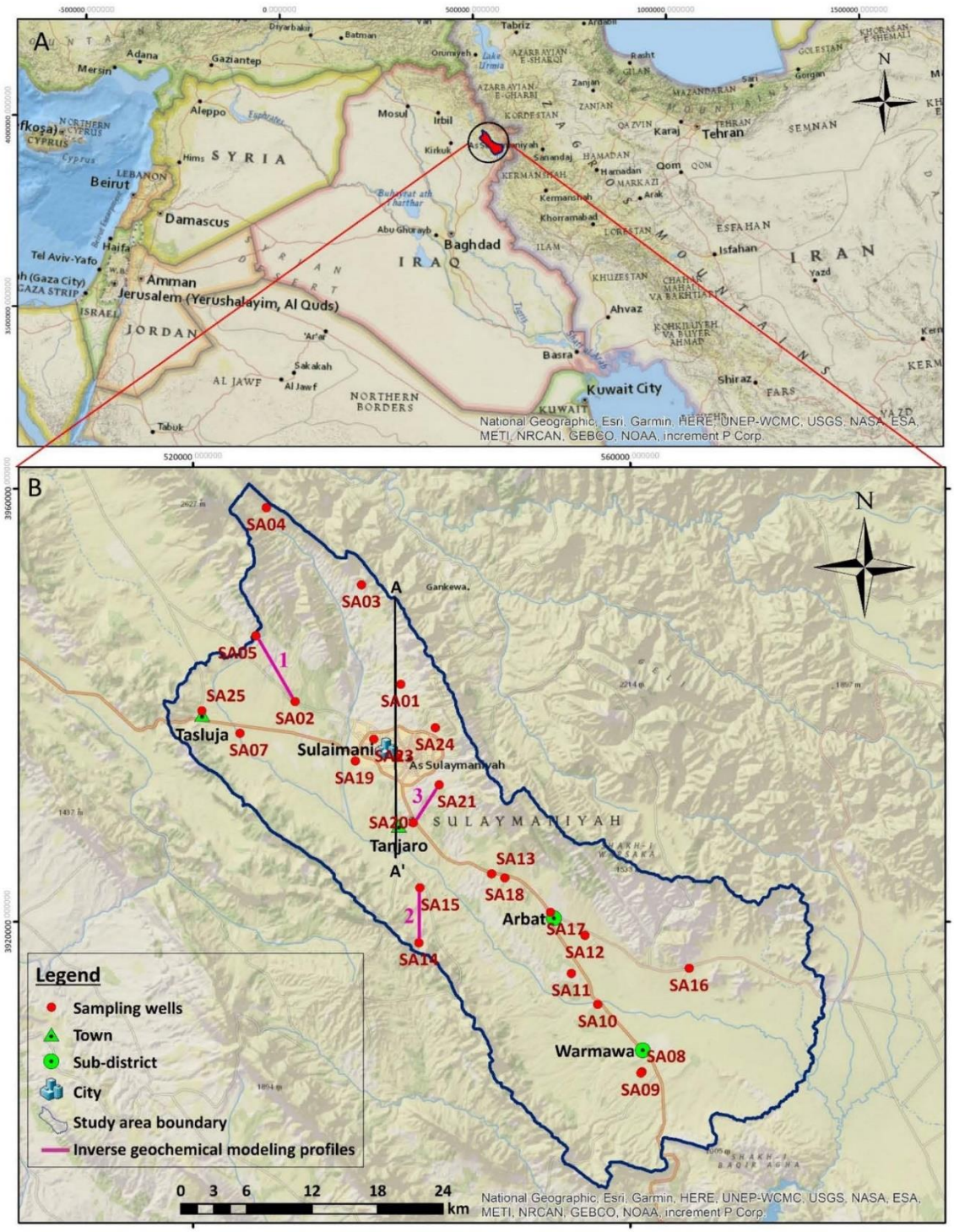

Fig. 1 **a** Location of the study site, **b** position of sampling points and modeling profiles, **c** geological cross section A-A' modified after Kareem et al. (2018), **d** slopes in the upper reaches of the basin with typical vegetation cover

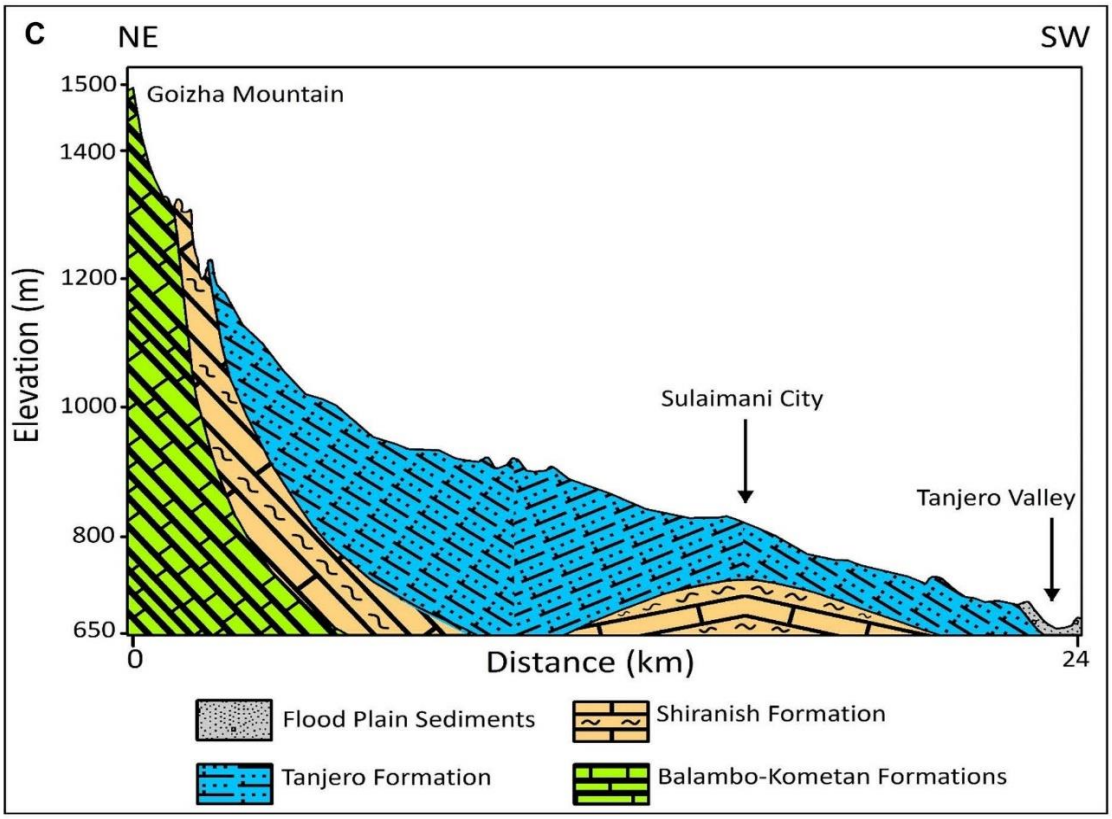

Fig. 1 (continued)

of thin well-bedded radiolarian limestone (Bellen et al., 1959; Jassim & Goff, 2006; Ali, 2007). In addition, the Qamchuqa Formation mostly outcrops in the northern part of the Sub-basin and is composed of grey massive dolomites, and dolomitic limestone (Ali, 2007). The Kometan Formation is described as white-weathering, light grey, thin-bedded, globigerial-oligosteginal limestone, and locally silicified (Bellen et al., 1959). In addition, it is also described as well-bedded fine crystalline limestone (Sissakian, 2015).

The Late Cretaceous Formations in the study area are the Shiranish and Tanjero Formations. The Shiranish Formation is mostly composed of bluish-grey marl and marly limestone (Sissakian, 2015). The Tanjero Formation is widespread in the Sulaimani-Warmawa Sub-basin, especially around the city of Sulaimani, and extends from the foothills of Goizha Mountain in the north and northeast towards the Tanjero valley in the south and the Chaq-Chaq valley in the northwest (Mustafa, 2006). It is composed of silty marl, siltstone, shale, sandstone, conglomerate, and sandy or silty organic detrital limestone (Bellen et al., 1959). The Tanjero Formation has been divided into three parts based on its lithological composition, i.e., Lower, Middle, and Upper part (Karim, 2004). The lower part is mostly composed of the alteration of thin sandstone sliced between thick dark grey calcareous shale with a transition to a thick bed of boulder and coarse gravel conglomerate beds. The middle part consists of bluish marl and the upper part is composed of mixed siliciclastic-carbonated beds represented as the alteration of thick-bed biogenic limestone, and calcareous shale on the shelf.

The Tertiary geological formations in the area are Kolosh, Sinjar, Gercus, and Pila Spi. The Kolosh Formation is composed of dark grey claystone, shale, and siltstone with rare conglomerate (Sissakian, 2015). The Sinjar, Gercus, and Pila Spi Formations are outcropped in the study area with low thickness and mostly represented in the northwest and southwest. They are composed of well-bedded limestone, dolomite, and marly limestone and sandstone; alteration of red claystone, sandstone, and conglomerate; limestone and chalky marl with chert nodules; and cyclic deposits of claystone, marl, gypsum, and sandstone with occasional limestone (Jassim & Goff, 2006; Sissakian, 2015). The Quaternary deposits generally consist of alluvial fans and flood plain sediments. They are mostly composed of gravel, sand, silt, mud, sandy, and silty clay soil (Mustafa, 2006; Sissakian, 2015).

The hydrogeological map for the study area has been created based on a previous study which was conducted in Iraq, Kurdistan Region, and Sulaimani Governorate. In addition, to the hydrogeological data from (DoGWS) and the data were collected from 32 water wells in the study area during July and August 2020 and the depth of wells are varied from 24 to 450 m. The hydrostratigraphic units in the study area have been grouped according to their lithology and hydrogeologic characteristics into the Karstic-fissured aquifer (KFA), the Kometan aquifer (KA), the Tanjero aquifer (TA), an Aquiclude, and a Quaternary intergranular aquifer (QIA) (Stevanovic & Markovic, 2004; Mustafa, 2006 and Ali, 2007). The type of aquifers and associated hydrostratigraphic information are summarized in Table 1. According to the hydrogeological data and report from the Directorate of Groundwater of Sulaimani (DoGWS), the main productive aquifers in the study area are the Quaternary Intergranular Aquifer (QIA) and the Tanjero Aquifer (TA) in terms of groundwater quantity and quality (Mustafa, 2006; Kareem et al, 2018; DoGWS, 2020). However, they are recharged from relatively permeable karstic formations close to the basin boundaries. The groundwater flow direction is generally from the north and northwest towards Sulaimani and the Tanjero river which flows into the Darbandikhan Lake out of the basin in southeast (Fig. 2).

Material and methods

The hydrogeological map has been created for the Sub-basin based on previous studies of Iraq including a study on the Kurdistan Region and Sulaimani Governorate as well as based on hydrogeological data which were obtained from (DoGWS). In addition, the collected data from 32 water wells during the fieldwork in 2020. The direction of groundwater flow in the study area has been illustrated by measuring and updating the groundwater level data from several water wells in July–August 2020 (Fig. 2).

Groundwater was sampled from already existing wells after the pumping of several well volumes (Fig. 1b). Field parameters of temperature, pH, and electrical conductivity (EC) were measured on-site.

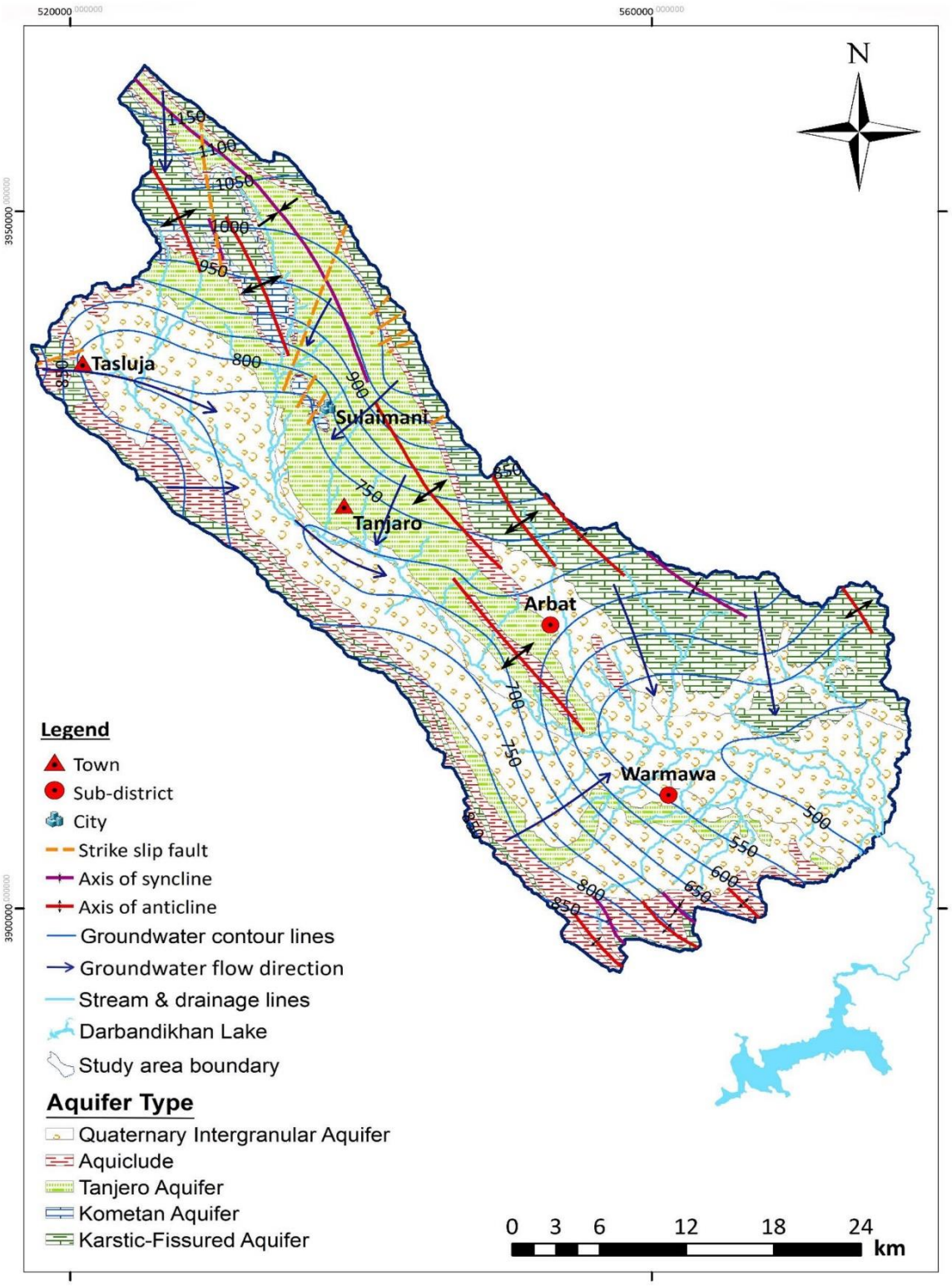
520000
560000
3950000
3900000
N
1150
1100
1050
1000
950
800
900
850
750
700
650
600
550
500
Tasluja
Sulaimani
Tanjaro
Arbat
Warmawa
Legend
Town
Sub-district
City
Strike slip fault
Axis of syncline
Axis of anticline
Groundwater contour lines
Groundwater flow direction
Stream & drainage lines
Darbandikhan Lake
Study area boundary
Aquifer Type
Quaternary Intergranular Aquifer
Aquiclude
Tanjero Aquifer
Kometan Aquifer
Karstic-Fissured Aquifer
0 3 6 12 18 24
km

◂**Fig. 2** Hydrogeological map and groundwater flow pattern in the study area

Groundwater samples have been collected for major cation, anion, and trace element analysis. Samples collected for cation and trace element analyses were filtered in the field with 0.45 mm Millipore filters, acidified with HNO_3-Suprapur, and stored in 50 mL HDPE bottles. Cations and trace elements were analyzed with the ICP-MS technique at the analytical laboratories of Charles University in Prague. The analytical error of the individual solution analyses was below 2%. Concentrations of anions were determined by HPLC, Dionex ICS. Ferrous iron was determined by potassium dichromate titration. Values of alkalinity were determined by HCl titration with the Gran plot to determine the endpoint. Sample of rain was collected about 3 km south of Sulaimani City and analyzed for Cl^-. The QA/QC was performed using standard procedures. About 10% of samples was analyzed in duplicate and there was good agreement between analyses.

Isotopes δ^2H and $\delta^{18}O$ were determined at the Czech Geological Survey in Prague with a LWIA 3000 laser analyzer (LGR). The analysis precision was ± 0.4‰ for δ^2H and 0.12‰ for $\delta^{18}O$. The results were normalized to the international standard (V-SMOW) and reported in common δ-notation. For $\delta^{13}C$ analyses, BaCl2 was added to precipitate $BaCO_3$ (Clark & Fritz, 1997). The precipitate was then decomposed in 100% H_3PO_4 under vacuum at 25 °C. The C isotope ratio in the generated CO_2 was determined by a Thermo Delta V mass spectrometer with a precision of $\delta^{13}C$ values better than ± 0.1‰. Results were expressed using the PDB standard.

Strontium (corresponding to at least 2 µg of Sr in solution) was isolated from water samples using exchange chromatography techniques based on Triskem's Sr resin (Pin et al., 1994). Isotopic composition was determined by a Neptune Plus instrument (MC-ICP-MC; ThermoFisher Scientific) in the Stable and Radiogenic Isotope Research Laboratory at Charles University in Prague. Analytical mass bias was corrected to $^{88}Sr/^{86}Sr = 8.375209$ (defined as $\delta^{88}/^{86}Sr = 0$ and related to NIST SRM 987, Nier, 1938). The analytical uncertainty was determined by repeated analyses of the SRM 987 standard, with resulting 87Sr/86Sr = 0.7102777 ± 0.0000099 in (2 S.E.M; $n = 8$).

The USGS program PHREEQC (Parkhurst & Appelo, 1999) with the minteq.dat database was used to calculate speciation and saturation indices and to determine mass transfer between selected mineral phases and groundwater using the inverse geochemical modeling module. The program Geochemist Workbench was used to prepare the Eh–pH diagram and the maps were prepared in an ArcGIS 10. The programs PAST (Hammer et al., 2001) and Statistica 13.3 were used for statistical treatment of data including hierarchical cluster analysis (HCA) where samples and wells are grouped based on their similarity.

Results

Principal ions and trace elements

Samples in the Piper diagram were sorted according to their mineralization, here represented by their electrical conductivity (Fig. 3). The general trend is the evolution from Ca-HCO_3 groundwater type towards Mg-Ca-HCO_3 groundwater type with increasing EC, which roughly corresponds to the direction of flow. However, there are some exceptions. Especially anomalous is sample SA15 with Na-Cl water type and sample SA25 with mixed Na-Ca-HCO_3-SO_4-Cl groundwater type. There is also sample SA19 of Ca-HCO_3-SO_4 groundwater type and high EC, located close to the Tanjero River (Fig. 1b).

Water chemistry parameters are given in Table 2. Values of pH are in the range from 7.02 (wells SA19) to 8.75 (well SA25), with an average of 7.67. Values of electrical conductivity range from 328 to 2460 µS/cm, average 663 µS/cm, but the maximum value in SA15 is an outlier. Concentrations of Ca are from 6.07 to 113 mg/L, average 51.24 mg/L. Concentrations of Mg are from 2.3 to 40.5 mg/L, average 11.9 mg/L. Concentrations of Na are from 2.7 to 480 mg/L, average 55.6 mg/L, and concentrations of K are from 0.25 to 2.66 mg/L, average 0.86 mg/L. Concentrations of HCO_3 are from 140 to 320 mg/L, average 215.3 mg/L. Concentrations of SO_4 are from 7.3 to 200.7 mg/L, average 47.3. Concentrations of Cl are from 1.9 to 462.4 mg/L, average 43.4 mg/L.

In general, redox processes influence the quality of water and can affect the mobility status of the toxic elements that are available naturally in aquifer materials, in addition to organic and inorganic

Table 1 Aquifer types and lithostratigraphy in the study area (after Stevanovic & Markovic, 2004; Mustafa, 2006; Ali, 2007 and SGI, 2011)

Aquifer type	Geological Formation	Lithology	Hydraulic conductivity K (m/s)
Quaternary intergranular aquifer (QIA)	Quaternary deposits	Sand, silt, rock fragments, mud, pebbly, sandy, silty, and clayey soil	$9.83 * 10^{-6}$
Tanjero aquifer (TA)	Tanjero	Silty marl, siltstone, shale, sandstone, conglomerate, and sandy or silty organic detrital limestone	$1.17 * 10^{-6}$
Aquiclude	Shiranish, Kolosh, and Gercus	Claystone, shale, siltstone, sandstone, marl, marly limestone, and rare conglomerate	Not available
Kometan aquifer (KA)	Kometan	Limestone	$2.3 * 10^{-5}$
Karstic-fissured aquifer (KFA)	Balambo, Qamchuqa, Pila Spi, and Sinjar	Limestone, dolomite and dolomitic limestone, and chalky marl	$6.2 * 10^{-6}$

components. In the aquifer, these processes contribute to the degradation or preservation of anthropogenic contaminants (McMahon & Chapelle, 2008). Regarding redox indicators, NO_3 concentrations are from 1.2 to 36 mg/L, average 15.4 mg/L; concentrations of Fe are from 0.03 to 0.68 mg/L, average 0.32 mg/L; and concentrations of Mn are generally below the detection limit and maximum concentration reaches only 8.28 µg/L.

Concentrations of geogenic contaminants, except for Ba with a maximum of 383 µg/L in well SA 12, are low. Only sample SA15 has a high As concentration of 4.27 µg/L, all other samples show concentrations less than 1 µg/L. Concentrations of F are low, with a maximum of 0.54 mg/L again in SA15. All other samples have concentrations close to or below 0.2 mg/L. The maximum concentration of Cr is 3.25 µg/L in SA19 and concentrations in other wells are generally less than 1 µg/L. Concentrations of Sr are frequently higher than 1 mg/L with a maximum of 2.68 mg/L in SA19.

The concentration of Cl^- in rain collected in the field out of Sulaimani was 2.2 mg/L. The correlation matrix for principal groundwater chemistry parameters is in Table S1 in Supplementary Material. Notable is a high positive correlation between EC and Na, Cl, and SO_4. The correlation between F and Ca is negative as expected based on fluorite precipitation control.

Stable isotopes

The stable isotopic compositions of the groundwater samples from the Sulaimani-Warmawa Sub-basin expressed in δ-notation per mil deviation from the internationally accepted standard V-SMOW (Vienna Standard Mean Ocean Water) are summarized in Table 3 and in Fig. 4. They range from (−7.0‰) to (−5.5‰) $\delta^{18}O$ and from (−36.9 ‰) to (−25.5 ‰) $\delta^{2}H$ for sampling in July–August 2020. Values of deuterium excess are high, in some samples more than 20‰. Mook (2001), Mazor (2004), and Al-Charideh (2011), stated that the isotopic composition of local rainwater can be influenced by several factors such as surface air temperature and humidity, altitude, and geographic location (longitude and latitude). According to the results of the isotopic composition of the groundwater samples in the study area, the most negative value ($\delta^{18}O = -7.0$‰) was measured for the highest altitude sample which is 1224 m above sea level. Samples collected around Sulaimani (altitude 882 m) have more positive $\delta^{18}O$ values close to −5.0‰. The global meteoric water line (GMWL) has a higher slope and intercept than the local groundwater line (GWL) for samples from the study area (Craig, 1961; Gat & Carmi, 1970) (Fig. 2). The local GWL for the groundwater samples in the study area has a higher slope and intercepts the local meteoric

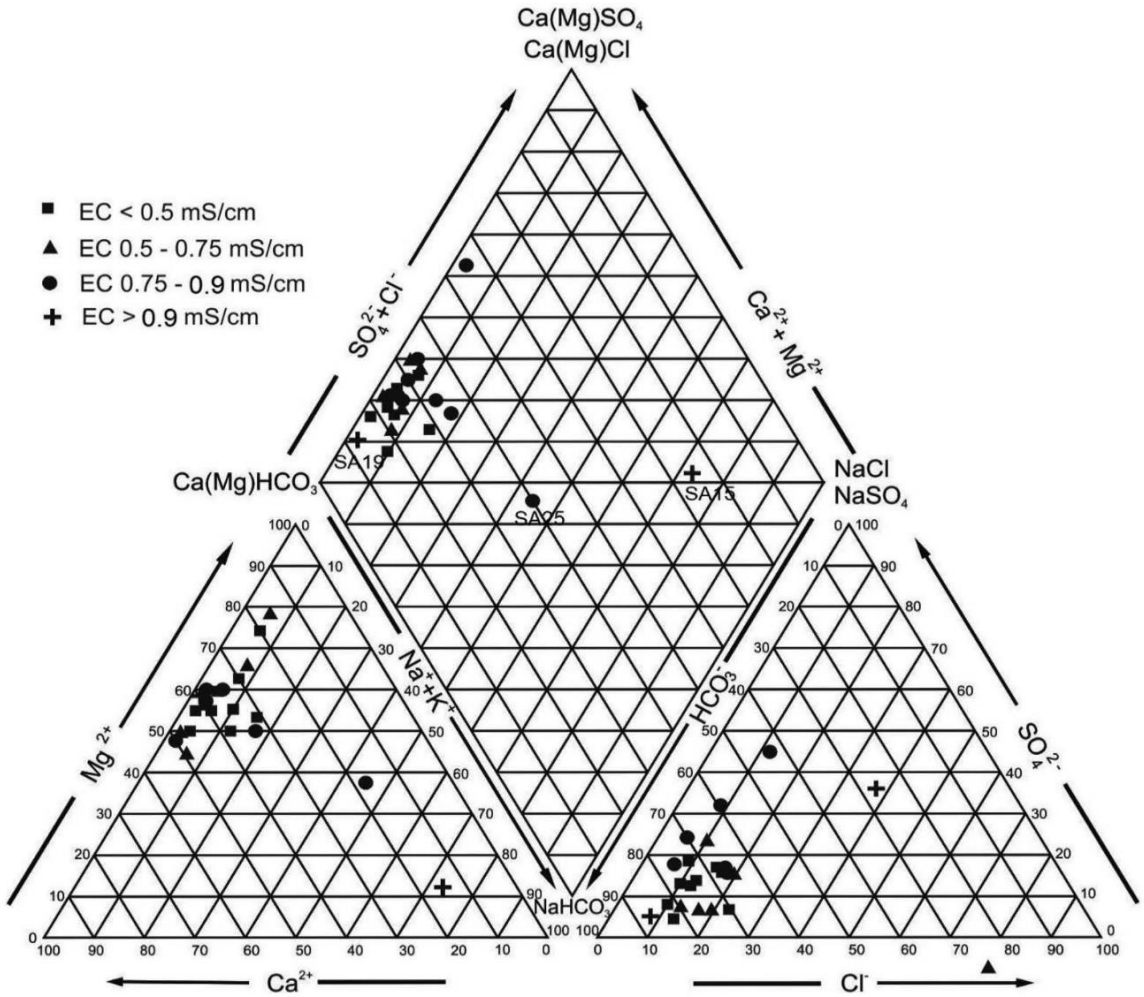

Fig. 3 Piper diagram, samples are sorted based on their EC values. Outliers SA19, SA25, and SA15 are marked

water lines (LMWL) developed for Zagros by Osati et al. (2014). The local GWL for the groundwater samples in the study area showed slopes and intercepts between local meteoric water lines (LMWL) developed for the Zagros by Osati et al. (2014) ($\delta^2H=6.80\delta^{18}O+10.1$) and Mohammadzadeh et al., 2020 ($\delta^2H=6.44\delta^{18}O+8.514$). However, there is a very good agreement of the local GWL with the LMWL for winter precipitation ($\delta^2H=6.67\delta^{18}O+9.766$) (Mohammadzadeh et al., 2020). This indicates that the groundwater in the study area has been recharged almost exclusively from winter rainfall with minimum evaporation during infiltration. This is different from groundwater data from western Iraq where a significant evaporation impact with a slope of the groundwater line of 5.19 was observed (Ali et al., 2015). The deviation in precipitation isotopic data in the Iraqi and Irani Kurdistan LMWL from the global meteoric water line (GMWL) is caused by the mixing of air masses from the Eastern Mediterranean with high deuterium excess and the Persian Gulf, where the latter is more important in Fall when the slope of the Kurdistan LMWL decreases to 6.08 (Mohammadzadeh et al., 2020). In Fall, some influence of precipitation from highly evaporated Caspian Sea is also possible (Mohammadzadeh & Heydarizad,

Table 2 Water chemistry parameters

Indicators	Unit	SA02	SA03	SA05	SA08	SA12	SA14	SA15	SA16	SA18	SA19	SA20	SA21	SA23	SA24	SA25
Well depth	m	180	100	80	140	198	235	100	100	160	71	100	120	142	450	
pH		7.55	7.54	7.53	7.37	7.86	7.84	8.55	7.22	7.4	7.02	7.03	7.65	7.16	8.57	8.75
Temperature	°C	24.9	21.8	25.5	23.3	22.9	23.3	22.3	22.4	26.8	26.3	23	24.9	25	26.7	25.5
EC	µS/cm	475	450	565	450	602	467	2460	408	401	935	642	328	483	486	792
Alkalinity as HCO_3	mg/L	190	180	180	240	220	240	140	220	180	320	200	240	210	240	230
Ca	mg/L	52.2	47.3	45.6	37.8	57	45.6	19.1	63.2	55	113	84.1	47.6	69.5	25.5	6.07
K		0.39	0.67	0.70	0.65	0.42	0.64	1.84	0.25	2.66	0.47	0.39	0.35	0.51	0.64	2.3
Mg		8.35	8.64	10.3	8.71	12.1	26.5	2.33	5.05	10.7	40.4	19.3	7.27	9.58	6.62	2.45
Na		4.32	14.7	16.4	41.9	3.98	4.79	480	2.67	4.8	19.4	10.6	3.52	8.15	61.5	157
Si		6.52	7.77	7.22	8.19	6.35	7.23	6.21	5.36	7.69	12.08	9.97	8.10	6.61	7.54	17.46
Cl^-		3.47	2.38	4.24	5.77	4.46	2.81	462.37	1.89	5.31	43.51	43.55	6.63	11.37	8.73	44.07
SO_4		30.91	19.03	31.81	27.05	7.35	23.59	200.7	7.65	16.00	84.32	44.74	7.97	34.73	53.15	121.1
F		0.20	0.20	0.20	0.20	0.20	0.20	0.54	0.20	0.20	0.20	0.20	0.20	0.20	0.29	0.20
NO_3		23.2	8.96	26.7	6.75	17.3	2.64	0.20	14.2	25.0	18.5	36.0	27.3	20.4	4.01	0.20
Li	µg/L	2.63	4.27	7.05	4.93	4.69	4.09	13.48	2.09	4.33	8.67	5.22	2.21	3.54	30.85	2.14
Al		19.31	18.15	17.33	16.32	18.21	16.29	17.01	17.32	6.07	5.35	5.87	6.03	5.79	6.16	6.04
Ti		204.64	183.35	168.21	142.88	214.39	177.95	81.61	225.31	198.72	394.34	293.79	172.75	256.94	94.52	26.34
V		3.85	1.90	1.27	4.01	3.11	2.27	16.72	3.45	4.98	10.39	7.09	4.21	2.12	0.86	1.79
Cr		3.13	0.91	0.72	1.19	1.75	1.89	0.65	1.31	1.63	3.25	1.06	2.89	0.97	2.97	0.54
Fe		347.05	312.18	278.36	234.54	372.90	307.52	130.89	395.96	335.10	689.54	505.99	292.43	445.98	147.93	27.59
Mn		0.465	BDL	2.52	8.28	1.22	BDL	1.89	0.09	BDL	BDL	BDL	BDL	0.025	6.93	2.01
As		BDL	BDL	BDL	1.5	BDL	BDL	4.27	0.2	0.1	0.33	BDL	BDL	BDL	BDL	0.12
Co		0.16	0.12	0.11	0.21	0.16	0.10	0.07	0.13	0.12	0.31	0.18	0.09	0.15	0.04	0.01
Ni		1.13	0.97	1.83	0.84	1.40	1.78	0.734	1.65	0.97	3.44	1.46	0.85	1.46	0.57	0.57
Cu		0.37	0.47	0.19	0.61	12.80	2.36	7.20	0.65	BDL	0.42	0.01	BDL	BDL	0.60	1.95
Zn		0.38	BDL	3.62	289.67	339.68	27.11	2.31	140.45	7.10	127.63	0.17	BDL	1.37	28.71	25.10
Rb		0.40	0.51	0.56	0.92	0.24	0.32	0.837	0.21	0.99	0.69	0.41	0.33	0.33	0.42	4.17
Sr		1002.01	1663.85	1286.81	900.03	1181.95	866.83	556.70	332.45	952.67	2682.28	1768.78	547.64	970.35	1108.00	171.86
Cd		0.10	0.04	0.01	0.02	0.02	0.05	0.09	0.02	0.03	0.02	0.01	0.0	0.02	0.010	0.02
Ba		32.72	51.85	74.77	24.10	383.4	21.96	11.99	214.11	46.04	144.29	165.97	63.441	173.7	101.72	7.45

Table 2 (continued)

Indicators	Unit	SA02	SA03	SA05	SA08	SA12	SA14	SA15	SA16	SA18	SA19	SA20	SA21	SA23	SA24	SA25
Ce		0.03	0.03	0.03	0.03	0.04	0.02	0.03	0.03	0.01	0.01	0.01	0.01	0.01	0.01	0.01
Pb		0.03	0.01	0.04	0.64	0.52	0.37	1.59	0.97	0.46	0.39	0.41	0.25	0.15	0.09	0.17
Bi		0.87	0.86	0.77	0.73	0.72	0.69	0.87	0.68	0.67	0.66	0.66	0.64	0.65	0.64	0.64
U		0.85	0.46	0.30	0.49	0.59	1.14	0.08	0.46	0.58	1.94	1.28	0.46	0.54	0.32	0.01

BDL below detection limit

2019). A limited evaporation impact is possible in the Tanjero Formation because of slow infiltration in low permeability marly limestone (Mustafa et al., 2015).

Values of $\delta^{13}C$(DIC) are in Table 3 and a plot of $\delta^{13}C$(DIC) vs. HCO_3 is in Fig. 5. Most values of $\delta^{13}C$(DIC) are between −3.0 and −1.0‰. Samples SA12 and SA15 with respective values −3.4 and −4.3‰ are an exception. High values indicate equilibrium with carbonate rocks under closed-system conditions consistent with high SI values for calcite especially in wells close to Sulaimani (Table 4). The dominant vegetation in recharge areas on the slopes around Sulaimani is grass, i.e., C4 plants (Fig. 1d) with high $\delta^{13}C$ values close to −12‰, (Clark & Fritz, 1997), which are the source of CO_2 interacting with Cretaceous carbonate rocks with values of $\delta^{13}C$ typically between −1 and −2‰ (Razmjooei et al., 2020).

Values of $^{87}Sr/^{86}Sr$ ratios in groundwater are in Table 3 and a plot of $^{87}Sr/^{86}Sr$ vs. Sr concentration is in Fig. 6. Most $^{87}Sr/^{86}Sr$ ratios range from 0.7081 to 0.7082. Slightly lower values below 0.708 are shown in samples SA3, SA5, SA24, and SA25 from wells located close to recharge areas close to the groundwater divide (Fig. 1b). The lowest value of 0.7076 has groundwater from well SA15 with anomalous water chemistry. However, all values are typical for groundwater in contact with carbonates of the Cretaceous age (Veizer, 1989).

Speciation modeling

Selected results of speciation modeling are shown in Table 4. Values of Eh calculated on the basis of the Fe(II)/Fe(III) couple are in the range −0.122 to +0.114 V, indicating post-oxic, moderately reducing conditions.

Values of total C expressed as CO_2 in mmol/kgw increase from 2.2 to 6.81 and increasing values generally follow the flow direction. Low values are in recharge zones close to the groundwater divide, e.g., for wells SA05 and SA25; high values are located in the axis of the valley, e.g., for wells SA19 and SA21. Values of log P_{CO2} are again generally low in recharge zones close to the basin boundaries with a value of −3.43 in SA25 and higher in the axis of the valley with a value of −1.54 in SA19. However, well SA15 with anomalous Na-Cl groundwater has minimum values of both total C and log P_{CO2} (Table 4). Groundwater in most wells is supersaturated with or at equilibrium with calcite. Groundwater in some

Table 3 Isotopes in groundwater samples from the Sulaimani-Warmawa Sub-basin, Kurdistan Region, Iraq, during the period July–August 2020

Samples	δ^2H (‰)	$\delta^{18}O$ (‰)	Deuterium excess	$\delta^{13}C$(DIC) (‰)	$^{87}Sr/^{86}Sr$
SA01	−28.5	−6.1	20.0	−2.4	n.a
SA02	−25.5	−5.6	19.2	−1.6	0.7082
SA03	−32.9	−6.6	19.6	−1.5	0.7078
SA04	−34.7	−7.0	21.7	−1.8	n.a
SA05	−30.3	−6.3	20.4	−1.7	0.7079
SA08	−26.2	−5.5	18.0	−2.5	0.7080
SA12	−28.7	−5.7	16.9	−3.4	0.7082
SA14	−33.7	−6.5	18.4	−1.7	0.7081
SA15	−39.5	−6.7	13.9	−4.3	0.7076
SA16	−29.8	−6.5	22.1	−1.3	0.7081
SA18	−29.1	−5.6	16.0	−1.6	0.7082
SA20	−28.5	−5.5	15.2	−1.6	0.7082
SA 21	−27.5	−6.2	22.1	−1.5	0.7082
SA23	−29.9	−6.2	19.3	−1.2	0.7081
SA24	−36.9	−6.9	18.4	−1.4	0.7078
SA25	−36.9	−6.9	18.1	−2.3	0.7077

n.a. not available

wells also reaches supersaturation or equilibrium with dolomite, especially wells along the axis of the valley.

On the other hand, all samples are undersaturated with respect to gypsum and strontianite, $SrCO_3$, suggesting conservative behavior of both sulfate and Sr. Groundwater is generally undersaturated with respect to ferrihydrite, but supersaturated with respect to more crystalline goethite. Groundwater is also undersaturated with respect to all Mn minerals and is generally undersaturated with respect to barite. Finally, all samples are undersaturated with respect to amorphous silica, but generally supersaturated with quartz. Also, supersaturation with respect to kaolinite is observed, but calculated values are uncertain because of the possible presence of colloidal aluminum.

Discussion

The flow system in the study area is a gravity-driven flow system in the sense of Tóth (2009). In such systems, mineralization expressed as EC and pH increase along the flow direction, and values of Eh decrease (Tóth, 1999). Based on values of δ^2H and $\delta^{18}O$ (Table 3) and only small Cl^- enrichment compared to rain in recharge area wells, evaporation of infiltrating water is limited.

In terrains with carbonate lithology, equilibrium with carbonates and high mineralization can occur already in recharge areas or even in epikarst especially when infiltration is slow and contact time with carbonate rocks is long (Frost & Toner, 2004; Ford & Williams, 2007; Faimon et al., 2012). Dissolution of evaporate minerals locally present in carbonates contribute Na^+, Ca^{2+}, Cl^-, and SO_4^{2-} and may cause precipitation of carbonate minerals due to the common ion effect (Appelo & Postma, 2005; Khosravi et al., 2020).

Hierarchical cluster analysis (HCA) divides groundwater samples or groundwater parameters into different clusters based on their similarity, i.e., similar wells and parameters are located in the same clusters (Davies, 2002). Results of HCA performed in Ward's mode are provided in Fig. 7. Sample SA15 with high concentrations of Na and Cl and samples SA25 and SA19 with high sulfate concentration are clearly separated in different clusters. In contrast, other samples with Ca-Mg-HCO_3 chemistry are in the right part of the HCA plot. This is consistent with the Piper diagram in Fig. 3 and with almost constant ratios of $^{87}Sr/^{86}Sr$ between 0.7076 and 0.7082 indicating the interaction of groundwater with carbonates. Interactions with clastic non-carbonate material would result in higher ratios (Frost & Toner, 2004). Also, $^{87}Sr/^{86}Sr$ ratios in groundwater samples are close to the $^{87}Sr/^{86}Sr$ ratios in

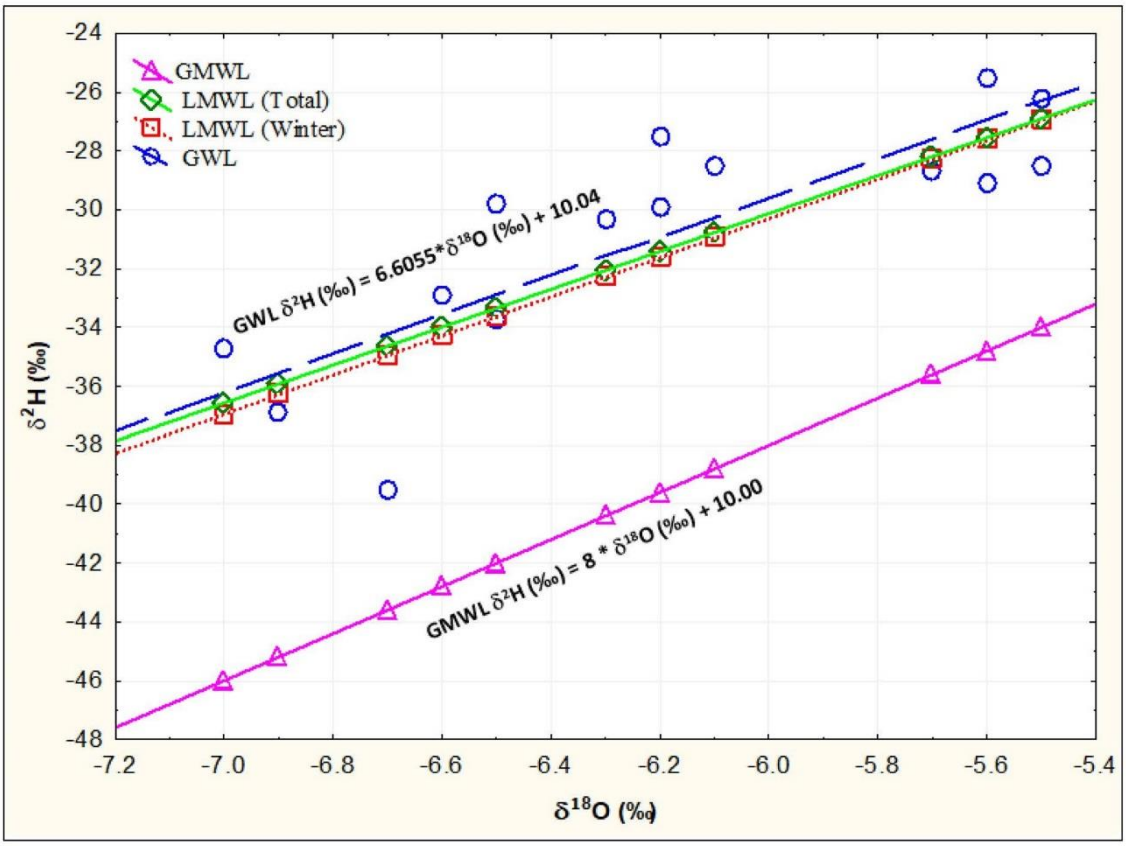

Fig. 4 Diagram of δ^2H vs. $\delta^{18}O$, GWL is groundwater line for the study area, LMWL (Total) is average local meteoric water line for Zagros, LMWL (Winter) is local meteoric water line for winter precipitation in Zagros, and GMWL is world global meteoric water line. For more explanation, see text

precipitation of the Kurdistan Region (mean = 0.7083) as reported by Mustafa et al. (2016).

Results of the HCA for groundwater parameters also in Ward's mode are shown in Fig. 8. In this diagram, Na and Cl as well as Ca and SO_4 are in separate clusters, suggesting their origin in the dissolution of evaporates. Bicarbonate and EC are linked to all parameters as they represent groundwater mineralization. Then, T, pH, Si, Mg, and NO_3 are in a distinct cluster at the right as Si and Mg are linked to high pH values and most other parameters are in the large central cluster.

Inverse geochemical modeling has been performed to elucidate groundwater chemistry evolution on selected profiles (Fig. 1b). Modeled profiles were Profile 1: SA02-SA05 (profile close to the recharge zone); Profile 2: SA14-SA15 (profile affected by the significant dissolution of evaporites); and Profile 3: SA21-SA20 (profile in the axis of the valley, also with some impact of evaporites). Modeling was calibrated using measured $\delta^{13}C$(DIC) because interaction with carbonates is important on all profiles. A $\delta^{13}C$ value for carbonate rocks was set to −2‰ (Razmjooei et al., 2020), and a value of $\delta^{13}C$ for organic matter CH_2O composed of C4 plants was set to −14‰ (Clark & Fritz, 1997).

Results of inverse geochemical modeling are provided in Table 5. On Profile 1 (SA02-05) close to the recharge zone, there are only minor mass transfers because groundwater chemistry does not change very much downgradient. Small amounts of calcite dissolve and only very minor amounts of Na-silicate (here albite) account for increasing Na^+ because Cl^- concentrations

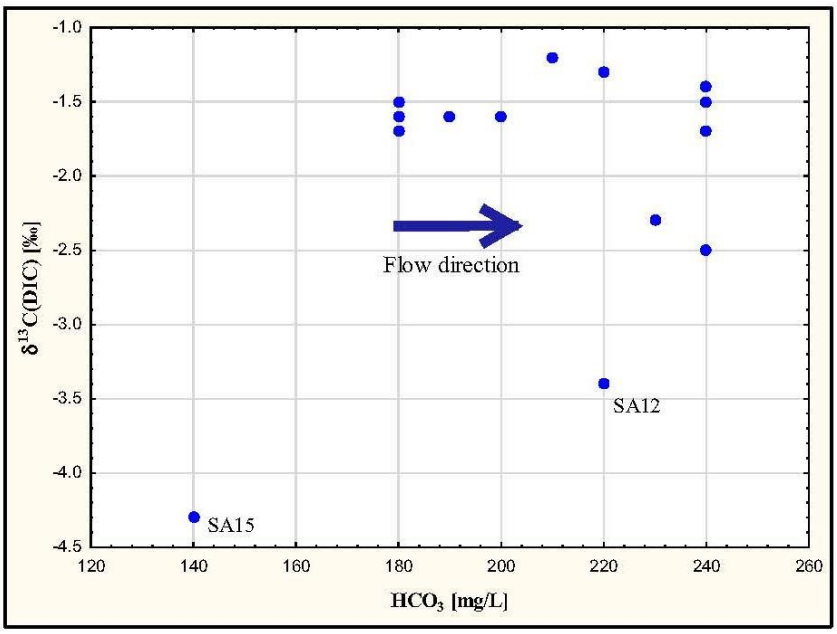

Fig. 5 Diagram of $\delta^{13}C(DIC)$ vs. HCO_3 concentration, outliers are marked

on the profile remain almost constant. In contrast, on Profile 2 (SA14-15), a very high amount of halite and some gypsum dissolves to account for large changes of Cl^- and SO_4^{2-} and some dolomite precipitates due to the common ion effect. On Profile 3 (SA21-20), changes are less dramatic than on Profile 2, but small amounts of halite and gypsum dissolve and a minor amount of calcite precipitates. Also, small amounts of organic matter CH_2O are introduced to account for changes in redox state, also indicated by the dissolution of ferric hydroxide and slightly increasing dissolved iron concentrations downgradient. Amorphous quartz precipitates on Profiles 2 and 3 and cation exchange operates on all profiles. There is an excellent agreement between calculated and measured values of $\delta^{13}C$, confirming realistic values of mass transfer in interactions with carbonates. The modeling results are also consistent with Pearson's correlation coefficients in Table S1.

The redox state of aquifers can be determined based on redox parameters, i.e., O_2, NO_3, Mn(II), Fe(II), SO_4, and CH_4, and the redox state gradually decreases in the sequence (McMahon & Chapelle, 2008). In some wells, the value of Eh calculated using the iron couple indicates a moderately reducing environment (Table 4). Concentrations of NO_3 were elevated especially in some wells, and reached up to 36 mg/L in SA20 (Table 2). Nitrate pollution from grazing in hills and from sewage at the valley bottom could be a possible source for these elevated concentrations (Mustafa & Ahmad, 2008). Samples from some wells, e.g., SA19, had elevated iron and NO_3 concentrations, probably indicating overlap of nitrate reduction and dissolution of Fe(III) mineral zones or mixing in long-screen pumping wells (Sracek et al., 2018). The Eh–pH diagram for the Fe-S system is shown in Fig. 9. The points are aligned along $Fe(OH)_3$(ppd) and Fe^{2+} boundary suggesting that precipitation of amorphous $Fe(OH)_3$(ppd) controls dissolved iron concentration. More crystalline goethite, FeOOH, crystalizes later from the amorphous phase.

The principal geogenic contaminant is Ba with concentrations up to 0.383 mg/L in well SA12, but still much lower compared to the WHO limit of 0.7 mg/L (WHO, 2017). Even in this well, the S1 value for barite is negative (Table 4); thus, this mineral cannot control Ba concentrations. The presence of barite impurities in carbonate rocks of the area was reported and represents a possible geogenic source for Ba (Mustafa & Merkel, 2015; Mustafa et al., 2015). The maximum concentration of F, 0.54 mg/L is in well SA15 and is below the WHO limit of 1.5 mg/L, and concentrations in most wells are below the detection limit. This is expected in carbonate-dominated systems with high dissolved Ca^{2+} concentrations where precipitation

Table 4 Selected results of speciation modeling

Sample	Total CO_2	Log P_{CO2}	Eh	Barite	Calcite	Dolomite(o)	Ferrihydrite	Goethite	Gypsum	Kaolinite	Manganite	Rhodochrosite	SiO_2(a)	Strontianite
	mmol/kgw													
SA02	3.27	−2.28	0.033	−0.65	0.1	−0.24	4.71	5.71	−2.16	2.5	−10.52	−2.5	−1.25	−1.15
SA03	3.12	−2.31	0.051	−0.61	−0.01	−0.44	0.0	5.78	−2.39	3.0	N/A	N/A	−1.15	−0.99
SA05	3.11	−2.28	0.039	−0.28	0.01	−0.28	−0.21	5.69	−2.2	2.46	−9.74	−1.88	−1.21	−1.09
SA08	4.26	−1.99	0.071	−0.84	−0.11	−0.51	−0.25	5.66	−2.35	2.83	−9.17	−1.41	−1.16	−1.29
SA12	3.67	−2.55	−0.01	−0.18	0.48	0.61	−0.03	5.79	−2.75	2.05	−9.98	−1.91	−1.25	−0.74
SA14	4.01	−2.49	−0.02	−0.96	0.39	0.87	−0.05	5.78	−2.38	2.07	N/A	N/A	−1.2	−0.87
SA15	2.22	−3.48	−0.1	−0.53	0.3	0.00	−0.04	5.75	−2.01	0.59	−9.42	−1.53	−1.27	−0.77
SA16	4.05	−1.9	0.094	−0.4	−0.11	−0.99	−0.12	5.68	−2.67	3.18	−11.17	−3.58	−1.32	−1.92
SA18	3.17	−2.14	0.049	−0.8	−0.02	−0.37	−0.31	5.64	−2.42	1.71	N/A	N/A	−1.2	−1.34
SA19	6.18	−1.54	0.099	0.2	0.06	0.03	−0.41	5.53	−1.59	2.74	N/A	N/A	−0.99	−1.12
SA20	3.89	−1.76	0.115	0.14	−0.25	−0.83	−0.23	5.59	−1.88	3.04	N/A	N/A	−1.05	−1.47
SA21	4.09	−2.28	0.022	−0.92	0.27	0.07	−0.16	5.73	−2.77	1.48	N/A	N/A	−1.16	−1.22
SA23	3.91	−1.85	0.089	0.09	−0.13	−0.78	−0.28	5.61	−2.02	2.2	−11.97	−4.17	−1.25	−1.54
SA24	3.8	−3.22	−0.12	0.04	0.87	1.53	−0.33	5.62	−2.26	−0.66	−9.41	−0.8	−1.23	−0.04
SA25	3.6	−3.43	−0.1	−0.8	0.33	0.62	−0.31	5.6	−2.58	−0.2	−9.19	−1.32	−0.87	−0.76

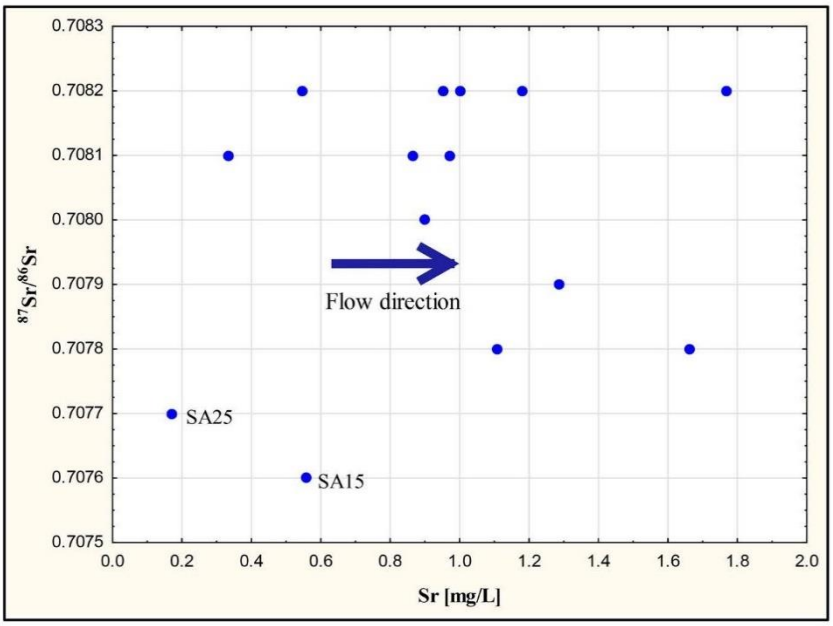

Fig. 6 Diagram of $^{87}Sr/^{86}Sr$ ratio vs. Sr concentration, outliers are marked

of fluorite, CaF_2, keeps F^- at low concentrations (Alarcón-Herrera et al., 2013; Sracek et al., 2015). The maximum concentration of As is 4.27 µg/L, below the WHO limit of 10 µg/L. The maximum concentration of Cr is 3.25 µg/L in well SA19, also below the WHO limit of 50 µg/L. Both contaminants form oxyanionic species desorbed at high pH (Appelo & Postma, 2005; Sracek et al., 2018), but they remain adsorbed and immobile at slightly alkaline pH in the studied system. Concentrations of dissolved Mn are only up to 8.28 µg/L in well SA08 and in many wells are below the detection limit. However, Kareem et al. (2018) found concentrations of Mn up to 911 µg/L south of Sulaimani, downgradient from the waste pile located between the city and the Tanjero River. It seems that most of the dissolved Mn is from waste material and is mobilized under reducing conditions. Concentrations far from the dump were much lower and similar to those found in the study.

Analysis of the interaction of groundwater with surface water in the hyporheic zone of the Tanjero River was beyond the scope of the study. The river is very

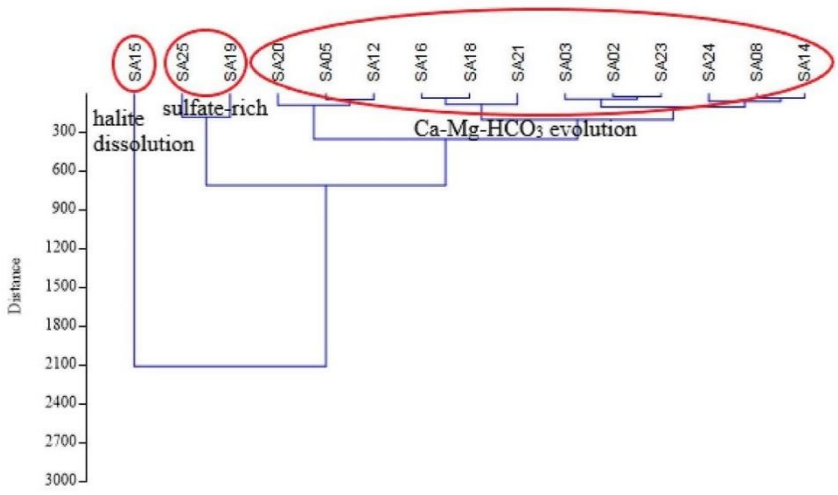

Fig. 7 Hierarchical cluster analysis (HCA) of sampled wells

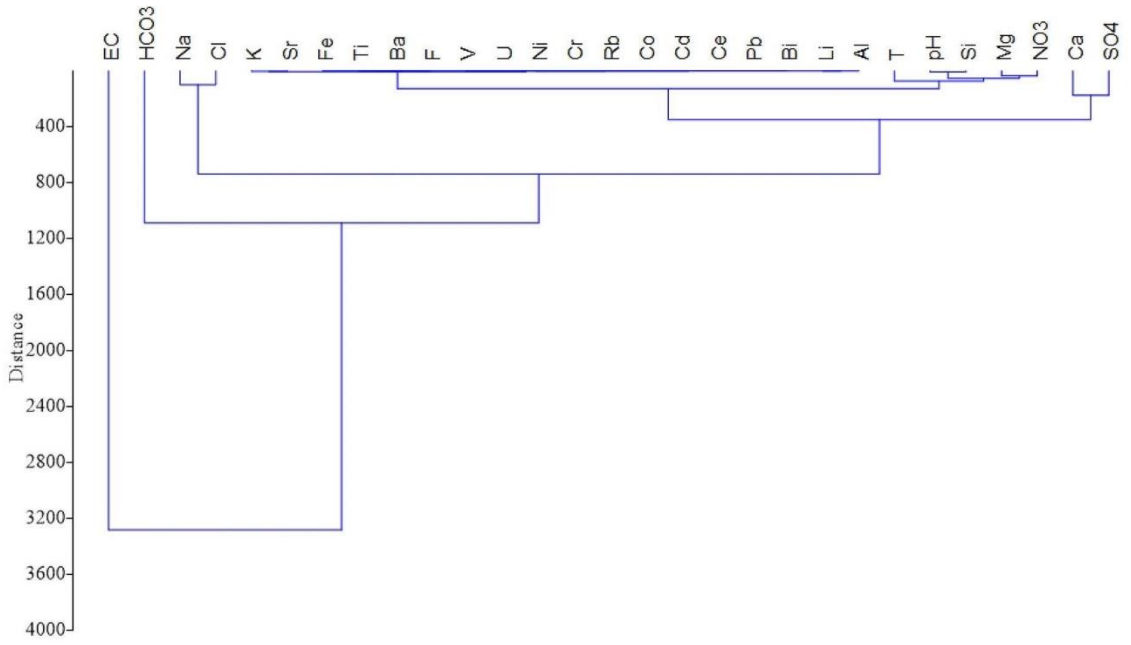

Fig. 8 Hierarchical cluster analysis (HCA) of groundwater parameters

Table 5 Transfer of phases calculated by inverse geochemical modeling. Mass transfer coefficients in mmol/L

Profile	Calcite	Dolomite	Halite	Albite	Gypsum	$Fe(OH)_3$	CH_2O	$SiO_2(a)$	NaX	CaX2	MgX2	$\delta^{13}C$ calc	$\delta^{13}C$ meas
1	+0.104	-	-	+0.001	−0.009	+0.001	+0.0003	-	+0.67	−0.1	−0.24	−1.6	−1.6
2	-	−1.286	+12.96	+3.40	+1.84	+0.027	-	−6.84	+1.85	−1.22	+0.29	−4.1	−4.3
3	−0.027	-	+1.11	-	+0.382	+0.004	+0.001	+0.31	−0.79	+0.07	+0.34	−1.6	−1.6

+ dissolution, − precipitation, X cation exchange

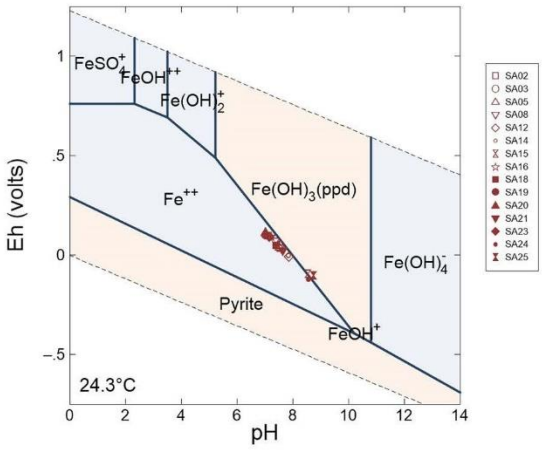

Fig. 9 Eh–pH diagram for system Fe-S, ppd-precipitated, $Fe_T = 1 \times 10^{-5}$ mol/L, $S_T = 5 \times 10^{-4}$ mol/L

contaminated (Mustafa, 2006), and dries out in late summer and fall, and water flow re-appears in early October. Cyclic drying and flooding may induce redox changes with re-mobilization of contaminants like Mn (Sengupta et al., 2018). The waste dump with a resulting increased Mn plume is located close to the river already contaminated by communal sewage. In that case, the behavior of Mn and other redox-sensitive contaminants should be investigated in piezometric profiles perpendicular to the river.

Conclusions

Investigation of groundwater chemistry in the Sulaimani-Warmawa Sub-basin in Sulaimani Governorate, Iraqi

Kurdistan Region, using hydrogeochemical and isotopic methods, provided data for developing a conceptual model of groundwater chemistry evolution. This is a semiarid region with seasonal precipitation which is maximum in January. Water chemistry generally evolves from Ca-HCO_3 groundwater type close to the recharge area in the basin boundaries towards a Ca-Mg-HCO_3 groundwater type close to the Tanjero River in the axis of the basin. Principal dissolution of carbonates occurs already in recharge areas close to the groundwater divide. Some samples have higher concentrations of Na, Cl, and SO_4 because of dissolution of halite and gypsum embedded in carbonates with resulting decrease in bicarbonate concentration due to common ion effect. Values of pH are slightly alkaline or alkaline and redox parameters indicate a moderately reducing environment and simultaneous presence of iron and NO_3 in some samples is probably caused by mixing of groundwater in long-screen pumping wells. Isotopes δ^2H and $\delta^{18}O$ indicate recharge from winter precipitation with no or limited evaporation. Values of dissolved $\delta^{13}C$ (DIC) correspond to interaction with carbonates and C4 plants as the source of CO_2. They show only small variability along the flow path. Values of $^{87}Sr/^{86}Sr$ in groundwater also show small variability and are in good agreement with carbonate dissolution as a principal process. Concentrations of Ba reach up to 0.383 mg/L. Concentrations of other geogenic contaminants such as Mn, As, F, and Cr are low or below the detection limit. Inverse geochemical modeling on selected profiles calibrated using $\delta^{13}C$ values provided mass transfer coefficients in geochemical reactions. Mass transfer coefficients for interaction with carbonates are low, but values for halite and gypsum are much higher. Future work should focus on interactions in the hyporheic zone of the Tanjero River and the seasonal impact of cyclic drying and flooding of river sediments.

Acknowledgements We thank Martin Mihaljevič for water analyses performed at Charles University in Prague and František Buzek from Czech Geological Survey for comments on isotopes. Thanks to Directorate of Groundwater of Sulaimani for providing archived water well data.

Author contribution Rebar Mahmmud—collecting data and interpretation; Ondra Sracek—interpretation and modeling; Omed Mustafa—collecting data and evaluation of contaminant sources; Bohuslava Čejková—carbon isotope analysis; Ivana Jačková—carbon isotope analysis; Lenka Vondrovicova—strontium isotope analysis.

Funding The first author (MR) received Fisher's scholarship awarded by Palacky University in Olomouc (Univerzita Palackého v Olomouci).

Availability of data and materials The used and analyzed datasets in this study are available from the corresponding author on reasonable request.

Declarations

Ethical approval Not applicable.

Consent to participate Not applicable.

Consent for publication Not applicable.

Competing interests The authors declare no competing interests.

References

Alarcón-Herrera, M. T., Bundschuh, J., Nath, B., Nicolli, H. B., Gutierrez, M., Martín-Dominguez, I. R., Reyes-Gomez, V. M., Nuñez, D., Martín-Domínguez, A., & Sracek, O. (2013). Co-occurrence of arsenic and fluoride in groundwater of semi-arid regions in Latin America: Genesis, mobility and remediation. *Journal of Hazardous Materials, 262*, 960–969.

Al-Charideh, A. R. (2011). Environmental isotope study of groundwater discharge from the large karst springs in the west Syria. *Environment and Earth Science, 63*, 1–10.

Al-Jiburi, H. K. et al. (2015). Hydrogeological map of Iraq, scale 1: 1000 000, 2013. *Iraqi Bulletin of Geology and Mining, 11*(1):17–26. Available at: https://www.iasj.net/iasj/download/69d0ec38d854102b

Ali, K. K., Al-Kubaisi, Q. Y., & Al-Paruany, K. B. (2015). 'Isotopic study of water resources in a semi-arid region, western Iraq. *Environmental Earth Sciences, 74*(2), 1671–1686. https://doi.org/10.1007/s12665-015-4172-6

Ali, S. S., (2007). Geology and hydrogeology of Sharazoor - Piramagroon Basin in Sulaimani Area, Northeastern Iraq. Unpublished Ph.D. Thesis, Faculty of Mining and Geology, University of Belgrade, Serbia, 330 p.

Appelo, C. A. J., & Postma, D. (2005). *Geochemistry, groundwater and pollution* (2nd ed.). CRC Press.

Bellen, R. C., Dunnington, H. V., Wetzel, R., & Morton, D. (1959). Lexique Stratigraphique International, Iraq. Vol. III, Asie, Fasc. 10a, Paris. 336 p.

Bertolo, R., Bourotte, C., Hirata, R., Marcolan, L., & Sracek, O. (2011). Geochemistry of natural chromium occurrence in a sandstone aquifer in Bauru Basin, São Paulo State, Brazil. *Applied Geochemistry, 26*, 1353–1363.

Bondu, R., Cloutier, V., Rosa, E., & Roy, M. (2020). An exploratory data analysis approach for assessing the sources and

distribution of naturally occuring contaminants (F, Ba, Mn, As) in groundwater from southern Quebec (Canada). *Journal of Hydrology, 114*, 104500.

Buday, T. (1980). Regional geology of Iraq: Vol. 1, Stratigraphy, I. I. Kassab & S. Z. Jassim (Eds.) D. G. Geo Survey. Min. Invest. Publication. 445 p.

Buday, T., & Jassim, S. Z. (1987). The regional geology of Iraq: Tectonis, magmatism, and metamorphism. I. I. Kassab & M. J. Abbas (Eds.), Baghdad, 445 p.

Clark, I., & Fritz, P. (1997). Environmental isotopes in hydrogeology, Lewis, 328 p.

Craig, H. (1961). Isotopic variations in meteoric waters. *Science, 133*, 1702–1703. https://doi.org/10.1126/science.133.3465.1702

Davies, J. C. (2002). *Statistics and data analysis in geology* (3rd ed.). John Wiley & Sons.

Directorate of Groundwater of Sulaimani, DoGWS. (2020). Ministry of Agriculture and Water Resources, Kurdistan Regional Government, Kurdistan Region, Iraq. https://gov.krd/moawr

Faimon, J., Ličbinská, M., Zajíček, P., & Sracek, O. (2012). Partial pressures of CO2 in epikarstic zone deduced from hydrogeochemistry of permanent drips, the Moravian Karst. *Czech Republic, Acta Carsologica, 41*(1), 47–57.

Ford, D., & Williams, D. (2007). Karst hydrogeology and geomorphology, 2nd Edition, John Wiley & Sons, Ltd.

Frost, C. D., & Toner, R. (2004). Strontium isotopic identification of water-rock interaction and ground water mixing. *Ground Water, 42*(3), 418–432.

Gat, J. R., & Carmi, I. (1970). Evolution of the isotopic composition of atmospheric waters in the Mediterranean Sea area. *Journal of Geophysical Research, 75*, 3039–3048. https://doi.org/10.1029/JC075i015p03039

Halm, D., Gaiser, T., & Stahr, K. (2002). Seepage and groundwater recharge in sandy soils of the semi-arid region of Picos, Northeast Brazil. *Neues Jahrbuch Fur Geologie Und Palaontologie-Abhandlungen, 225*, 85–101.

Hamamin, D. F., et al. (2018). 'Hazard and risk intensity maps for water-bearing units: A case study', International. *Journal of Environmental Science and Technology, 15*(1), 173–184. https://doi.org/10.1007/s13762-017-1376-1

Hammer, Ø., Harper, D. A. T., & Ryan, P. D. (2001). PAST: Paleontological software for education and data analysis. Paleontological Association. https://palaeo-electronica.org/2001_1/past/issue1_01.htm

Harrington, G. A., Cook, P. G., & Herczeg, A. L. (2002). Spatial and temporal variability of groundwater recharge in central Australia: A tracer approach. *Ground Water, 40*, 518–527.

Jassim, S. Z., & Goff, J. C. (2006). Geology of Iraq. Jassim (Eds.) D. G. Geo Survey. Min. Invest. Publication. 445 p.

Johnson, C. A., & Bretzler, A. (2015). Geogenic Contamination Handbook, Eawag, Switzerland. https://www.eawag.ch/fileadmin/Domain1/Forschung/Menschen/Trinkwasser/Wrq/Handbook/geogenic-contamination-handbook.pdf

Kareem, A., Mustafa, O., & Merkel, B. (2018). Geochemical and environmental investigation of thae water resources of the Tanjero area, Kuristan region, Iraq. *Arabian Journal of Geosciences, 11*, 461.

Karim, K. H. (2004) Basin analysis of Tanjero Formation in Sulaimaniya area, NE-Iraq. PhD Thesis, University of Sulaimani, Iraq.

Karim, K., & Ali, S. S. (2004). Origin of dislocated limestone blocks on the slope side of Baranan (Zirgoez) Homocline: An attempt to outlook the development of western part of Sharazoor Plain. *(JZS) Journal of Zankoy Sulaimani, 3*(1), 5–21.

Khosravi, R., Zarei, M., & Sracek, O. (2020). Hydraulic and geochemical interactions between surface water and sediment pore water in seasonal hypersaline Maharlu Lake, Iran. *Hydrological Processes, 34*, 3358–3369.

Markovich, K. H., Manning, A. H., Condon, L. E., & McIntosh, J. C. (2019). Mountain-block recharge: A review of current understanding. *Water Resources Research, 55*(11), 8278–8304.

Mazor, E. (2004). *Chemical and isotopic groundwater hydrology* (3rd ed., p. 465p). Weizmann Institute of Science Rehovot.

McMahon, P. B., & Chapelle, F. (2008). Redox processes and water quality of selected principal aquifer systems. *Ground Water, 46*, 259–271.

Mohammadzadeh, H., & Heydarizad, M. (2019). $\delta^{18}O$ and $\delta^{2}H$ characteristics of moisture sources and their role in surface water recharge in the north-east of Iran. *Isotopes in Environmental and Health Studies, 55*(6), 550–565. https://doi.org/10.1080/10256016.2019.1680552

Mohammadzadeh, H., Eskandari Mayvan, J., & Heydarizad, M. (2020). The effects of moisture sources and local parameters on the 18O and 2H contents of precipitation in the west of Iran and the east of Iraq. *Tellus, Series B: Chemical and Physical Meteorology, 72*(1), 25–39. https://doi.org/10.1080/16000889.2020.1721224

Mook, W. G. (2001) 'Environmental isotopes in the hydrological cycle: Principles and applications, Volume I: Introduction: Theory, Methods, Review', International Hydrological Programme IHP-V, 1, pp. 1–165. Available at: http://wwwnaweb.iaea.org/napc/ih/documents/global_cycle/Environmental%20Isotopes%20in%20the%20Hydrological%20Cycle%20Vol%201.pdf

Mustafa, O. (2006). Impact of sewage waste water on the environment of Tanjero River and its basin with Sulaimani City/NE-Iraq, M.Sc. Thesis, University of Sulaimani-College of Science, Dep. of Geology.

Mustafa, O., & Ahmad, H. (2008). Nitrate pollution in groundwater of Sulaimaniyah City, Kurdistan Region, NE Iraq. *Iraqi Bulletin of Geology and Mining, 4*(2), 73–82.

Mustafa, O., & Merkel, B. (2015). Geochemical evolution and water–rock interactions in Makook Karst aquifers, Kurdistan Region, Iraq. Topical issues of rational use of natural resources, April 22–24, 2015a, St. Petersburg, Russia, National Mineral Resources University, p. 12–14.

Mustafa, O., Merkel, B., & Weise, S. (2015). Assessment of hydrogeochemistry and environmental isotopes in karst springs of Makook Anticline, Kurdistan Region, Iraq. *Hydrology, 2*, 48–68.

Mustafa, O., Tichomirowa, M., Kummer, N. A., & Merkel, B. (2016). Assessment of water-rock interaction processes in the karst springs of Makook anticline (Kurdistan Region, Iraq) using Sr-isotopes, rare earth, and trace elements. *Arabian Journal of Geosciences, 9*, 368. https://doi.org/10.1007/s12517-016-2344-7

Nier, A. O. (1938). The isotopic constitution of strontium, barium, bismuth, thallium and mercury. *Physical Review, 5*, 275–279.

Omar, A. A., Lawa, F. A., & Sulaiman, S. H. (2015). Tectonostratigraphic and structural imprints from balanced sections across the north-western Zagros fold-thrust belt, Kurdistan region, NE Iraq. *Arabian Journal of Geosciences, 8*(10), 8107–8129. https://doi.org/10.1007/s12517-014-1682-6

Osati, K., et al. (2014). Spatiotemporal patterns of stable isotopes and hydrochemistry in springs and river flow of the upper Karkheh River Basin, Iran. *Isotopes in Environmental and Health Studies, 50*(2), 169–183. https://doi.org/10.1080/10256016.2014.857317

Parkhurst, D. L., & Appelo, C. A. J. (1999). Guide to PHREEQC (Version 2)-a computer program for speciation, batch-reaction, one-dimensional transport, and inverse geochemical calculations. Water-Resources Investigations Report 99–4259, U.S. Geological Survey.

Pin, C., Briot, D., Bassin, C., & Poitrasson, F. (1994). Concomitant separation of strontium and samarium-neodymium for isotopic analysis in silicate samples, based on specific extraction chromatography. *Analytica Chimica Acta, 298*(2), 209–217.

Rashid, C, Tahir, J., & Mustafa, O. (2018). Solid waste management: A case study in Chamchamal (Dwbra Valley Open Dump), Sulaimani, Kurdistan Region. (August):210–19.

Ravenscroft, P., Brammer, H., & Richards, K. (2009). Arsenic pollution, A Global synthesis, Wiley-Blackwell, 588 p.

Razmjooei, M. J., Thibault, N., Kani, A., Ullman, C. V., & Jani, A. M. (2020). Santonian-Maastrichtian carbon-isotope stratigraphy and calcareous nannofossil biostratigraphy of the Zagros Basin: Long-range correlation, similarities and differences of carbon-isotope trends at global scale. *Global and Planetary Change, 184*, 103075.

Scanlon, B. R., Keese, K. E., Flint, A. L., Flint, L. E., Gaye, B. C., Esmunds, W. M., & Simmers, I. (2006). Global synthesis of groundwater recharge in semiarid and arid regions. *Hydrological Processes, 20*, 3335–3370.

Sengupta, S., Sracek, O., Jean, J. -S., Yang, H. -J., Wang, C. -H., Kar, S., Babek, O., Lee, C. -Y., & Das, S. (2018). Difference in attenuation among Mn, As, and Fe in riverbed sediments. *Journal of Hazardous Materials, 341*, 277–289.

Sissakian, V. K. (2015). Geological map of Sulaimaniyah, Scale 1:250000', (October). https://doi.org/10.13140/RG.2.1.5109.0642

Sracek, O., Berg, M., & Müller, B. (2018). Redox buffering and de-coupling of arsenic and iron in reducing aquifers across the Red River Delta, Vietnam, and conceptual model of de-coupling processes. *Environmental Science and Pollution Research, 25*(16), 15954–15961.

Sracek, O., Wanke, H., Ndakunda, N. N., Mihaljevič, M., & Buzek, F. (2015). Geochemistry and fluoride levels of geothermal springs in Namibia. *Journal of Geochemical Exploration, 148*, 96–104.

Stadler, S., Osenbrück, K., Suckow, A. O., Himmelbach, T., & Hötzl, H. (2010). Groundwater flow regime, recharge and regional-scale solute transport in the semi-arid Kalahari of Botswana derived from isotope hydrology and hydrochemistry. *Journal of Hydrology, 388*(3–4), 291–303.

Stevanovic, Z., & Markovic, M. (2003). Hydrogeology of northern Iraq, climate, hydrology, geomorphology, Geology. Ed. Filed documents, Vol. 1.

Stevanovic, Z., & Markovic, M. (2004). Hydrogeology of Northern Iraq, Vol.2, General Hydrogeology and Aquifer Systems. *Food and Agriculture Organization of the United Nations, Rome P 264.*

Studio Galli Ingegneria (SGI). (2011). Hydrogeological study for the governorate of around the center of the city, Final Report, January, 2011, Kurdistan Region, Iraq. 200p.

Tóth, J. (1999). Groundwater as a geological agent: An overview of the causes, processes, and manifestations. *Hydrogeology J., 7*, 1–14.

Tóth, J. (2009). *Gravitational systems of groundwater flow.* Cambridge University Press.

Uugulu, S., & Wanke, H. (2020). Estimation of groundwater recharge in savannah aquifers along a precipitation gradient using chloride mass balance method and environmental isotopes, Namibia. *Physics and Chemistry of the Earth, Parts a/b/c, 116*, 102844.

Veizer, J. (1989). Strontium isotopes in seawater through time. *Annual Review of Earth and Planetary Sciences, 17*, 141–167.

WHO. (2017). Guidelines for Drinking-water Quality. https://www.who.int/publications/i/item/9789241550017

Appendix 3: Second published article

water

MDPI

Article

Geogenic Sources of Arsenic and Fluoride in Groundwater: Examples from the Zagros Basin, the Kurdistan Region of Iraq

Omed Mustafa [1,2,*], Rebar Mahmmud [3], Ondra Sracek [3] and Shwan Seeyan [4]

[1] Research Center, University of Sulaimani, Sulaimani 46001, Kurdistan Region, Iraq
[2] Department of Civil and Structural Engineering, University of Sheffield, Broad Lane, Sheffield S1 3JD, UK
[3] Department of Geology, Faculty of Science, Palacky University Olomouc, 17. listopadu 12, 771 46 Olomouc, Czech Republic; rebar.mahmmud@upol.cz (R.M.); ondrej.sracek@upol.cz (O.S.)
[4] Soil and Water Department, Agriculture Engineering Science College, Salahaddin University-Erbil, Erbil 44001, Kurdistan Region, Iraq; shwan.seeyan@su.edu.krd
* Correspondence: omed.mustafa@univsul.edu.iq

Abstract: Groundwater is one of the crucial water resources for domestic, agriculture and other purposes in the Kurdistan Region of Iraq, which is counted as a semiarid region with seasonal precipitation in winter. The geogenic source of arsenic and fluoride in groundwater has been studied in the Kurdistan Region of Iraq, which is a part of the Zagros Basin, using the hydrogeochemical method. The analysis results showed that the concentrations of arsenic and fluoride range from 0.19 to 7.8 µg/L and from 0.01 to 2.1 mg/L, respectively. The hydrogeochemical characteristics of the groundwater in the studied area were connected to the fluoride F^- and arsenic As concentrations for understanding their sources and behavior. The hydrogeochemical relations between F and As indicate geogenic sources and relatively simple aquifer conditions. Some samples may indicate the presence of contamination sources in addition to geogenic sources. Considering the WHO guidelines, the concentrations of As in most of the samples do not exceed the WHO limit, but the F in some samples shows a higher concentration than the WHO limit, indicating a serious risk of fluorosis in some spots. Connecting the changes in F concentrations to depth and aquifer types, a higher F concentration is associated with an intergranular aquifer and decreases in a karst aquifer. The speciation of F^- and As is controlled by pH and redox conditions. Adsorption, cation exchange, and the dissolution of carbonate minerals with the possible dissolution of fluorite are the most dominant geochemical processes that control the concentrations of As and F^- in groundwater. The principal sources of F^- and As in the study area seem to be geogenic.

Keywords: geogenic; arsenic; fluoride; groundwater; karst; Zagros Basin

check for updates

Citation: Mustafa, O.; Mahmmud, R.; Sracek, O.; Seeyan, S. Geogenic Sources of Arsenic and Fluoride in Groundwater: Examples from the Zagros Basin, the Kurdistan Region of Iraq. *Water* **2023**, *15*, 1981. https://doi.org/10.3390/w15111981

Academic Editor: Domenico Cicchella

Received: 5 April 2023
Revised: 2 May 2023
Accepted: 19 May 2023
Published: 23 May 2023

1. Introduction

Geogenic arsenic (As) and fluoride (F^-) are observed worldwide in groundwater [1,2] and groundwater also represents the main source of their intake [3]. A high As concentration in drinking and irrigation water usually enters the food chain and causes health problems [4]. Arsenic can be derived from anthropogenic and geogenic sources, but the latter causes larger groundwater contamination. As is released from the oxidation of sulfide minerals in sedimentary rocks (mostly shale with mean values of 28 ppm), which is higher than those of igneous and metamorphic rocks, by the reductive dissolution of ferric oxyhydroxides, and is also a component of thermal waters [5,6]. Geogenic sources of As are arsenic minerals such as arsenopyrite, orpiment, realgar, claudetite, arsenolite, pentoxide, scorodite, and arsenopalledenite. Alluvial deposits rich in organic matter driving reductive dissolution of ferric oxyhydroxides with adsorbed As are major sources of As in sedimentary formations in countries such as Bangladesh and West Bengal in India [5]. Besides this, industrial waste, coal combustion, oil, cement, phosphate, fertilizers, mine tailing, smelting, ore processing, metal extraction, metal purification, chemicals, glass, leather, textiles, alkalis,

petroleum refineries, acid mines, alloys, pigments, insecticides, herbicides, fungicides, and catalysts contribute to arsenic contamination of the groundwater, soil, and air [7].

Fluorine is essential for human health and low F^- concentrations in water possibly cause dental decay [8], while high F^- concentrations in drinking water have unfavorable health effects, including dental fluorosis (occurrence of yellow-brown spots in the teeth), skeletal fluorosis, and neurological problems resulting from drinking such water for long periods of time [9,10]. Regarding rock-forming minerals, fluorine is only an essential component in fluorite (CaF_2) and topaz (Al_2SiO_4 (F, $OH)_2$), but it is also found in accessory minerals such as cryolite (Na_3AlF_6) and apatite ($Ca_5(PO_4)_3$ (F, Cl_2). Minerals such as phlogopite, biotite, epidote, and amphibole (tremolite and hornblende) also have F. Ultramafic rocks have less than 100 ppm of F, while granitic rocks have F in the order of 800 ppm [11]. Fluoride is released into the groundwater mainly through water–rock interaction by various fluoride-bearing minerals. Fluorite (CaF_2) is the principal mineral of fluorine occurring in nature and is commonly found as an accessory in granitic gneiss [12,13]. Fluorine is also abundant in other rock-forming minerals such as apatite, micas, amphiboles, and clay minerals [14–19].

Fluoride concentration in groundwater is influenced by a number of factors, such as temperature, pH, DIC, the presence or absence of complexing or precipitating ions and colloids [20], the solubility of fluorine-bearing minerals, the anion exchange capacity of aquifer materials, the dimensions and types of geological formations that water flows through, and the length of time that the water is in touch with a specific formation [21]. The concentration of F^- is generally related to the flow systems and is controlled by the water–rock interaction and the residence times in aquifers [10]. The fluorine concentration in metamorphic rocks is between 100 and 5000 ppm in regional metamorphic and contact metamorphic rocks [22]. Moreover, fluoride enters the groundwater through soil contamination as a result of fertilizers and phosphate pesticide application [23]. High F^- concentrations in groundwater are typically linked to Na-HCO_3 waters with low Ca^{2+} concentrations [24,25]. In high Ca^{2+} concentration waters, the F^- concentration is controlled by fluorite, CaF_2, and precipitation [26]. High F^- concentrations are typical for low Ca^{2+} groundwater, e.g., at the Ethiopian Rift [27].

Long-term exposure to arsenic and fluoride, mainly through drinking water intake, can lead to arsenicosis and fluorosis [3]. The initial symptoms of arsenicosis are skin lesions (hyperkeratosis), and the long-term consumption of As-rich water leads to cancer of lungs and bladder [28]. The primary health problems caused by excessive fluoride are dental fluorosis, skeletal fluorosis, and the deformation of bones in children and adults [29]. Fluorosis has the most significant impact on growing teeth, and children under seven years old are particularly vulnerable [30]. There is also evidence that the adverse health effects of fluoride are enhanced by the lack of Ca, vitamins, and protein in the diet [31,32].

The purpose of this study was (1) to review As and F occurrences in Iraqi Kurdistan with a focus on geogenic sources and (2) to determine the factors responsible for their release and mobility control in groundwater.

2. Study Area

The area of interest is located in the Kurdistan Region, north of Iraq and north-west of the Zagros Basin. It is divided into two zones. The first zone is in the Sulaimani governorate, and the second is in Erbil governorate.

Sulaimani Area (Sulaimani city, Tanjero, Arbat, Tasluja, Bazian, Piramagroon, Makook)

This zone is located mainly in the Sulaimani governorate, Ranya, Halabja, and Sulaimani districts in the foothills of the Zagros Mountains, Kurdistan Region, Iraq (Figure 1). The Sulaimani city, Tanjero, Arbat, and Tasluja zones are parts of Tanjero Basin. It is situated within latitudes 35°50′–36°30′ north and longitudes 45°52′–45°05′ east in the elevation range from 700 m to >2000 m above sea level (a.s.l.).

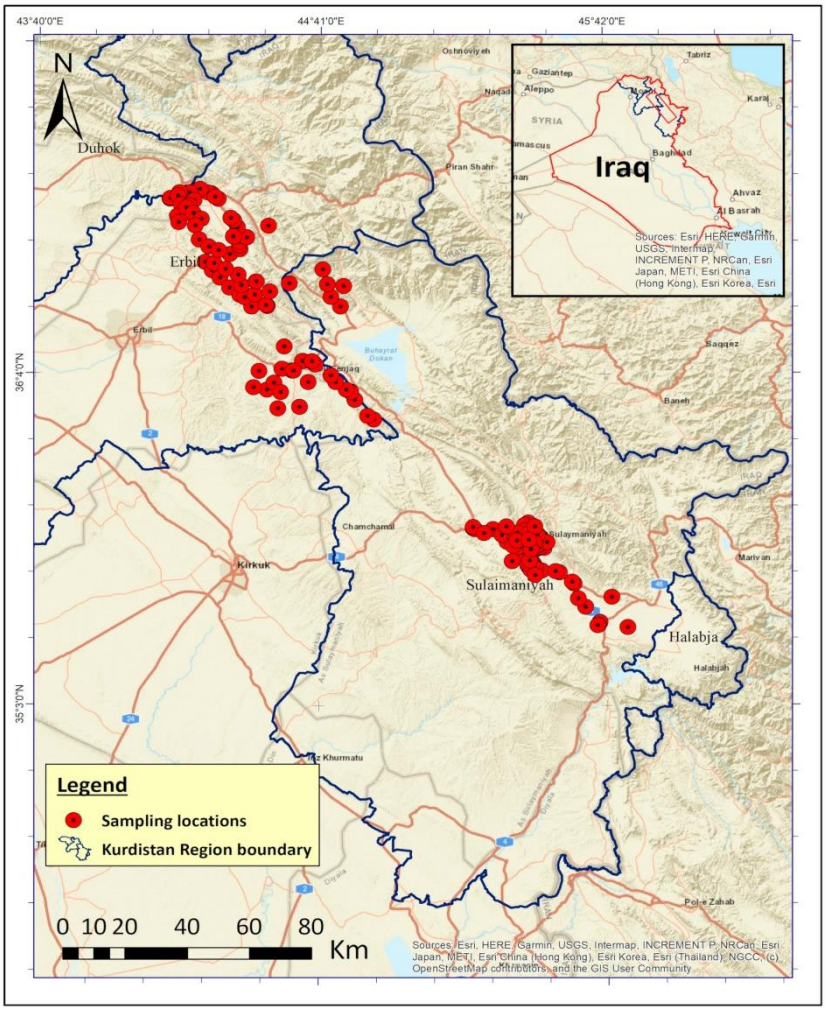

Figure 1. Location of the study area and sampling points.

Erbil Area (Koysinjaq, Shiwashok, Shaqlawa, Harrir)

This zone is located mainly in the Erbil governorate, Erbil, Koysinjaq, and Shaqlawa-Harrir districts in the Kurdistan Region, Iraq (Figure 1). The Koysinjaq and Shiwashok zone is part of the Koysinjaq-Surdash basin and the Shaqlawa-Harrir Basin is located in the northeast of Erbil city. The Shaqlawa and Harrir Basin is divided into three small basins: Tawska, Hiran, and Harash. The area is situated within latitudes 35°50′–36°45′ north and longitudes 44°04′–44°57′ east in the elevation range from 400 m to >1000 m above sea level (a.s.l.).

The climate in the study area is semiarid, with a distinct rainy period in winter and a dry period in summer when temperatures reach more than 40 °C. The average annual temperature is 21 °C. The mean annual precipitation in the Sulaimani area is 669 mm, and most pre-precipitation falls in January and February when most of the aquifer recharge occurs [33]. Meanwhile, Meteorological data obtained from the ground meteorological station in Salahaddin district/Erbil Governorate (Pirmam meteorological station) for the

period between 1992 and 2012 show that the annual precipitation is about 589 mm in Erbil zone [34].

2.1. Geologic Setting

From a geological viewpoint, the study area is divided into two provinces: Sulaimani and Erbil. The geological units that cropped out in the area are presented in Figure 2 and Table 1. The age of the units ranges from Early Cretaceous to Quaternary. The oldest unit of the Lower Cretaceous age is the Qamchuqa Formation, predominantly composed of carbonates. The Upper Cretaceous formations are represented by carbonates of the Aqra-Bekhme Formation and impure carbonate rocks of the Shiranish and Tanjero Formations. Alternation of flysch and carbonates of the Kolosh, Khurmala, Gercus, and Pila Spi Formations overlie the Cretaceous rocks.

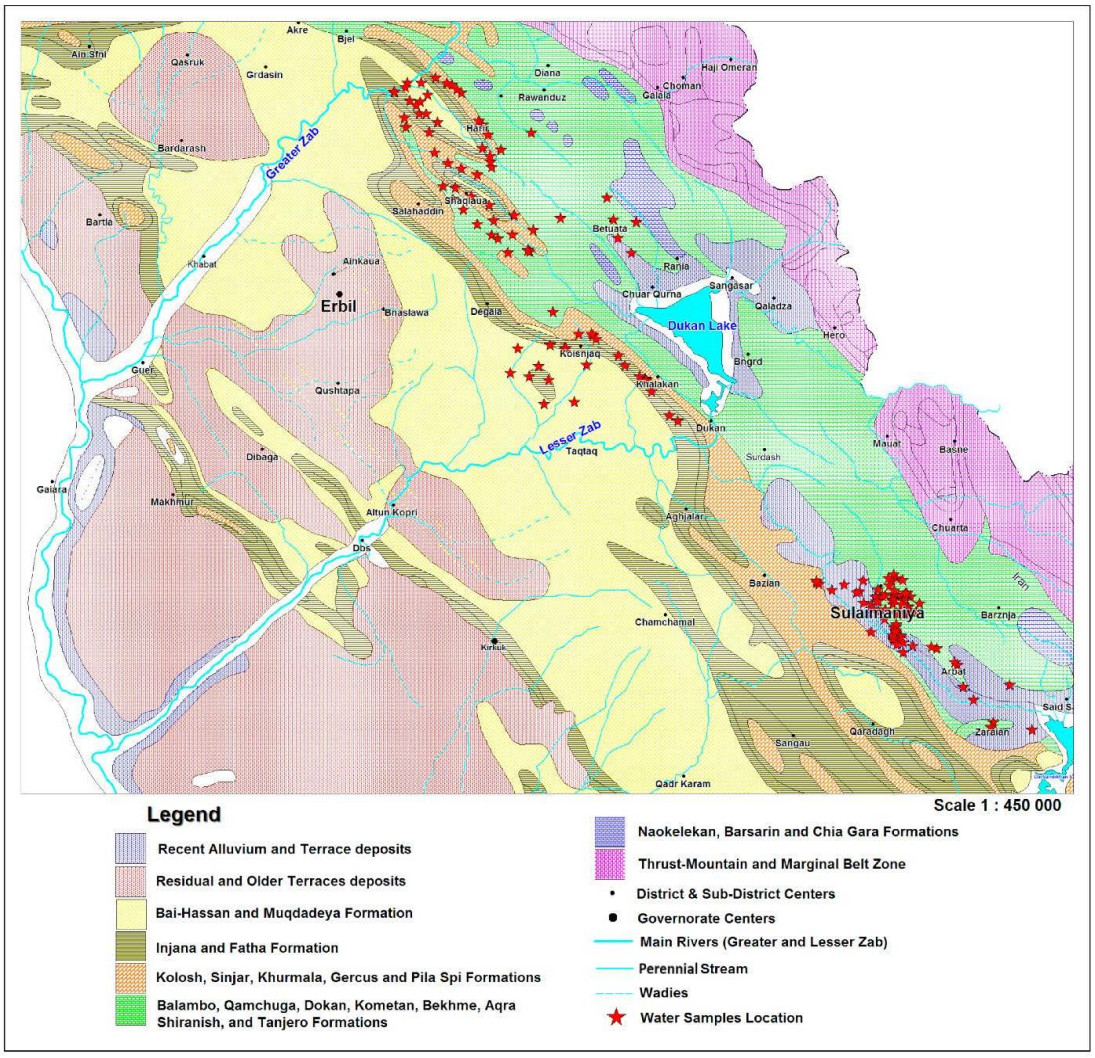

Figure 2. Geology of the study area.

Table 1. Geology and stratigraphy [24,35,36].

Stratigraphic Unit	Age	Lithology	Location
Recent alluvial deposits and River Terraces	Quaternary	Clastic sediments, clay, sand, pebbles, and boulders	Sulaimani, Koysinjaq
Bai Hassan and Muqdadiya Formation	Pliocene	Sandstone, siltstone, and conglomerate	Sulaimani, Koysinjaq
Injana Formation	Late Miocene	Claystone, siltstone, and sandstone	Sulaimani, Koysinjaq
Fatha Formation	Middle Miocene	Alternation of sandstone, claystone, limestone, gypsum, rock salt, and anhydrite	Sulaimani, Koysinjaq,
Pila Spi Formation	Middle-Late Eocene	Bituminous, chalky, and crystalline limestone with chert nodules	Sulaimani, Koysinjaq
Sinjar, Khurmala and Gercus Formation	Early Eocene	Red mudstone, sandstone, shale, and conglomerate	Sulaimani, Koysinjaq
Kolosh Formation	Paleocene	Clastic, shale, limestone, marl, and mudstone	Koysinjaq, Shaqlawa, Harrir, Erbil Area
Tanjero and Shiranish Formations	Late Cretaceous	Blue marl overlaying limestone and marly limestone	Sulaimani, Koysinjaq, Makook
Aqra-Bekhme, Kometan and Qamchuqa Formations	Late Cretaceous	Bituminous dolomitic limestone and massive organic limestone	Sulaimani, Koysinjaq, Makook
Sarki and Sehkaniyan Formation, Naokelekan and Barsarin Formation and Chia Gara Formation	Jurassic	Limestone, dark dolomite, bituminous limestone, marl, and shale	Sulaimani, Koysinjaq and Makook

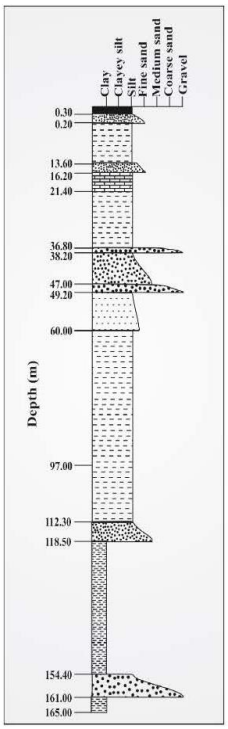

2.2. *Hydrogeology*

Four aquifer systems are recognized in the study area: karst, fissured karst, Tanjero, and intergranular aquifers. The rocks of the Tanjero Formation often form an aquitard and are composed of alternating marly limestone, sandstone, marl, and occasionally conglomerate beds, but they are highly deformed and fractured (especially in the Sulaimani city area), which allows the formation of secondary porosity [37]. Where permeability is increased due to secondary porosity, the Tanjero Formation becomes a medium-depth to deep aquifer (25–120 m) that yields a good quantity of water in the sandstone and marly limestone facies. The majority of the wells in the study area are drilled within the Tanjero porous aquifer. The shallow Quaternary intergranular aquifer (0–25 m depth) is represented by shallow terraces and recent alluvium deposits, which are composed of unconsolidated gravel and sand that yield a good quantity of water [38]. Another part of the intergranular aquifer is represented by the Bai Hassan and Muqdadiya Formations. Typical characteristics of these aquifers are the inter-bedded layers of fine, medium, and coarse-grained textures and variations in permeability from one site to another within the same aquifer horizon. Karst aquifers are represented by the Bekhme and Qamchuqa Formations and are anisotropic and heterogeneous, with very high permeability and transmissivity [39] and a conduit flow regime containing large groundwater reserves [40]. Wells in these formations have high specific yields and the drawdowns in pumping wells are very small [39]. Most freshwater in the Shaqlawa and Harrir basins is produced from this aquifer [34]. Fissured karst aquifers are represented by the Kometan and Pila Spi Formations containing medium to large groundwater reserves. The aquifer is characterized by high permeability and transmissivity and a turbulent flow regime [39]. Both karst and fissured karst are developed in limestone, dolomites, marly limestones, and dolomitic limestones. The other formations,

such as Injana, Fatha, and Kolosh, contain a limited amount of groundwater because they are composed mainly of impermeable layers such as claystone and marls (mostly forming aquiclude) and partially alternate with permeable fractured limestone, which, in turn, results in low permeability and a limited amount of groundwater.

2.3. Material and Methods

Ninety-two wells within the Sulaimani area and seventy-eight wells and springs in the Erbil area were sampled in this study from three different aquifers: intergranular, fissured, and karst. Therefore, the total number of samples was 170. The water samples were collected in a sterilized polyethene bottle. The samples selected for analysis were filtered with 0.2 µm cellulose acetate filters and then acidified with an ultra-pure nitric acid (30% HNO_3). All water samples were stored in a cool box at 4 °C until analysis in the laboratory. Physical parameters such as temperature, pH, electrical conductivity (EC), and redox potential (Eh) were measured in the field and corrected with respect to the H_2 electrode. Chemical parameters for the samples were determined in the laboratories of Technische Universität Bergakademie Freiberg, Germany, Sulaimanyiah Environmental Protection Office, Iraq, and Charles University in Prague, Czech Republic, according to [41]. Cations and trace elements were examined with the ICP-MS technique at the analytical laboratories of Charles University in Prague, and the laboratories of the Hydrogeology Department, Technical University Bergakademie Freiberg, Germany. The analytical error of the individual solution analyses was below 2%. Anion concentrations were determined by HPLC, Dionex ICS. Ferrous iron was determined by potassium dichromate titration. Alkalinity values were determined by HCl titration with the Gran plot to determine the endpoint. Major cations and anions were determined with ion chromatography (Metrohm-Compact IC Pro). Trace elements were analyzed with ICP-MS (Thermo Scientific-XSERIES 2). Total inorganic carbon (TIC) was measured with an Elementar Liqui-TOC. As was measured with ICP-MS (Thermo Scientific-XSERIES 2) and F with ion chromatography (Metrohm-Compact IC Pro). The raw data were subject to statistical tests using SPSS [42]. The ion balance and saturation indices of minerals and molar concentrations were calculated by PHREEQC code [43], using the WATEQ4F and PHREEQC databases. Location maps and spatial distribution maps were made using ArcGIS 10.7.1.

3. Results and Discussion

3.1. Groundwater Chemistry

3.1.1. Sulaimani Area

The statistical parameters of the water chemistry for each zone in the studied areas are given in Table 2, and the complete data set is given in the Supplementary Materials in Table S1. The Piper plot for the groundwater chemistry data is presented in Figure 3. In the Piper plot, the evolution from Ca-HCO_3 groundwater type to Na-HCO_3 groundwater type is evident, indicating favorable conditions for F^- enrichment in groundwater [20,44].

Table 2. Field and laboratory parameter statistics for the groundwater samples.

Area	Zone	Depth	Aquifer	Statistics	Tem.	pH	pE	EC	TDS	Ca^{2+}	Mg^{2+}	K^{+}	Na^{+}	HCO_3^{-}	SO_4^{2-}	Cl^{-}	NO_3^{-}	F^{-}	As
Sulaimani area	Zone 1 Sulaimani Tanjero	45–145	Intergranular, Karst, Fissured	Min.	20.1	6.8	5	NA	NA	6.9	1	0.4	20.7	214.5	28.2	13.8	2.4	0.1	0.0002
				Max.	25.5	8.8	6.2	NA	NA	138	29.8	3.9	222	424	144	110.0	25.9	1.65	0.0078
				Mean	22.1	7.5	5.6	NA	NA	68.3	15.0	1.4	100.1	329.1	82.9	51.9	7	0.34	0.0020
	Zone 2 Sulaimani Bazian	6–190	Intergranular, Karst, Fissured	Min.	5.8	5.8	NA	16	1.6	8	0.2	0.9	25.6	NA	46	2.5	0.1	NA	NA
				Max.	9.3	9.3	NA	1177	80	68	2.9	164.9	145	NA	220	50.5	1.7	NA	NA
				Mean	7.1	7.1	NA	360	23.1	37.8	1.2	31.8	212.2	NA	205.8	30.3	0.3	NA	NA
	Zone 3 Sarwchawa-Diyana	Springs	Karst	Min.	9.5	7.3	21.7	310	NA	42.7	10.7	0.3	0.9	172.2	10	1.4	2.6	0.04	0.0002
				Max.	17.4	7.8	23.5	602	NA	76.1	21.6	1.8	4.4	340.4	70.4	8.3	21	0.13	0.0003
				Mean	13.4	7.5	22.7	460	NA	58.2	17.5	0.7	1.8	253.3	20.3	2.7	6.3	0.07	0.0003
	Zone 4 Sulaimani-Warmawa	71–450	Intergranular, Karst, Fissured	Min.	21.8	7.0	NA	328	NA	6.1	2.3	0.3	2.7	140	7.4	1.9	0.2	0.2	0.0001
				Max.	26.8	8.8	NA	2460	NA	113	40.4	2.7	480	320	200.7	462.4	36	0.54	0.0043
				Mean	24.3	7.7	NA	663	NA	51.2	11.9	0.9	55.6	215.3	47.3	43.4	15.4	0.23	0.0011
Erbil area	Zone 5 Shiwashok	80–210	Intergranular, Karst, Fissured	Min.	7.3	NA	NA	500	11.7	6.3	1.2	25.7	198	59	23.3	4.6	0.3	NA	0.0002
				Max.	8.5	NA	NA	1193	164	77.7	19.2	320.2	293	790.7	223	209.3	1.3	NA	0.0012
				Mean	7.8	NA	NA	793	72.3	32	5.1	117.4	237.5	253.8	91.3	49.3	0.5	NA	0.0005
	Zone 6 Koysinjaq	96–281	Intergranular, Karst, Fissured	Min.	24.1	7.3	9.6	462	300.3	64.2	7.1	0.5	0.9	258.7	14	4.7	1.4	0.04	0.0002
				Max.	24.9	7.6	12.7	751	488.2	89.4	30.7	1.2	9.5	382.7	31.7	12.2	8.7	0.64	0.0012
				Mean	24.5	7.4	11.0	572	372	75.2	23.5	0.7	2.9	322	20	6.4	4.5	0.14	0.0005
	Zone 7 Shaqlawa–Harrir	68–239, Springs	Intergranular, Karst, Fissured	Min.	21.2	7.2	6.4	297	193	4	4.1	0.3	1.1	168.9	10.6	4.3	0.1	0.04	0.0002
				Max.	22.5	8.3	13.2	1355	880.8	118	74.7	8.3	117.6	532.1	272.2	114.1	41.5	2.12	0.0020
				Mean	21.8	7.6	10.1	612	397.6	67.1	27.3	1.2	16.5	322.7	38.8	15.5	10.1	0.33	0.0007

Note: Concentration is in mg/L, temperature = °C, EC = µS/cm, depth = meters, and NA = not available.

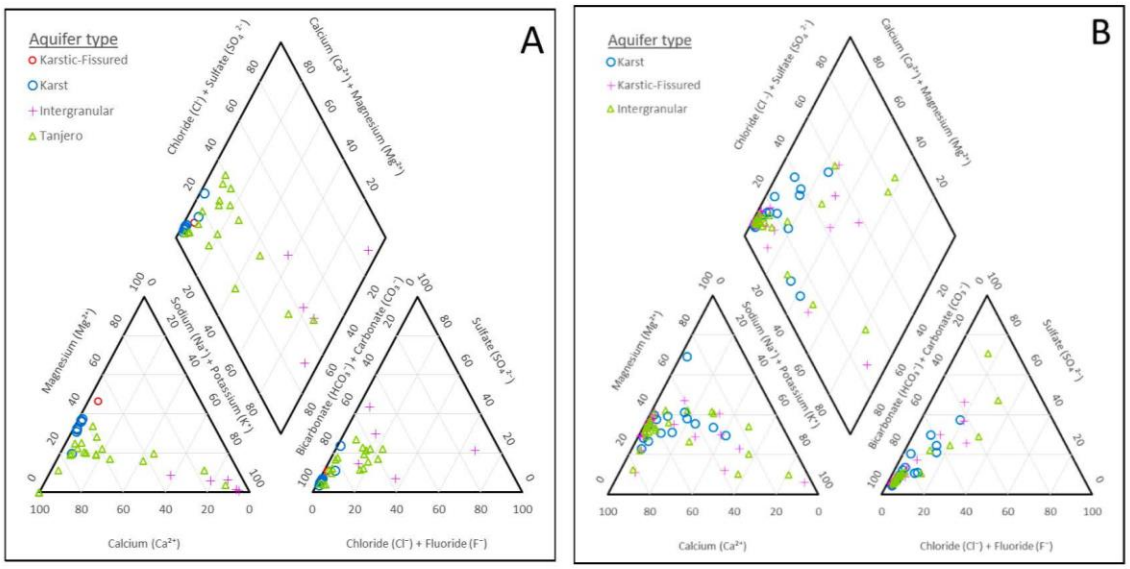

Figure 3. Piper diagram for groundwater samples: (**A**) Sulaimani area, (**B**) Erbil area.

The values of electrical conductivity range from 25 to 2460 µS/cm; the average is 558.6 µS/cm. The EC values for Tanjero, karst, and intergranular aquifers are in the range from 25 to 935, 310 to 602, and 538 to 2460 µS/cm, respectively. The pH values in the Sulaimani area are in the range from 5.8 to 9.3 and the average pH value is 7.5. The pH value in the Tanjero aquifer is in the range of 5.8 to 8.6, in the karst aquifer in the range of 7.3 to 7.8, and in the intergranular aquifer ranges from 7.3 to 8.8. The average value of Ca is 52.4 mg/L with concentrations from 1.6 to 138 mg/L. In the Tanjero aquifer, the concentration of Ca is in the range from 1.6 to 138 mg/L, in the karst aquifer is in the range from 42.7 to 76.1, and in the intergranular aquifer is in the range from 6.9 to 73.9 mg/L. Concentrations of Mg range from 1 to 77.7 mg/L, with the average being 25.7 mg/L. The concentrations are from 4.7 to 68 mg/L in the Tanjero aquifer, 10.7 to 21.6 mg/L in the karst aquifer, and 1 to 59 mg/L in the intergranular aquifer. Concentrations of Na are from 0.9 to 480 mg/L, with the average being 33.8 mg/L; in the Tanjero aquifer, the concentration of Na is in the range from 0.9 to 222 mg/L, in the karst aquifer is in the range from 0.9 to 1.8 mg/L, and in the intergranular aquifer from 7 to 480 mg/L. The concentration of K ranges from 0.2 to 19.2 mg/L, and the average is 1.3 mg/L; the concentrations of K for the Tanjero, karst, and intergranular aquifers are in the range of 0.2 to 3.9, 0.3 to 1.84, and 0.5 to 2.3 mg/L, respectively. Concentrations of HCO_3 range from 25.6 to 532.1 mg/L, with an average of 264 mg/L; HCO_3 ranges from 25.6 to 424 mg/L in the Tanjero aquifer, from 172.2 to 340.4 mg/L in the karst aquifer, and 140 to 297.8 mg/L in the intergranular aquifer. The concentration of SO_4 ranges from 7.35 to 790 mg/L with an average of 55.19 mg/L; in the Tanjero aquifer, the SO_4 concentration is in the range of 7.35 to 118 mg/L, in the karst aquifer is from 10 to 70.4 mg/L, and in the intergranular aquifer is from 28.2 to 200.7 mg/L. The concentration of Cl ranges from 1.4 to 462.4 mg/L, the average is 63.9 mg/L, and the concentrations of Cl for the Tanjero, karst, and intergranular aquifers are in the range of 1.9 to 288, 1.4 to 8.3, and 13.8 to 462.6 mg/L, respectively.

3.1.2. Erbil Area

In the Erbil area, the values of EC range from 297 to 1355 µS/cm, the average is 596.2 µS/cm, and the EC values for the karstic-fissured, karst, and intergranular aquifers are in the range from 412 to 695, 297 to 1319, and 313 to 1355 µS/cm, respectively. The pH

values are in the range from 7.2 to 8.5, and the average pH value is 7.5. The pH value in the karst-fissured aquifer is in the range of 7.2 to 8.5, the pH in the karst aquifer is in the range of 7.2 to 8.1, and in the intergranular aquifer ranges from 7.25 to 8.2. The average value of Ca is 69.5 mg/L with concentrations from 4 to 164 mg/L; in the karstic-fissured aquifer, the concentration of Ca is in the range from 4 to 90.5 mg/L, in the karst aquifer is in the range from 18.9 to 118.2, and in the intergranular aquifer is in the range from 12 to 164 mg/L. Concentrations of Mg are from 4 to 77.7 mg/L, the average is 26.8 mg/L, and is in the range of 4 to 77.7 mg/L for the karstic-fissured aquifer, from 8.7 to 66.3 mg/L in the karst aquifer, and from 7.1 to 74.7 mg/L in the intergranular aquifer. Concentrations of Na are from 0.9 to 320.2 mg/L, the average is 23.3 mg/L, and in the karstic-fissured aquifer, the concentration of Na is in the range from 0.9 to 117.6 mg/L, in the karst aquifer is in the range from 1.4 to 74.9 mg/L, and in the intergranular aquifer is in the range from 1 to 320.2 mg/L. In addition, concentrations of K are from 0.2 to 19.3 mg/L, the average is 1.46 mg/L, and the concentrations of K for the karstic-fissured, karst, and intergranular aquifers are in the range from 0.2 to 8.26, 0.4 to 5.58, and 0.3to 19.2 mg/L, respectively. Concentrations of HCO_3 are from 168.9 to 532.1 mg/L, the average is 313.8 mg/L, and the values are from 195.9 to 410.5 mg/L in the karstic-fissured aquifer, from 168.9 to 500.8 mg/L in the karst aquifer, and from 172.3 to 532.1 mg/L in the intergranular aquifer. Concentrations of SO_4 are from 10.5 to 790.7 mg/L, the average is 56 mg/L, and in the karstic-fissured aquifer, the SO_4 concentration is in the range from 12.4 to 224 mg/L, in the karst aquifer is in the range from 10.5 to 272.18 mg/L, and in the intergranular aquifer is in the range from 13.9 to 790.7 mg/L. Concentrations of Cl are from 4.3 to 233 mg/L, the average is 20.9 mg/L, and the concentrations of Cl for the karstic-fissured, karst, and intergranular aquifers are in the range of 4.3 to 99, 4.5 to 98.3, and 4.71 to 223 mg/L, respectively.

3.2. *Statistical Analysis*

Correlation between F^- and As

In the groundwater of the Sulaimani area, the concentrations of As and F show a significant (R^2 = 0.736) positive correlation (Figure 4A). This relation may reflect their similar adsorption behavior, i.e., their desorption at higher pH values due to their anionic form [1,11,45]. In the case of high calcium and low As concentrations, a positive correlation with F^- may reflect the presence of a contamination source in addition to the geogenic source [19]. The groundwater of the Erbil area shows only a positive, but not significant correlation (R^2 = 0.37) (Figure 4B).

3.3. *Occurrence and Geogenic Sources*

3.3.1. Variation of Concentrations with Depth

The concentration of As appears not to be depth-dependent because there is no clear trend of As concentration with changing depth. A low As concentration is linked to the shallower aquifer and roughly increases with depth (Figure 5A). Two distinctive groups are recognized from the As–depth relation: Group A and Group B. This grouping is based on the type of aquifer, in which the karst aquifer shows relatively higher As concentrations (0.2–2 µg/L) with a wide range of depth variation (60–280 m). Group B represents groundwater from an intergranular aquifer with a lower As concentration compared to Group A (0.2–0.7 µg/L). The behavior of F^- concentration is completely opposite to the As concentration because a higher F concentration is associated with the intergranular aquifer and decreases in the karst aquifer (Figure 5B).

3.3.2. Speciation of As and F

According to the Eh–pH diagram, the low observed As concentration corresponds to a neutral pH and moderate to high Eh values (Figure 6A). The $HAsO4^{2-}$ is the dominant species of As in both the Sulaimani and Erbil areas. This may be linked to the affinity of Fe-oxyhydroxide minerals for As (V) in adsorption and co-precipitation reactions [46]. The neutral pH and oxidizing conditions assist in retaining As (V) onto Fe minerals. With

the rising pH value above 7.8, the As concentration increases (especially in the Sulaimani samples) and reflects the dependency of pH on desorption [5,47]. In the groundwater of the Sulaimani area, As speciation is controlled by pH, redox conditions, temperature, and the dissolution of calcite and dolomite minerals [48].

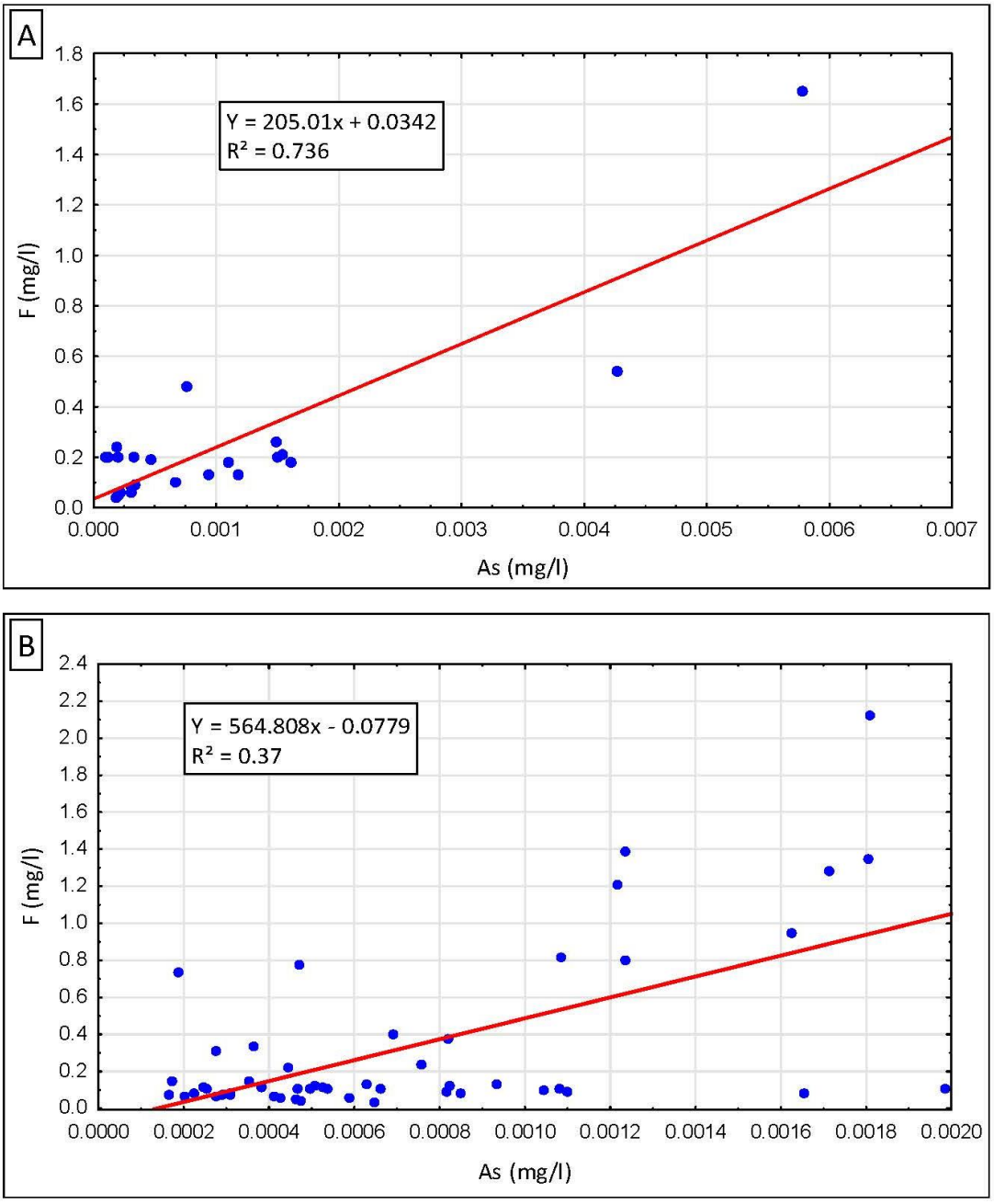

Figure 4. Correlation between fluoride and arsenic in groundwater: (**A**) Sulaimani area, (**B**) Erbil area.

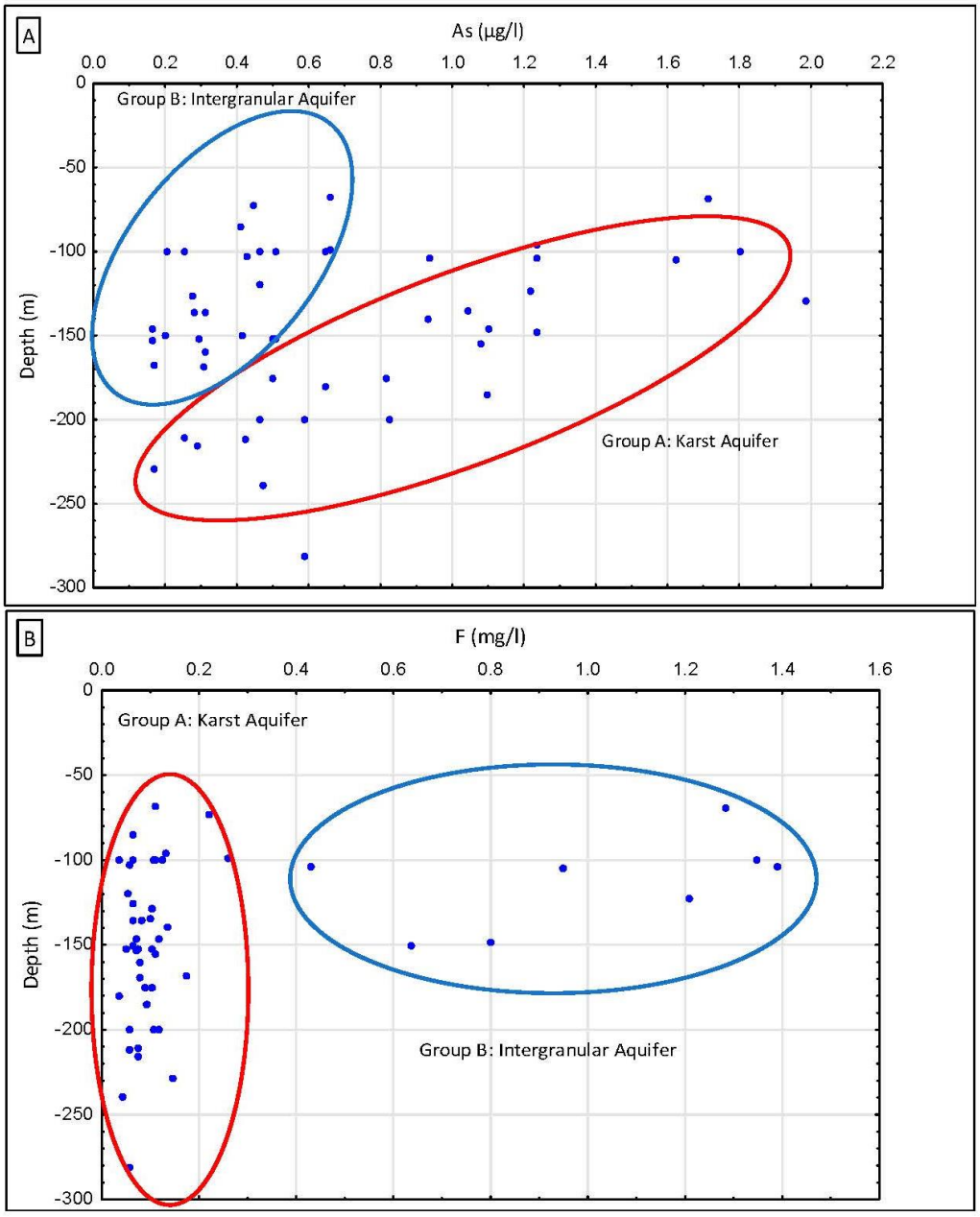

Figure 5. Variation of As (**A**) and F (**B**) with depth.

Regarding F, there is only one oxidation state, F^-—i.e., it is Eh-independent and samples with F concentration >1 mg/L are characterized by lower pH values of 6.5–7.5. An increasing pH value results in F release due to the competition with adsorbed OH^- [49]. The high concentrations of HCO_3^- and pH conditions are responsible for F enrichment [20,47]. Notably, F concentrations show a positive correlation with HCO_3^- and Cl^- concentrations

($R^2 = 0.37$) in the groundwater of the Erbil area. A high HCO_3^- concentration in groundwater may remove Ca^{2+} and promote CaF_2 dissolution, causing the release of F^- [49].

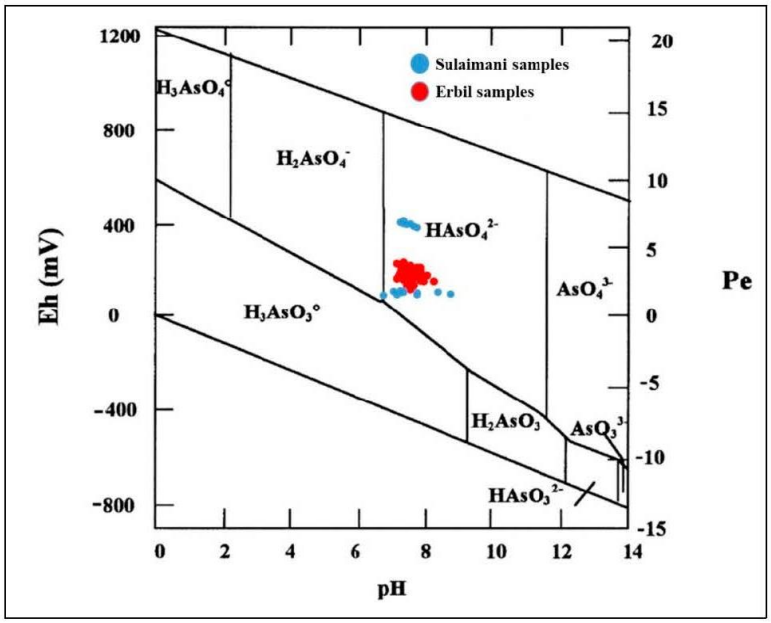

Figure 6. Eh–pH diagrams of As.

3.3.3. Saturation Indices

There is no clear trend in relation to As and F^- concentrations and saturation indices for calcite and dolomite (Figure 7A,B). Some high F^- groundwaters are mostly supersaturated with respect to calcite (Figure 7B), and most samples are undersaturated with respect to fluorite (Figure 7C) and dolomite (Figure 7D), which is compatible with the findings of [50]. Fast recharge may lead to the dilution of groundwater and cause low F^- concentrations and undersaturation with respect to calcite and dolomite [47]. In addition, undersaturation with respect to fluorite in some samples can be caused by sampling from long screen wells in which the concentrations of F^- were diluted [26]. In general, negative saturation indices for fluorite suggest the dissolution of the mineral when present in the solid phase of the studied aquifers.

3.4. Correlation of As and F with Hydrochemical Parameters

The correlation matrix of As and F with hydrochemical parameters is given in Table 3. In the samples from the Sulaimani area (Table 3(A)), the correlation coefficients show that the most significant correlations are those between SO_4, Cl, Ca, and Na against electric conductivity (EC) and pH. Some samples have increased concentrations of Na, Cl, and SO_4 as a consequence of the dissolution of halite and gypsum embedded in carbonates [33]. This may also be reflected by the predominance of sulphate and sodium chloride facies in some groundwater samples [51]. These correlations may indicate the geological sources of these components [52]. The correlation matrix for Erbil area samples (Table 3(B)) shows a significant correlation of Mg with SO_4, Cl, and bicarbonate. This may be caused by the dolomite dissolution from the dolomite and dolomitic limestone in the karst aquifers of the Erbil area, as indicated by the presence of hydrochemical facies of Mg-Ca-Na-SO_4-HCO_3 groundwater in the Erbil area [40,53]. There is a negative correlation between Na^+ and Ca^{2+}, suggesting cation exchange. This is further supported by intermediate, but significant, correlation between Na^+ and F^- in both areas, linking high F^- to Na^+-rich

groundwater [25,44]. Cation exchange removes Ca^{2+} (Equation (1)) and promotes the dissolution of fluorite (Equation (2)), resulting in Na-HCO_3 groundwater rich in F^-:

$$CaCO_3 + CO_2 + H_2O + Na_2\text{-}X = 2Na^+ + 2HCO_3^- + Ca^{2+} \quad (1)$$

$$CaF_2 = Ca^{2+} + 2F \quad (2)$$

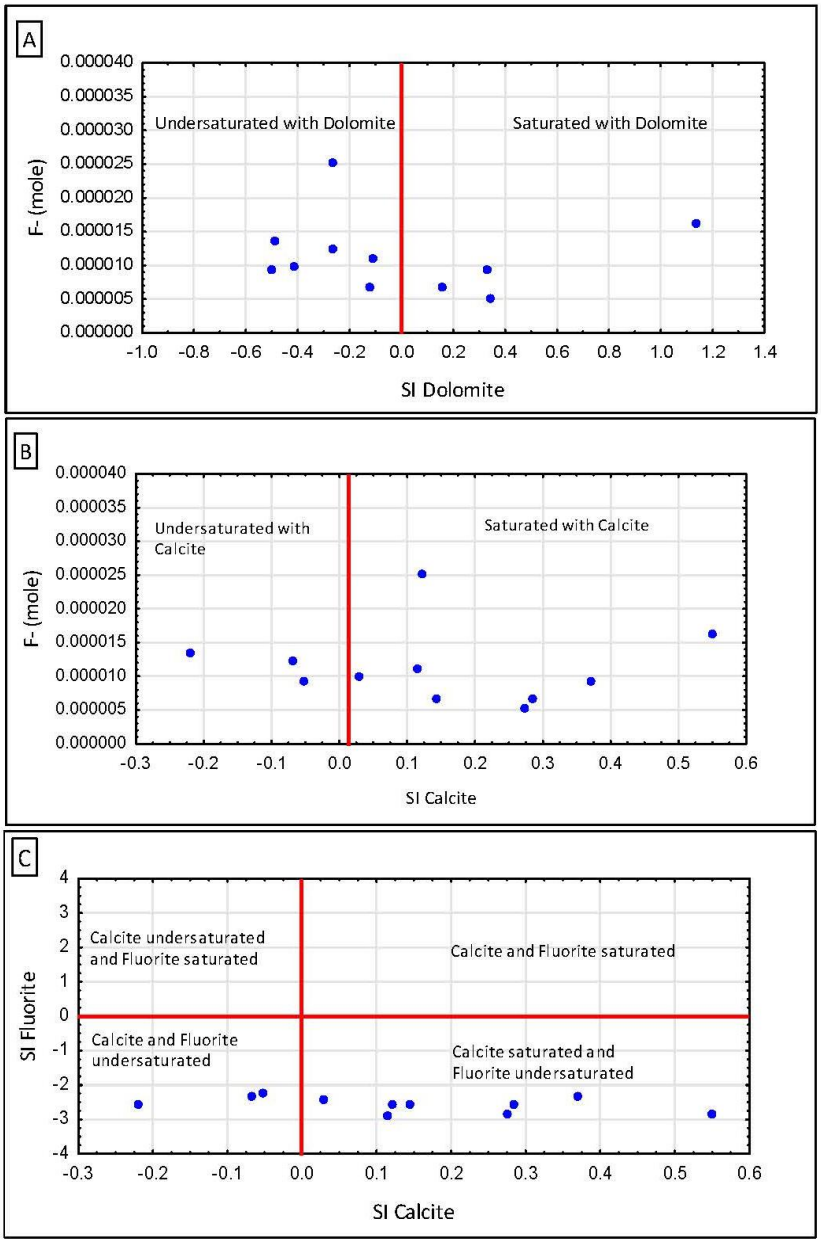

Figure 7. *Cont.*

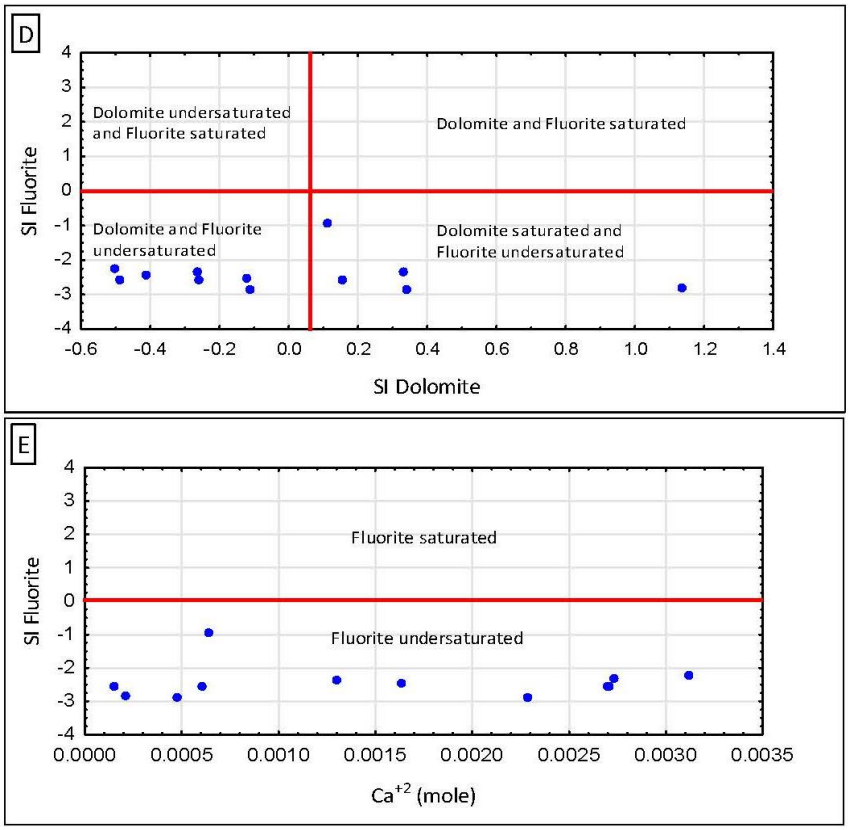

Figure 7. Correlation between (**A**) F^- and SI-dolomite, (**B**) F^- and SI-calcite, (**C**) SI-fluorite and SI-calcite, (**D**) SI-fluorite and SI-dolomite, and (**E**) SI-fluorite and Ca^{2+}.

Table 3. Correlation matrix for groundwater parameters: A, Sulaimani area; B, Erbil area.

	pH	EC	Ca^{2+}	Mg^{2+}	K^+	Na^+	HCO_3^-	SO_4^{2-}	Cl^-	NO_3^-	F^-	As
pH	1											
EC	0.16	1										
Ca^{2+}	−0.8	0.1	1									
Mg^{2+}	−0.63	0.03	0.76	1								
K^+	−0.17	0.44	0.46	0.14	1							
Na^+	0.54	0.79	−0.44	−0.45	0.16	1						
HCO_3^-	−0.39	0.24	0.56	0.5	0.45	−0.07	1					
SO_4^{2-}	0.25	0.77	−0.02	−0.05	0.34	0.8	0.19	1				
Cl^-	0.31	0.93	−0.12	−0.19	0.28	0.85	−0.05	0.67	1			
NO_3^-	−0.36	−0.22	0.27	0.1	−0.13	−0.42	−0.22	−0.29	−0.21	1		
F^-	0.27	0.27	−0.31	−0.33	−0.07	0.45	−0.01	0.12	0.38	−0.15	1	
As	0.42	0.46	−0.27	−0.29	0.07	0.6	0.08	0.41	0.51	−0.28	0.63	1
A—Sulaimani area												

Table 3. *Cont.*

	pH	EC	Ca^{2+}	Mg^{2+}	K^{+}	Na^{+}	HCO_3^{-}	SO_4^{2-}	Cl^{-}	NO_3^{-}	F^{-}	As
pH	1											
EC	−0.28	1										
Ca^{2+}	−0.61	0.56	1									
Mg^{2+}	−0.3	0.86	0.52	1								
K^{+}	−0.09	0.27	0.1	0.09	1							
Na^{+}	0.35	0.48	−0.23	0.29	0.28	1						
HCO_3^{-}	−0.5	0.75	0.74	0.74	0.09	0.19	1					
SO_4^{2-}	−0.13	0.87	0.49	0.73	0.29	0.59	0.54	1				
Cl^{-}	−0.04	0.89	0.36	0.79	0.34	0.66	0.56	0.89	1			
NO_3^{-}	0.34	−0.07	−0.05	−0.13	0.22	−0.11	−0.36	−0.06	−0.03	1		
F^{-}	−0.06	0.65	0.32	0.5	0.32	0.47	0.4	0.74	0.65	0.08	1	
As	0.05	0.34	0.36	0.33	0.07	0.16	0.25	0.44	0.37	0.19	0.59	1
B—Erbil area												

3.5. Health and Environmental Impact

The concentrations of As and F range from 0.19 to 7.8 µg/L and 0.01 to 2.1 mg/L, respectively. According to the World Health Organization [54], the permissible limit of As in drinking water is 10 µg/L, and for fluoride, it is 1.5 mg/L. Fluoride levels above 1.5 mg/L in drinking water cause dental fluorosis and skeletal fluorosis in higher concentrations [55]. Considering these guidelines, all groundwater samples are below this guideline for As, but some samples show higher concentrations than the permissible level for F, especially in the Sulaimani area. Arsenic and fluoride are two natural components affecting human health. In this study, both areas are considered to be of no or low risk for arsenicosis, but there is the risk of fluorosis, which was not considered in the area previously. In their investigation, the authors in [56] pointed out that there is no indication of the risk of fluorosis in the groundwater of the area, as they only detect low F^{-} concentrations (less than 0.15 mg/L). However, this investigation did not represent the whole studied area and the different groundwater resources and aquifers, as they took only 22 samples. In the current investigation, the mentioned criteria were taken into consideration, including sample number, frequency, distribution, depth, and aquifer types. Therefore, the risk of fluorosis in these spots in the studied area should be seriously considered. The reason for the observed low concentration of arsenic may be due to its limited geogenic and anthropogenic sources [36,37]. This interpretation also applies to the groundwater of the Erbil area, as indicated by [54].

Spatial Distribution of As and F

The available groundwater data were used to make a geostatistical interpolation and construction of predictive maps for As and F concentrations in groundwater. The maps for As and F^{-} (Figure 8A,B) indicate vulnerable areas. This can help authorities to become aware of potentially contaminated groundwater, especially close to industrial areas.

The spatial distribution of As and F in the studied area is patchy, and different concentration hotspots are present. This may suggest the existence of local sources [45].

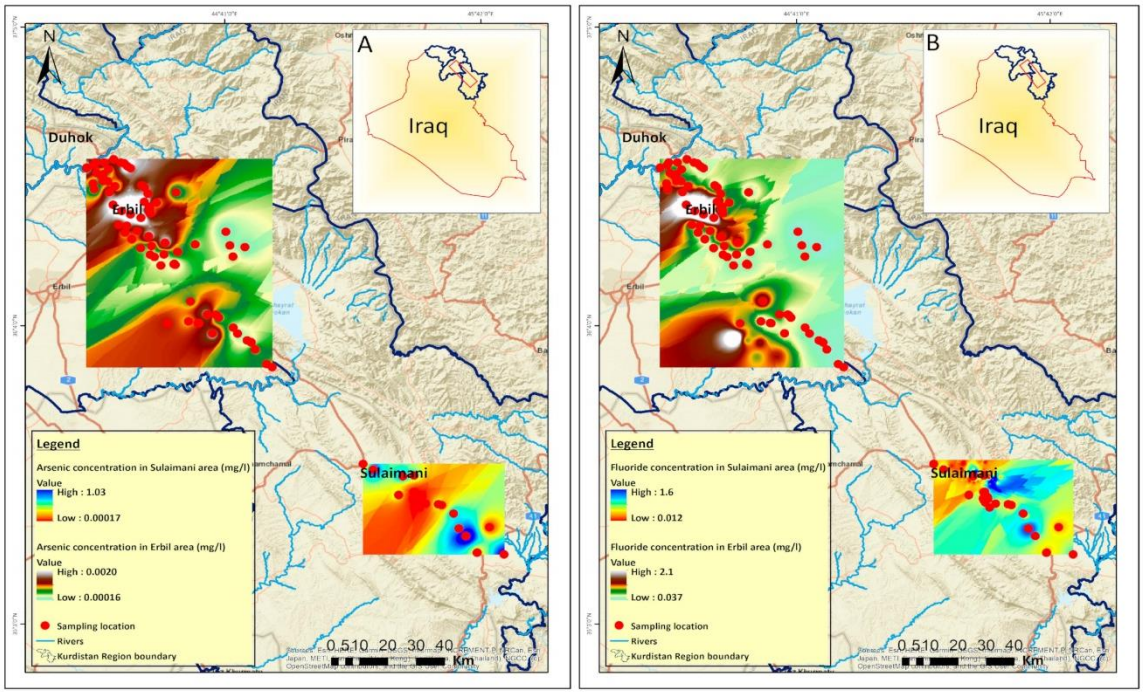

Figure 8. Spatial distribution of (**A**) As and (**B**) F.

4. Conclusions and Recommendations

4.1. Conclusions

The primary outcome of the current study can be summarized as follows:

Concentrations of F^- and As range from 0.01 to 2.1 mg/L and 0.19 to 7.8 µg/L, respectively. Concentrations of F^- and As in groundwater are correlated to the hydrogeochemical processes and their similar adsorption behavior due to their anionic speciation. The results of the examined samples suggest that the primary sources of F^- and As are geogenic. There is no or low risk for arsenicosis. However, the fluoride in some groundwater samples was found in a higher concentration than the permissible WHO limit, indicating a risk of fluorosis in some areas. The risk of fluorosis should be considered seriously, and the monitoring of F is necessary.

The speciation of As and F^- is controlled by pH, redox conditions, and groundwater temperature. Adsorption, desorption, cation exchange, the dissolution of carbonate minerals, and possibly fluorite dissolution are the dominant geochemical processes that govern and control F^- and As concentrations.

Future studies should focus on concentrations of geogenic contaminants in other governorates of the Iraqi Kurdistan area and on the identification of factors controlling their concentrations.

4.2. Recommendations

It is recommended to take the risk of fluorosis into consideration in areas with high fluoride concentrations and to study each hotspot separately to distinguish between geogenic and contamination sources.

Supplementary Materials: The following supporting information can be downloaded at: https://www.mdpi.com/article/10.3390/w15111981/s1, Table S1 is the raw data.

Author Contributions: O.M.—preparing the original draft, statistical plot, collecting data, and interpretation; R.M.—collecting data, mapping, statistical plot, and interpretation; O.S.—interpretation and validation; S.S.—mapping and interpretation. All authors have read and agreed to the published version of the manuscript.

Funding: The second author (R.M.) received a Fisher's scholarship awarded by Palacky University Olomouc (Univerzita Palackého v Olomouci).

Institutional Review Board Statement: Not applicable.

Informed Consent Statement: Not applicable.

Data Availability Statement: The used and analyzed datasets in this study are available from the corresponding author upon reasonable request.

Acknowledgments: We thank Martin Mihaljevič for the water analyses performed at Charles University in Prague. In addition, thanks go to the Laboratories of Technische Universität Bergakademie Freiberg, Germany and Sulaimanyiah Environmental Protection Office, Iraq, for the water analyses.

Conflicts of Interest: The authors declare no conflict of interest.

References

1. Alarcón-Herrera, M.T.; Bundschuh, J.; Nath, B.; Nicolli, H.B.; Gutierrez, M.; Martín-Dominguez, I.R.; Reyes-Gomez, V.M.; Nuñez, D.; Martín-Domínguez, A.; Sracek, O. Co-occurrence of arsenic and fluoride in groundwater of semiarid regions in Latin America: Genesis, mobility and remediation. *J. Hazard. Mater.* **2013**, *262*, 960–969. [CrossRef] [PubMed]
2. Johnson, C.A.; Bretzler, A. (Eds.) *Geogenic Contamination Handbook—Addressing Arsenic and Fluoride in Drinking Water*; Eawag: Dübendorf, Switzerland, 2015; 173p.
3. He, X.; Li, P.; Ji, Y.; Wang, Y.; Su, Z.; Elumalai, V. Groundwater Arsenic and Fluoride and Associated Arsenicosis and Fluorosis in China: Occurrence, Distribution and Management. *Expo. Health* **2020**, *12*, 355–368. [CrossRef]
4. Estrada-Capetillo, B.L.; Ortiz-Perez, M.D.; Salgado-Bustamante, M.; Calderón-Aranda, E.; Rodríguez-Pinala, C.J.; Reynaga-Hernández, E.; Corral-Fernandez, N.E.; González-Amaro, R.; Portales-Perez, D.P. Arsenic and fluoride co-exposure affects the expression of apoptotic and inflammatory genes and proteins in mononuclear cells from children. *Mutat. Res.* **2014**, *731*, 27–34. [CrossRef] [PubMed]
5. Ravenscroft, P.; Brammer, H.; Richards, K. *Arsenic Pollution: A Global Synthesis*; Wiley-Blackwell: Hoboken, NJ, USA, 2009.
6. Appelo, T.; Heederik, J.P. *Arsenic in Groundwater: A World Problem*; IGRAC International Groundwater Resources Assessment Centre: Delft, The Netherlands, 2006; pp. 7–8.
7. Rajmohan, N.; Prathapar, S. Occurrence and Extent of Arsenic, Fluoride and Iron Contamination in Groundwater in Selected Districts in Eastern Ganges Basin-A Review. *J. Appl. Geochem.* **2016**, *18*, 386–407.
8. Fawell, J.; Bailey, K.; Chilton, J.; Dahi, E.; Fewtrell, L.; Magara, Y. *Fluoride in Drinking Water*; IWA Publishing: London, UK, 2001; pp. 15–37.
9. USEPA. Fluorine (Soluble Fluoride) (CASRN 7782-41-4) | IRIS | US EPA. 2012. Available online: https://cfpub.epa.gov/ncea/iris2/chemicalLanding.cfm?substance_nmbr=53 (accessed on 6 February 2022).
10. Sung Ahn, J. Geochemical occurrences of arsenic and fluoride in bedrock groundwater: A case study in Geumthesan County, Korea. *Environ. Geochem. Health* **2012**, *34*, 43–54.
11. Blarasin, M.; Bécher Quinodóz, F.; Cabrera, A.; Matteoda, E.; Felizzia, J. Arsenic and Fluoride in Groundwater of a Loessical Unconfined Aquifer, Cordoba, Argentina. *J. Appl. Geol. Geophys.* **2016**, *4*, 59–65.
12. Ozsvath, D.L. Fluoride concentrations in a crystalline bedrock aquifer Marathon County, Wisconsin. *Environ. Geol.* **2006**, *50*, 132–138. [CrossRef]
13. Saxena, V.; Ahmed, S. Inferring the chemical parameters for the dissolution of fluoride in groundwater. *Environ. Geol.* **2003**, *43*, 731–736. [CrossRef]
14. Karro, E.; Uppin, M. The occurrence and hydrochemistry of fluoride and boron in carbonate aquifer system, central and western Estonia. *Environ. Monit. Assess.* **2013**, *185*, 3735–3748. [CrossRef]
15. Narsimha, A.; Sudarshan, V. Hydro-Geochemistry of Ground Water in Basara Area, Adilabad District, Andhra Pradesh, India. *J. Appl. Geochem.* **2013**, *15*, 224–237.
16. Rafique, T.; Naseem, S.; Usmani, T.H.; Bashir, E.; Khan, F.A.; Bhanger, M.I. Geochemical factors controlling the occurrence of high fluoride groundwater in the Nagar Parkar area, Sindh, Pakistan. *J. Hazard. Mater.* **2009**, *171*, 424–430. [CrossRef] [PubMed]
17. Naseem, S.; Hamza, S.; Bashir, E. Groundwater geochemistry of Winder agricultural farms, Balochistan, Pakistan and assessment for irrigation water quality. *Eur. Water* **2010**, *31*, 21–32.
18. Jha, M.K.; Chowdary, V.M.; Chowdhury, A. Groundwater assessment in Salboni Block, West Bengal (India) using remote sensing, geographical information system and multi-criteria decision analysis techniques. *Hydrogeol. J.* **2010**, *18*, 1713–1728. [CrossRef]
19. Carrillo Rivera, J.; Cardona, A.; Edmunds, A. Use of abstraction regime knowledge of hydrogeological conditions to control high-fluoride concentration in abstracted groundwater: The San Luís Potosí basin, México. *J. Hydrol.* **2022**, *261*, 24–47. [CrossRef]

20. Nordstrom, D.K. Fluoride in thermal and non-thermal groundwater: Insights from geochemical modeling. *Sci. Total Environ.* **2022**, *824*, 153606. [CrossRef]
21. Apambire, W.B.; Boyle, D.R.; Michel, F.A. Geochemistry, genesis, and health implications of fluoriferous groundwaters in the upper regions of Ghana. *Environ. Geol.* **1997**, *33*, 13–24. [CrossRef]
22. Brunt, R.; Vathesak, L.; Griffin, J. *Fluoride in Groundwater: Probability of Occurrence of Excessive Concentration on Global Scale*; IGRAC International Groundwater Resources Assessment Centre: Delft, The Netherlands, 2004; pp. 1–4.
23. Brunt, R.; Vasak, L.; Griffioen, J. Arsenic in groundwater: Probability of occurrence of excessive. *Int. Groundw. Resour. Assess. Cent.* **2004**, *1*, 15.
24. Daessle, L.W.; Ruiz-Montoya, L.; Tobschall, H.J.; Chandrajith, R.; Camacho-Ibar, V.F.; Mendoza-Espinosa, L.G.; Quintanilla-Montoya, A.L.; Lugo-Ibarra, K.C. Fluoride, nitrate and water hardness in groundwater supplied to the rural communities of Ensenada County, Baja California, Mexico. *Environ. Geol.* **2009**, *58*, 419–429. [CrossRef]
25. Bhattacharya, P.; Claesson, M.; Bundschuh, J.; Sracek, O.; Fagerberg, J.; Jacks, G.; Thir, J.M. Distribution and mobility of arsenic in the Río Dulce alluvial aquifers in Santiago del Estero Province, Argentina. *Sci. Total Environ.* **2006**, *358*, 97–120. [CrossRef]
26. Sracek, O.; Wanke, H.; Ndakunda, N.N.; Mihaljevic, M.; Buzek, F. Geochemistry and fluoride levels of geothermal springs in Namibia. *J. Geochem. Explor.* **2015**, *148*, 96–104. [CrossRef]
27. Appelo CA, J.; Postma, D. *Geochemistry, Groundwater and Pollution*; CRC press: Boca Raton, FL, USA, 2004.
28. Rango, T.; Kravchenko, J.; Atlaw, B.; McCornick, P.G.; Jeuland, M.; Merola, B.; Vengosh, A. Groundwater quality and its health impact: An assessment of dental fluorosis in rural inhabitants of the Main Ethiopian Rift. *Environ. Int.* **2012**, *43*, 37–47. [CrossRef] [PubMed]
29. Smith, A.H.; Marshall, G.; Roh, T.; Ferreccio, C.; Liaw, J.; Steinmaus, C. Lung, Bladder, and Kidney Cancer Mortality 40 Years After Arsenic Exposure Reduction. *J. Natl. Cancer Inst.* **2017**, *110*, 5576. [CrossRef]
30. Susheela, A.; Kumar, A.; Bhatnagar, M.; Bahudur, R. Prevalence of endemic fluorosis with gastro-intestinal manifestations in people living in some North-Indian villages. *Fluoride* **1993**, *26*, 97–104.
31. Murray, K.S. Hydrology and geochemistry of thermal waters in the Upper Napa Valley, California. *Groundwater* **1996**, *34*, 1115–1124. [CrossRef]
32. Jacks, G.; Rajagopalan, K.; Alveteg, T.; Jönsson, M. Genesis of high-F groundwaters, southern India. *Appl. Geochem.* **1993**, *8*, 241–244. [CrossRef]
33. Mahmmud, R.; Sracek, O.; Mustafa, O.; Čejková, B.; Jačková, I.; Vondrovicová, L. Groundwater geochemistry evolution and geogenic contaminants in the Sulaimani-Warmawa Sub-basin, Sulaimani, Kurdistan Region, Iraq. *Environ. Monit. Assess.* **2022**, *194*, 352. [CrossRef]
34. Seeyan, S.; Merkel, B. Determination of Recharge by Means of Isotopes and Water Chemistry in Shaqlawa-Harrir Basin, Kurdistan Region, Iraq. *Hydrol. Curr. Res.* **2014**, *5*, 179. [CrossRef]
35. Buday, T. *Regional Geology of Iraq: Vol. 1, Stratigraphy*; Kassab, I.I., Jassim, S.Z., Eds.; Publications of Geological Survey of Iraq: Baghdad, Iraq, 1980; 445p.
36. Jassim, S.Z.; Goff, J.C. *Geology of Iraq*; Jassim, S.Z., Ed.; GEOSURV: Baghdad, Iraq, 2006; 445p.
37. Mustafa, O. Impact of sewage wastewater on the environment of Tanjero River and its basin with Sulaimani City/NE-Iraq. Master Thesis, University of Sulaimani, Sulaymaniyah, Irak, 2006.
38. Kareem, A.; Mustafa, O.; Merkel, B. Geochemical and environmental investigation of the water resources of the Tanjero area, Kurdistan region, Iraq. *Arab. J. Geosci.* **2018**, *11*, 461. [CrossRef]
39. Stevanovic, Z.; Markovic, M. *Hydrogeology of Northern Iraq, General Hydrogeology and Aquifer System*; FAO: Rome, Italy, 2004; Volume 2.
40. Mustafa, O.; Merkel, B. Classification of karst springs based on discharge and water chemistry in Makook karst system, Kurdistan Region, Iraq. *Freib. Online Geosci.* **2015**, *39*, 1–24.
41. APHA; AWWA; WPCF. *Standard Methods for the Examination of Water and Wastewater*, 20th ed.; APHA American Public Health Association: Washington, DC, USA, 2006.
42. Landau, S.; Everitt, B. *A Handbook of Statistical Analyses Using SPSS*; Chapman & Hall/CRC: Boca Raton, FL, USA, 2004.
43. Parkhurst, D.; Appelo, C. *Description of Input and Examples for PHREEQC (Version 3)—A Computer Program for Speciation, Batch-Reaction, One-Dimensional transport, and Inverse Geochemical Calculations*; Chapter 43 of section A, Groundwater Books, Modeling Techniques; United States Geological Survey: Washington, DC, USA, 2013.
44. Bhattacharya, P.; Ahmed, K.M.; Hasan, M.A.; Broms, S.; Fogelström, J.; Jacks, G.; Sracek, O.; von Brömssen, M.; Routh, J. *Mobility of Arsenic in Groundwater in a Part of Brahmanbaria District, N.E. Bangladesh. Managing Arsenic in the Environment: From Soil to Human Health*; CSIRO Publishing: Melbourne, Australia, 2006; pp. 95–115.
45. Parrone, D.; Ghergo, S.; Frollini, E.; Rossi, D.; Preziosi, E. Arsenic-fluoride co-contamination in groundwater: Background and anomalies in a volcanic-sedimentary aquifer in central Italy. *J. Geochem. Explor.* **2020**, *217*, 106590. [CrossRef]
46. Dixit, S.; Hering, J.G. Comparison of arsenic (V) and arsenic (III) sorption onto iron oxide minerals: Implications for arsenic mobility. *Environ. Sci. Technol.* **2003**, *37*, 4182–4189. [CrossRef] [PubMed]
47. Pi, K.; Wang, Y.; Xie, X.; Su, C.; Ma, T.; Li, J.; Liu, Y. Hydrogeochemistry of co-occurring geogenic arsenic, fluoride and iodine in groundwater at Datong Basin, northern China. *J. Hazard Mater.* **2015**, *300*, 652–661. [CrossRef] [PubMed]
48. Mustafa, O. Speciation of U, Se, As and Sr in Karst waters of Makook System, Kurdistan Region, Iraq. *J. Zankoy Sulaimani* 2016.

49. Guo, Q.; Wang, Y.; Ma, T.; Ma, R. Geochemical processes controlling the elevated fluoride concentrations in groundwaters of the Taiyuan Basin, Northern China. *J. Geochem. Explor.* **2007**, *93*, 1–12. [CrossRef]
50. Mustafa, O.; Tichomirowa, M.; Kummer, N.A.; Merkel, B. Assessment of water-rock interaction processes in the karst springs of Makook anticline (Kurdistan Region, Iraq) using Sr-isotopes, rare earth, and trace elements. *Arab. J. Geosci.* **2016**, *9*, 368. [CrossRef]
51. Gomez, M.L.; Blarasin, M.T.; Martínez, D.E. Arsenic and fluoride in a loess aquifer in the central area of Argentina. *Environ. Geol.* **2009**, *57*, 143–155. [CrossRef]
52. Li, C.; Gao, X.; Wang, Y. Hydrogeochemistry of high-fluoride groundwater at Yuncheng Basin, northern China. *Sci. Total Environ.* **2015**, *508*, 155–165. [CrossRef]
53. Seeyan, S. Hydrochemical assessment and groundwater quality of Koysinjaq area in Kurdistan Region-Iraq. *Arab. J. Geosci.* **2020**, *13*, 491. [CrossRef]
54. WHO. *Guideline for Drinking-Water Quality*, 4th ed.; World Health Organization: Geneva, Switzerland, 2011.
55. Kumar, M.; Puri, A. A review of permissible limits of drinking water. Indian. *J. Occup. Environ. Med.* **2012**, *16*, 40–44.
56. Khursheed, D.A.; Abdulateeef, D.S.; Fatah, A.O.; Rauf, A.M. Fluoride concentration of well water in different areas of Sulaimani province. *Sulaimani Dent. J.* **2015**, *2*, 67–71. [CrossRef]